# Direct Synthesis of Gasoline from Syngas on Hybrid Catalyst

**Ting Ma**

# Abstract

The purpose of this study is to develop high-performance hybrid catalyst for direct synthesis gasoline-range hydrocarbons from syngas by methanol synthesis route and FTS route, respectively. The following conclusions have been achieved.

The catalytic performances of hybrid catalysts composed of Cu-ZnO and metal/ZSM-5 in the syngas conversion to light hydrocarbons via methanol in a near-critical *n*-hexane solvent have been studied.

1. The near-critical fluid was effective in the selective production of hydrocarbons in gasoline fraction during the syngas conversion over the hybrid catalyst. The employment of the near-critical solvent led to depressing the formation of $CO_2$ during the reaction.

2. Hydrocarbon distribution was strongly dependent on the particle size of ZSM-5 and Pd loading. A decrease in the particle size of ZSM-5 and an increase in the Pd loading improved the yield of hydrocarbons in gasoline fraction. It is likely that the improvement of the mass transfer due to the decrease of the particle size and the hydrogenation of unsaturated hydrocarbons over Pd suppress the deposition of carbonaceous species. Therefore, Pd/ZSM-5 composed of nano-sized particles is effective on the selective production of gasoline fractions from syngas via methanol with the near-critical fluid.

3. The hybrid catalyst consisting of 5 wt% Cu/ZSM-5 coupled with Cu-ZnO exhibited very similar catalytic performances to those over the hybrid catalyst containing 0.5 wt% Pd/ZSM-5, and produced selectively gasoline-ranged hydrocarbons from syngas.

For FTS reaction with $H_2$-deficient syngas as feed gas, the metal-added Fe-based

catalyst as a WGS catalyst was mixed with Co/β as an FTS catalyst to prepare a hybrid catalyst. The effect of different metal addition on the structure and WGS activity of Fe-based catalysts were investigated.

1. The effects of metal species in an Fe-based catalyst on structural properties were investigated through the synthesis of Fe-based catalysts containing various metal species, such as Mn, Zr, and Ce. The metal-added Fe-based catalysts exhibited much higher specific surface area than the conventional Fe-based catalyst due to the formation of mesoporous voids surrounded by the nanosized crystallites.

2. Among the catalysts, the hybrid catalyst containing the Mn-added Fe-based catalyst exhibited the highest activity for the CO hydrogenation and the WGS reaction with the CO conversion of 45.0%, the STY of hydrocarbons of 2.61mol kmol $kg^{-1}$ $h^{-1}$, and the STY of $CO_2$ of 1.92mol $kg^{-1}$ $h^{-1}$ after 6.5 h of the reaction.

3. Moreover, the loading of Pd species on the Mn-added Fe-based catalyst improved the durability due to the high hydrogenation ability of Pd species.

# Contents

# CHAPTER ONE

# INTRODUCTION

## 1.1 General remarks

Gasoline is an important liquid hydrocarbon-based fuel derived primarily from fractional distillation of petroleum fractions. Globally, gasoline is popularly employed as a major commodity for transportation and fuel and petrochemicals-based industrial applications [1]. While its global demand was projected to rise for many world regions, particularly due to increase in the number of automobiles and industrial-based internal combustion engines, the available crude oil reserves are on the decline. One major alternative given consideration today is the production from non-petroleum sources. Synthesis gas (syngas) ($CO + H_2$), which can be produced from a variety of carbon resources such as natural gas, biomass, and coal, has been focused on as a raw material for the production of fuels and chemicals. Catalytic conversion of syngas to hydrocarbons and alcohols is an important link to improve the carbon cycling with the increasing energy demand and environmental concern [2]. Gas-to-Liquids (GTL), Coal-to-Liquids (CTL), Biomass-to-Liquids (BTL) all rely on the catalytic conversion of syngas. Liquid fuels are preferred for use in transportation since they have higher energy density than coal but are more easily and safely stored than gas, which has the highest energy density of the three phases. Gasoline is one of the most important liquid fuels in transportation. In general, it was produced from petroleum refining. With the increasing gasoline demand and the shrinking petroleum reserves, it is attracting more and more attention for gasoline production from non-petroleum resources [3]. Currently, there are two typical commercialized processes for gasoline production from non-petroleum resources via syngas: Fisher-Tropsch synthesis (FTS) [4 - 10] and

methanol-to-gasoline (MTG) [11 -16]. Fischer-Tropsch (FT) produces a wide range of mainly linear paraffinic hydrocarbons, with a distribution depending on the catalyst and the specific process configuration. It should be noted that several studies have evaluated the combination of Fischer-Tropsch catalysts (e.g. Fe-, and Co-based) and zeolites (e.g., ZSM-5) for the conversion of syngas to gasoline-range hydrocarbons [17 - 21]. Hydrocracking and hydroisomerization of the primary Fischer-Tropsch olefins are considered to occur on the acidic sites and in the pore channels of the zeolite, which break the limit of the Anderson-Schultz-Flory (ASF) hydrocarbon product distribution [17] thus enabling direct conversion of liquid fuels without the need for further hydrotreatment. While integration of the two catalytic mechanisms holds promise there appears to be room for improvement in enhancing yield to gasoline-range hydrocarbons (e.g., $C_5$-$C_{11}$) [18, 21] and catalytic stability [20]. Post processing, generally hydrocracking, is required to maximize the desired product fraction. MTG operations take advantage of the relative ease with which methanol is formed from syngas, followed by direct conversion of this initial product into heavier fuels. The MTG process converts methanol to a mixture of hydrocarbons in the $C_2$ to $C_{10}$ range, including paraffins, aromatics, and olefins. As Figure 1.1 shows, FT synthesis and methanol synthesis are widely used for syngas effectively utilization, in which carbon monoxide hydrogenation can produce ultra clean fuels from coal, natural gas or biomass as feedstocks through chemical conversion.

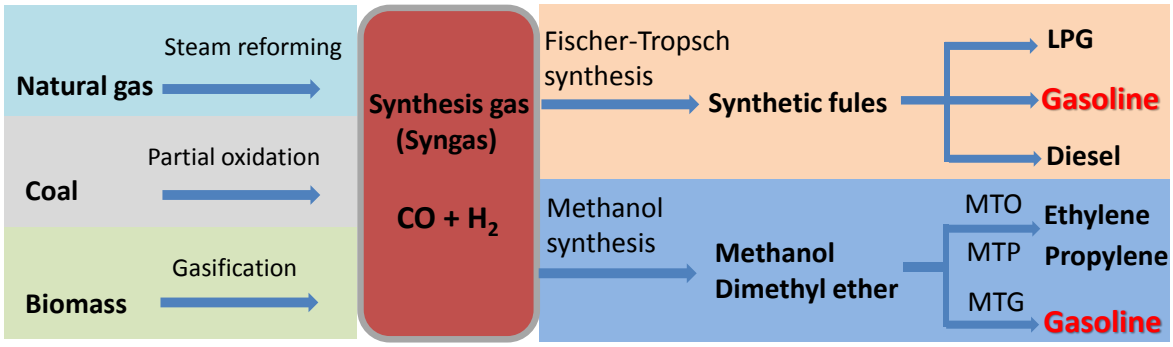


Fig. 1.1 XTL (GTL, CTL and BTL) process scheme

## 1.2 Methanol synthesis process

### 1.2.1 Methanol synthesis reaction

Methanol can be derived from synthesis gas ($H_2$, CO), which in principle can be produced from the reforming of abundant natural gas reserves or biomass-based materials. The reforming process, which involved the reaction of methane gas derived from biomass or natural gas with carbon dioxide or water, is achieved catalytically at normally high reaction temperatures, under controlled pressure conditions to produce hydrogen rich synthesis gas [22]. The principal raw materials for synthesis gas production are natural gas, methane gas from associated petroleum, shale gas, coal and biomass. Synthesis from fossil sources can be successfully achieved by the reforming technologies (i.e. dry and steam reforming) whereas pyrolysis and gasification processes for the biomass-based production option. The increasing global interest on the production and valorization of shale gas [23, 24], therefore imply that the syngas production will attract future shifts towards the shale gas utilization as the main feedstock. Currently, the production of shale gas takes place mainly in the countries like the United States, Canada and countries in the North America. Dry reforming proceeds via the interaction of methane with carbon dioxide, at usually high temperatures that

could be up to 800 °C, over reforming catalysts like the Ni based systems. An alternative to the dry reforming technology is the steam reforming process. Unlike the dry reforming process which employs $CO_2$ as the co-reactant, steam reforming proceeds by an endothermic reaction of purified methane feed with steam at comparable temperatures.

Following its successful production, the syngas is employed as an affordable feedstock for the production of high grade methanol. At the industrial scale, purified syngas, usually containing 2 - 2.5 M ratio of hydrogen to carbon monoxide, is employed for the reaction at 20 to 30 MPa pressure. This extreme pressure permits the compression of the reactant species. Under appropriate space velocity, the mixture can be fed into the reactor at temperatures in the range of 300 - 400 °C. The exothermic nature of the reaction implies that, sufficiently high pressure is desired to shift the equilibrium towards methanol production.

The predominant reactions are:

$CO_2 + 3\ H_2 \leftrightharpoons CH_3OH + H_2O$ - 47 kJ/mol (1-1)

or combined with the water-gas shift reaction (2)

$CO + H_2O \leftrightharpoons CO_2 + H_2$ - 41 kJ/mol (1-2)

$CO + 2\ H_2 \leftrightharpoons CH_3OH$ - 91 kJ/mol (1-3)

Although methanol had been employed previously for a variety of applications, covering the production of pigments, plastics and paints, as solvent, wastewater denitrification, biodiesel production and in electricity generation by driving turbines [25 - 27], the current status of the energy industry gave a considerable emphasis to hydrocarbon production. The methanol to gasoline (MTG) technology is a forefront catalytic route under exploration.

### 1.2.2 Methanol-to-gasoline (MTG) process

Modern processes for the conversion of methanol to gasoline gave emphasis to the methanol production from syngas before subsequent upgrade to gasoline in the MTG operation unit. Unlike other synthetic methods for gasoline production, the methanol to gasoline route produce gasoline with compatible octane properties that is also free from impurities. At the industrial scale, the MTG process, which can be achieved at complete conversion, is exothermic with heat of reaction of 1.74 MJ/kg methanol [28]. To successfully handle the reaction, two splitting steps are normally adopted. Initially, methanol gets transformed into water and dimethyl ether equilibrated with unreacted methanol over a catalyst that is usually non-zeolitic in nature. In the final/second stage, a zeolite catalyst like HZSM-5 is used to convert the mixture with a recycled gas to gasoline range hydrocarbons and water. Several MTG commercialization units are considered in different parts of the world. The petroleum giant Mobil, commercialized a plant in New Zealand in 1987. The operational unit comprised of a syngas production facility, which converts natural gas from field sources to methanol. The 14,500 barrels per day MTG unit uses fixed-bed configuration to generate clean gasoline with properties similar to those of the conventional fuel [29].

The actual reaction mechanism for the production of paraffins and other hydrocarbon products from methanol is still a debatable issue in the literature. Among the proposed mechanisms, direct coupling of C1 species, methylation of alkenes and their subsequent cracking (i.e. olefins methylation and cracking pathway) and the hydrocarbon pool pathways involving methylbenzene intermediates have been critically studied [30 -32].

### 1.2.3 Methanol-to-gasoline catalysts

Generally, methanol has been produced industrially from CO, $CO_2$ and $H_2$ using Cu/Zn/Al catalysts [33, 34]. The catalyst is typically prepared by co-precipitation method followed by calcination and reduction. Copper metal is the catalytically active phase, and ZnO is a chemical and structural promoter, while alumina is only a structural promoter which has been pointed out to work as the promoter to increase the stability and the activity [35]. Moreover, $ZrO_2$ is also a very promising catalyst promoter due to its high stability under reducing or reactive conditions [34]. Especially sintering of copper in ternary $Cu/ZnO/Al_2O_3$ catalysts has been identified as a major deactivation mechanism in this process.

The MTG reaction is catalyzed by Brønsted acidic zeolite and zeolite-like materials [36]. Their behaviors are based on shape-selectivity, dimensional structure, stability and acidity properties with possibility of modifications under controlled conditions. Catalysts based on H-ZSM-5 or the modified analogs were the main materials given preference by the Companies, with numerous literature studies document [37, 38]. The reaction mechanism was believed to consist of two key steps. Primarily, methanol undergo dehydration into dimethyl ether. In the secondary stages, the equilibrium mixture produces light olefins that are susceptible for conversion to higher hydrocarbon products. The mechanism of coke deposition during the MTG reaction is similarly dependent on the zeolite topology [29]. Most studies revealed that the acidic properties and mesopore formation of ZSM-5 catalysts were well altered, and the diffusion properties of the pore channels were improved. However, these catalysts still exhibited high selectivity toward the undesired aromatics and relatively fast deactivation due to the formation of carbonaceous species. Many researches on the improvement of ZSM-5

zeolites by alteration of preparation methods or modification technologies have been carried out to solve these problems. Nanocrystalline zeolites have attracted more attention due to the short diffusion path length, large external surface and easy accessibility to active sites [39]. Recently, researchers have confirmed that nanocrystalline ZSM-5 exhibited good resistance of coke deposition and excellent catalytic performance in MTG reaction [40].

## 1.3 Fischer-Tropsch synthesis process

### 1.3.1 Fischer-Tropsch synthesis reaction

In 1922 Franz Fischer and Hans Tropsch developed a heterogeneously catalysed process (Fischer–Tropsch synthesis (FTS)) for the transformation of synthesis gas (syngas, CO + $H_2$) into different hydrocarbons fractions (diesel fuels, gasoline, lower olefins, etc.). The motivation for this work was to allow nations with no natural oil reserves to produce liquid fuels for transportation from coal. Liquid fuels are preferred for use in transportation since they have higher energy density than coal but are more easily and safely stored than gas, which has the highest energy density of the three phases [41]. The FTS converts syngas into hydrocarbons which form the basis for gasoline, diesel, jet fuel, and chemicals such as olefins and waxes [42 - 45]. It forms the heart of the Gas-to-Liquids (GTL) and Coal-to-Liquids (CTL) plants in South Africa, Qatar, Malaysia and China. In addition to natural gas, coal and biomass can be converted to syngas by partial oxidation, steam reforming or gasification processes. Moreover, different hydrocarbons may be directly produced from syngas by developing highly selective FT catalysts. Therefore, FT synthesis is viewed as a valuable process to produce super-clean fuels from syngas derived from non-petroleum resources. The

product distribution is broader than liquids hydrocarbons alone, and includes methane and alkanes, $C_nH_{2n+2}$ (with n from 1 $\rightarrow$ 100), alkenes or olefins ($C_nH_{2n}$; $n \geq 2$), and to a lesser extent oxygenated products such as alcohols.

The following exothermic reactions take place during FT synthesis, with alkanes and alkenes the desired products:

Alkane production: $n\,CO + (2n + 1)\,H_2 \rightarrow C_nH_{2n+2} + nH_2O$ (1-4)

Alkene production: $n\,CO + 2nH_2 \rightarrow C_nH_{2n} + nH_2O$ (1-5)

Water-gas shift reactions: $CO + H_2O \leftrightharpoons CO_2 + H_2$ (1-6)

The water-gas shift (WGS) reaction also takes place over most of FT catalysts (reaction (1-6)) and provides a means to alter the CO : $H_2$ distributions. Side reactions such as those producing alcohols and undesired carbonaceous deposits via Boudouard reactions may occur (reactions (1-7) and (1-8)).

Alcohols: $n\,CO + 2n\,H_2 \rightarrow C_nH_{2n+2}O + (n - 1)\,H_2O$ (1-7)

Boudouard reaction: $2\,CO \rightarrow C + CO_2$ (1-8)

FT processes are usually categorised based on operating conditions; typically high-temperature FT (HTFT) operates at 300 - 350 °C and low-temperature FT (LTFT) operates at 200 - 240 °C [46]. The typical reactors designed for FT processes are fixed bed, slurry bubble column reactor, and circulating and fluidised-bed reactor, with fluidised bed reactors mostly applied for HTFT processes using Fe catalysts to produce $C_1$ - $C_{15}$ hydrocarbon fractions. Slurry-phase and fixed-bed reactors are typically used for LTFT process with both Co and Fe catalysts to produce linear long-chain hydrocarbons (such as paraffins and waxes).

### 1.3.2 Fischer-Tropsch synthesis catalysts

It has been reported that the activity of FT catalysts are dependent on $H_2$ adsorption capacity, ability to dissociatively adsorb CO the reducibility of other metal oxide components. Based on literature reviews [47- 49], it shown that transition metals belonging to groups III-VI of the periodic table are ineffective for FTS. While, they are desirable for dissociative adsorption of CO their tendency to form highly stable oxides, means catalysts are not easily reduced under usual FTS conditions. Moreover, transition metals belonging to groups XI and XII plus Ir, Pt and Pd are favour non-dissociative CO adsorption and are not sufficiently active in FTS. Fe, Co, Ni, Ru and Os are commonly accepted to be the best catalytic materials for use FT synthesis, with occasionally Re and Rh reported to exhibit acceptable catalytic activity for FTS. Ru is one of the most active catalysts for FTS operating at low reaction temperature producing long chain hydrocarbons without the need for any promoters. However, it is very expensive and a limited world resource and therefore it is not considered a sustainable option for use in industrial processes. Nickel, while another suggested catalyst for FT process, has a high hydrogenation activity and thus undesired high selectivity to methane production. Therefore, Co and Fe are the deemed to be the best metals for application in industrial scale FTS processes [50]. Fe while economically attractive and highly abundant, has a very low selectivity to paraffins, favouring the production of olefins and oxygen and unfortunately deactivates more quickly than Co based catalysts [46]. Although Co is more expensive than Fe, Co has a good selectivity to paraffins, low selectivity to olefins and oxygen, and is more resistant to deactivation. In fact, the iron-based catalyst is an iron carbide under reaction conditions, whereas cobalt works in the metallic state.

Therefore, Co is the preferred choice to create long chain paraffins, while Fe is the

better selection to produce olefins. To make a more informed selection between Fe and Co, the nature of the carbon feedstock is an essential factor that must be considered. Fe has a high activity for water gas shift (WGS) and hence it is appropriate for hydrogen-poor feed stocks derived from biomass or coal [46]. Fe is thus useful for syngas conversion with lower ratios of $H_2/CO$ = 0.5 - 2.5 obtained from biomass or coal, but it is not suitable for conversion of $H_2$-rich syngas derived from methane. Consequently, the Fe based catalysts are better for alkene production from syngas, BTL and CTL technologies. On the other hand, Co provides better catalytic performance at high $H_2/CO$ ratios (i.e. 2 and above) and is therefore, a better selection where the carbon feed stock is natural gas. Due to the instability of Fe, more modification is generally required to improve activity and selectivity, with rapid catalyst deactivation still the major challenge for Fe based catalysts [51].

Effective reduction of the active phase plays an important role in optimising catalyst performance, with the addition of small quantities of promoters during the formulation of the catalyst found to significantly enhance the reducibility of Co and Fe. Furthermore, promoters improve the activity and selectivity of heterogeneous catalysts by influencing the catalyst's structural properties through varying the active phase structure, or modifying the electronic character of the active phase. Generally, metal oxides (MnO and ZnO), alkali metals (Na, K, Rb, Cs) and certain transition metals (Cu, Pd, Pt, Ru) or carbonates are applied as promoters for the Fe and Co-based FT catalysts [52]. Additionally, the selection of support which stabilises the resulting Co or Fe nanoparticles is critical in determining FT-catalyst activity and stability. Altering the support's surface structure and pore size may improve the metal dispersion, reducibility and the diffusion coefficients of reactants and products. $Al_2O_3$, $SiO_2$, $TiO_2$ and $ZrO_2$ are

used as catalyst supports in the FTS due to their high surface area and strong mechanical strength. Low metal-support interactions are important for catalyst activity and stability [46].

## 1.4 Purpose of this study

This research focused on selective synthesis of light hydrocarbon, especially gasoline-range hydrocarbons from syngas on hybrid catalyst through methanol synthesis and FTS process. The purpose of this study is to develop the catalytic performance of the hybrid catalyst for direct synthesis gasoline from syngas by MTG route and FTS route, respectively.

For the syngas obtained from natural gas, the catalytic activity of a hybrid catalyst composed of Cu-ZnO and Pd/ZSM-5 in a near-critical *n*-hexane solvent in the conversion of syngas to hydrocarbons via methanol was investigated. During the experimental trials, the reaction in the near-critical phase was compared with those in conventional phases to clarify the effect of the near-critical solvent on the catalytic activity and product distribution. The effects of the acid amount and particle size of ZSM-5 as well as Pd loading on the hydrocarbon yield were also investigated. In addition, since low-cost sources are desirable for the preparation of catalysts, copper, cobalt and iron, which are non-precious metals, were employed for the preparation of metal-loaded ZSM-5 to compare their catalytic properties with those of Pd/ZSM-5.

Meanwhile, enormous efforts have been made to improve the gas utilization efficiency of these $H_2$-deficient biosyngas. The catalytic properties of hybrid catalysts composed of a catalyst for the WGS reaction and a catalyst for the FTS in the conversion of $H_2$-deficient syngas to hydrocarbons was investigated. In particular, the

catalytic activity of the WGS catalyst was focused on for the enhancement of the CO hydrogenation by the supply of hydrogen. Since Co-based catalysts have a higher activity for the CO hydrogenation than Fe-based catalysts, the Co-based catalyst and the Fe-based catalyst were employed as an FTS catalyst and a WGS catalyst, respectively. The effect of the addition of metal species to the Fe-based WGS catalyst on the physicochemical and catalytic properties had also been discussed.

References

[1] M. F. Chang, L. Evans, R. Herman, P. Wasielewski, 1976. Gasoline Consumption in Urban Traffic. Transportation Research Record.

[2] J. Wang, Q. Sun, S. Chan, H. Su, Appl. Catal. A: Gen. 509 (2016) 97–104

[3] C. Wang, D. Zhang, C Fang, Q. Ge, H. Xu, Fuel 134 (2014) 11–16

[4] R. B. Anderson, Fischer–Tropsch Synthesis, Academic Press, New York, 1984.

[5] M. E. Dry, Appl. Catal. A: Gen. 276 (2004) 1–3.

[6] B. H. Davis, Ind. Eng. Chem. Res. 46 (2007) 8938–8945.

[7] H. Schulz, in: B. H. Davis, M.L. Occelli (Eds.), Fischer–Tropsch Synthesis and Hydroformylation on Cobalt Catalysts, CRC Press/Taylor and Francis Group, Boca Raton/London/New York, 2010, pp. 165–183.

[8] L. Shi, Y. Jin, C. Xing, C. Zeng, T. Kawabata, K. Imai, K. Matsuda, Y. Tan, N. Tsubaki, Appl. Catal. A: Gen. 435-436 (2012) 217–224.

[9] B. Todic, T. Bhatelia, G.F. Froment, W. Ma, G. Jacobs, B.H. Davis, D.B. Bukur, Ind. Eng. Chem. Res. 52 (2013) 669–679.

[10] N. E. Tsakoumis, R. Dehghan, R. E. Johnsen, A. Voronov, W. van Beek, J. C. Walmsley, Ø. Borg, E. Rytter, D. Chen, M. Rønning, A. Holmen, Catal. Today 205 (2013) 86–93.

[11] Aghamohammadi, S., Haghighi, M., Chem. Eng. J. 264, (2015) 359–375.

[12] F. Yaripour, Z. Shariatinia, S. Sahebdelfar, A. Irandoukht, Microporous Mesoporous Mater. 203 (2015) 41–53.

[13] Olsbye U, Svelle S, Bjorgen M, Beato P, Janssens TVW, Joensen F, Angew Chem-Int Ed 51(2012) 5810–5831.

[14] M. Stöcker, Microporous Mesoporous Mater. 29 (1999) 3–48.

[15] M. Stöcker, Microporous Mesoporous Mater. 82 (2005) 257–292.

[16] T. Mokrani, M. Scurrell, Catal. Rev. 51 (2009) 1–145.

[17] Y. Li, T. Wang, C. Wu, H. Li, X. Qin, N. Tsubaki, Fuel Processing Technology 91 (2010) 388–393.

[18] Y. Yoneyama, J. He, Y. Morii, S. Azuma, N. Tsubaki, Catalysis Today 104 (2005) 37–40.

[19] P. Mohanty, K.K. Pant, J. Parikh, D.K. Sharma, Fuel Processing Technology 92 (2011) 600–608.

[20] F. G. Botes, W. Böhringer, Applied Catalysis A: General 267 (2004) 217–225.

[21] X. Huang, B. Hou, J.Wang, D. Li, L. Jia, J. Chen, Y. Sun, Applied Catalysis A: General 408 (2011) 38–46.

[22] J. H. Edwards, A. M. Maitra, Fuel Process. Technol. 42 (1995) 269–289.

[23] P. C. Bruijnincx, B. M. Weckhuysen, Angew. Chem. Int. Ed. 52 (2013) 11980–11987.

[24] K. A. Bowker, AAPG Bull. 91 (2007) 523–533.

[25] W. W. Kaeding, S. A. Butter, J. Catal. 61 (1980) 155–164.

[26] A. Hamnett, Catal. Today 38 (1997), 445–457.

[27] B. McNicol, D. Rand, K. Williams, J. Power Sources 83 (1999) 15–31.

[28] S. Yurchak, Surf. Sci. Catal. 36 (1988) 251–272.

[29] A. Galadima, O. Muraza, Journal of Natural Gas Science and Engineering 25 (2015) 303–316

[30] D. M. Marcus, K. A. McLachlan, M. A. Wildman, J .O. Ehresmann, P. W. Kletnieks, J. F. Haw, Angew. Chem. Int. Ed. 45 (2006) 3133–3136.

[31] R. M. Dessau, R. B. LaPierre, J. Catal. 78 (1982) 136–141.

[32] I. M. Dahl, S. Kolboe, J. Catal. 161 (1996) 304–309.

[33] M. Bowker, R. A. Hadden, H. Houghton, J. N. K. Hyland, K. C. Waugh, J. Catal., 109 (1988), 263–273

[34] X. M. Liu, G. Q. Lu, Z. F. Yan, J. Beltramini, Ind. Eng. Chem. Res., 42 (2003), 6518–6530

[35] C. Li, X. Yuan, K. Fujimoto, Appl. Catal. A: Gen., 469 (2014), 306–311

[36] U. Olsbye, S. Svelle, M. Bjørgen, P. Beato, T.V.W. Janssens, F. Joensen, S. Bordiga, K.P. Lillerud, Angew. Chem. Int. Ed. 51 (2012) 5810–5831.

[37] M. Bjørgen, S. Svelle, F. Joensen, J. Nerlov, S. Kolboe, F. Bonino, L. Palumbo, S. Bordiga, U. Olsbye, J. Catal. 249 (2007) 195–207.

[38] S. K. Saxena, N. Viswanadham, A. H. Al-Muhtaseb, J. Indust. Eng. Chem. 20, (2014) 2876–2882.

[39] A. A. Rownaghi, J. Hedlund, Ind Eng Chem Res, 50 (2011), 11872–11878

[40] B. Li, B. Sun, X. Qian, W. Li, Z. Wu, Z. Sun, J Am Chem Soc, 135 (2013), 1181–1184

[41] H. Jahangiri, J. Bennett, P. Mahjoubi, K. Wilson, S. Gu, Catal. Sci. Technol., 4 (2014) 2210–2229.

[42] H. Storch, N. Golumbic, R. B. Anderson, Wiley, New york, 1951.

[43] E. Iglesia, S. C. Reyes, R. J. Madon, S. L. Soled, Advances in Catalysis, 39 (1993) 221–302.

[44] G. P. van der Laan, A. A. C. M. Beenackers, Catalysis Reviews-Science and Engineering, 41 (1999) 255–318.

[45] A. P. Steynberg, M. E. Dry, Studies in Surface Science and Catalysis, Vol. 152, Elsevier, Amsterdam, 2004.

[46] A. Y. Khodakov, W. Chu, P. Fongarland, Chem. Rev., 107 (2007) 1692–1744.

[47] C. Perego, R. Bortolo, R. Zennaro, Catal. Today, 142 (2009) 9–16.

[48] O. O. James, A. M. Mesubi, T. C. Ako, S. Maity, Fuel Process. Technol., 91 (2012) 136–144.

[49] V. Ponec, Catal. Today, 12 (1992) 227–254.

[50] H. Schulz, Appl. Catal., A, 186 (1999) 3–12.

[51] E. de Smit, B. M. Weckhuysen, Chem. Soc. Rev., 37 (2008) 2758–2781.

[52] M. Feyzi, M. Irandoust, A. A. Mirzaei, Fuel Process. Technol., 92 (2011) 1136–1143.

CHAPTER TWO

# SYNTHESIS OF GASOLINE FROM SYNGAS VIA METHANOL SYNTHESIS IN NEAR-CRITICAL PHASE


## Abstract

The effect of solvents on the reaction performance of conversion of syngas ($CO + H_2$) to hydrocarbons in gasoline fraction over a hybrid catalyst composed of Cu-ZnO and Pd/ZSM-5 under near-critical condition was studied in a fixed bed reactor. Three kinds of solvents: *n*-pentane, *n*-hexane and *n*-heptane were chosen as the solvent. Methanol was synthesized from syngas over Cu-ZnO; subsequently, was converted to hydrocarbons through the formation of dimethyl ether (DME) over Pd/ZSM-5. The yield of hydrocarbons increased from ca. 29% to ca. 54% with increasing the partial pressure of *n*-hexane from 0 MPa to 1.5 MPa. By contrast, the yields of $CO_2$ and DME decreased with increasing the partial pressure of *n*-hexane. Influence of solvent used in near-critical phase on activity, $CO_2$ selectivity and hydrocarbon distributions were investigated. Similar CO conversion, $CO_2$ and DME yields and hydrocarbon distribution were obtained in different solvent. CO conversion increased with increasing the total pressure when the ratio of syngas partial pressure to *n*-hexane partial pressure was kept constant.

## 2.1 Introduction

Gasoline is an important liquid hydrocarbon-based fuel derived primarily from fractional distillation of petroleum fractions. Globally, gasoline is popularly employed as a major commodity for transportation and fuel and petrochemicals-based industrial applications [1]. While its global demand was projected to rise for many world regions, particularly due to increase in the number of automobiles and industrial-based internal combustion engines, the available crude oil reserves are on the decline. One major alternative given consideration today is the production from non-petroleum sources. Synthesis gas (syngas) ($CO + H_2$), which can be produced from a variety of carbon resources such as natural gas, biomass, and coal, has been focused on as a raw material for the production of fuels and chemicals. Gasoline is one of the most important liquid fuels in transportation. In general, it was produced from petroleum refining. With the increasing gasoline demand and the shrinking petroleum reserves, it is attracting more and more attention for gasoline production from non-petroleum resources [2]. Currently, there are two typical commercialized processes for gasoline production from non-petroleum resources via syngas: Fisher-Tropsch synthesis (FTS) [3-9] and methanol-to-gasoline (MTG) [10-15]. Fischer-Tropsch (FT) produces a wide range of mainly linear paraffinic hydrocarbons, with a distribution depending on the catalyst and the specific process configuration. It should be noted that several studies have evaluated the combination of Fischer-Tropsch catalysts (e.g. Fe-, and Co-based) and zeolites (e.g., ZSM-5) for the conversion of syngas to gasoline-range hydrocarbons [16-20]. Those reactions usually take place in a gas phase.

For example, gasoline-range hydrocarbons (e.g., $C_5$-$C_{11}$) could be directly synthesized from syngas over a hybrid catalyst, which is composed of methanol

synthesis catalyst and zeolite in the gas phase. Different from FT synthesis reaction mechanism, the syngas, which is produced by reforming of natural gas or gasification of coal or biomass, can be converted into hydrocarbons through an intermediate of methanol or DME in the reactions. The hybrid catalysts that composed of Cu–Zn methanol synthesis catalysts and MFI zeolite showed a good initial activity and selectivity for synthesis of gasoline-range hydrocarbons. But a considerable amount of $CO_2$ would be produced during the reactions. That will impair efficient utilization of syngas and will increase emission of greenhouse gas. Gas phase reactions will result in a high temperature rise because of intense exothermic reaction of synthesis of methanol and its conversion. The hybrid catalysts suffer from deactivation with time on stream at high temperature and an environment with water and $CO_2$ [21].

Reaction processes using solid catalysts in near- and supercritical solvents have received considerable attention in the fields of organic synthesis [22-25] and biomass conversion [26-30] in the recent decades because a reaction rate can be significantly improved in the solvents. Supercritical fluids have unique properties such as superior solubility and transfer characteristics due to gas-like viscosity and diffusivity as well as liquid-like density, which make them attractive for chemical reactions. The production of undesirable products can be reduced under the supercritical fluid reaction system and the deactivation of the catalysts can be mitigated through better heat and mass transfer, consequently prolonging the longevity of catalysts. Supercritical hydrocarbon fluids have been applied to the FTS to increase the hydrocarbon yield and to suppress the generation of undesired products due to the efficient extraction of products from catalysts [30-35]. In a manner similar to the FTS reaction in the supercritical phase, the LPG synthesis from syngas using a hybrid catalyst in a near-critical solvent has been

studied [21]. Efficient removal of heat generated during the reaction by the near-critical fluid leads to improvements in the stability of the catalyst as well as selectivity for light hydrocarbons.

The aim of this work is to investigate the solvent effect during the conversion of syngas to hydrocarbons via methanol over hybrid catalyst. During the experimental trials, the reaction in the near-critical phase was compared with those in conventional phases to clarify the effect of the near-critical solvent on the catalytic activity and product distribution.

## 2.2 Experimental

### 2.2.1 Catalyst preparation

A hybrid catalyst was prepared by physically mixing the 355-710 μm pellets of a Cu-ZnO methanol synthesis catalyst of 0.5 g with those of a Pd/ZSM-5 catalyst of 0.5 g. Cu-ZnO was a commercial catalyst (MK-121, TOPSØE). Pd/ZSM-5 was prepared by impregnation method with a 4.557 wt% $Pd(NH_3)_2(NO_3)_2$ aqueous solution and commercial ZSM-5 with the $SiO_2/Al_2O_3$ molar ratio of 23 (CBV2314, Zeolyst). Commercial $NH_4^+$- type ZSM-5 was calcined at 823 K for 3 h to become proton-type ZSM-5. Proton-type ZSM-5 was immersed in the $Pd(NH_3)_2(NO_3)_2$ aqueous solution with a supported metal weight at room temperature overnight. The proton-type ZSM-5 was immersed in a metal salt aqueous solution with a supported metal weight at room temperature overnight. The resultant was evaporated at 333 K, dried at 393 K for 3 h, and calcined at 823 K for 3 h.

### 2.2.2. Catalytic reaction test

A pressurized flow type of reaction apparatus with a fixed-bed reactor was used for this study. The experimental set-up scheme is shown in Fig. 2.1. The apparatus was equipped with an electronic temperature controller for a furnace, a vaporizer of a solvent, a stainless tubular reactor with an inner diameter of 6 mm, thermal mass flow controllers for gas flows and a back-pressure regulator. A solvent was pumped into the reactor by a high-pressure pump. 1 g of a hybrid catalyst was loaded in the reactor, and inert glass sand was placed above and below the catalyst. The length of the catalyst bed was about 6.0 - 6.5 cm. The catalyst was reduced in a flow of a mixture of 5% hydrogen and 95% nitrogen with 100 mL $min^{-1}$ at 573 K for 3 h. After the reduction of the

catalyst, the catalyst was cooled down to 473 K. Syngas (60% $H_2$, 32% CO, 5% $CO_2$, and 3% Ar) and *n*-pentane, *n*-hexane or *n*-heptane as a solvent were introduced into the catalyst to make the total pressure inside reach to 4.0 MPa in a He flow, and then the catalyst was heated up to 553 K. The partial pressure of syngas, $P_{syngas}$, of 2.5 MPa was retained, and the partial pressure of *n*-hexane, $P_{n\text{-hexane}}$, was varied from 0 MPa to 1.5 MPa. The catalyst weight to the flow rate ratio (W/F-syngas) was 9.7 $g_{\text{-cat}}$ h/$mol_{\text{-syngas}}$. CO, $CO_2$ and $CH_4$ of the reaction products were analyzed with an on-line gas chromatograph (Shimadzu GC-8A) equipped with a thermal conductivity detector (TCD) and a packed column of activated charcoal. The light hydrocarbon products were analyzed with another on-line gas chromatograph (Shimadzu GC-2014) equipped with a flame ionization detector (FID) and a capillary column of Porapak-Q. The products liquefied by condensation at room temperature were analyzed with an off-line gas chromatograph (Shimadzu GC-2014) equipped with an FID detector and a capillary column of TC-1. For the analyses of the liquefied products, decahydronaphthalene ($C_{10}H_{18}$) was used as an internal standard.

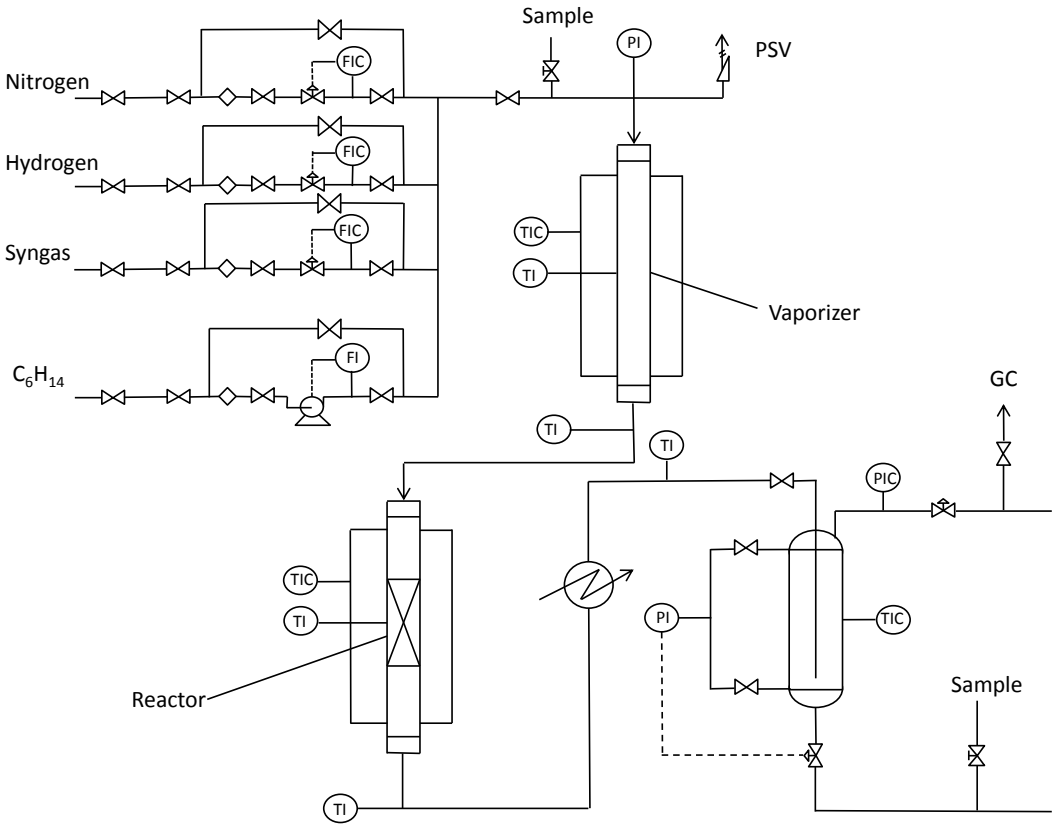


FIC, flow indicator and controller

PIC, pressure indicator and controller

TIC, temperature indicator

PI, pressure indicator

TI, temperature indicator

GC, gas chromatograph

Fig. 2.1. Scheme of experimental set-up.

2.2.3. Calculation method

The conversion of CO was defined as

$$\text{CO conversion (\%)} = \left(1 - \frac{\text{CO out (mol)}}{\text{CO in feed (mol)}}\right) \times 100$$

The yield of C-containing products was defined based on the atomic carbon. The yield of $CO_2$ was defined as

$$CO_2 \text{ yield (C-\%)} = \frac{CO_2 \text{ (mol)}}{\text{CO in feed (mol)}} \times 100$$

The yield of DME was defined as

$$\text{DME yield (C-\%)} = \frac{\text{DME (mol)} \times 2}{\text{CO in feed (mol)}} \times 100$$

The yield of hydrocarbon was defined as

$$C_n \text{ yield (C-\%)} = \frac{C_n \text{ (mol)} \times n}{CO \text{ in feed (mol)}} \times 100$$

## 2.3. Results and discussion

### 2.3.1 The performances of the hybrid catalysts in different reaction phases

In order to compare the performances of the hybrid catalysts in two-phase reaction systems including a near-critical fluid of hexane to that in gas phase system, a series of experiments were conducted. The hybrid catalysts were composed of Cu-ZnO and 0.5 wt% Pd/ZSM-5 according to the weight ratio of 1/1. Pd/ZSM-5 was the MFI zeolite with a ratio of 23 (silica to alumina) containing 0.5 wt% Pd. Fig. 2.2 shows product yields resulting from the syngas conversion over the hybrid catalyst. The partial pressure of *n*-hexane was varied from 0 MPa to 1.5 MPa with the syngas partial pressure of 2.5 MPa constant. The critical pressure and critical temperature of *n*-hexane are 507.5 K and 3.01 MPa, respectively. The total pressure in the reaction system of 4.0 MPa was kept with He as a carrier gas during the reaction. CO conversion decreased from ca. 90% to ca. 74% as the partial pressure of *n*-hexane increased from 0 to 1.5 MPa. The employment of supercritical fluids resulted in decreasing CO conversion in the FT synthesis due to lower diffusion efficiency of syngas compared with that in gas phase [34, 36, 37]. It is indicated that the near-critical fluid also suppressed the diffusion of syngas during the reaction to decrease the CO conversion in this study. Hydrocarbon yield was drastically increased by co-feeding n-hexane with syngas to the catalyst, and increased from ca. 29% to ca. 54% with the increase in the partial pressure of n-hexane from 0 to 1.5 MPa. Hydrocarbon distributions at 6.5 h after the reaction started are shown in Fig. 2.3. By employing the near-critical fluid ($P_{n\text{-hexane}}$ = 1.5 MPa), hydrocarbons with carbon numbers of 5 - 9 were efficiently produced, while the selectivities of ethane and propane decreased. In contrast to the hydrocarbon yield,

DME yield was decreased from 33% to 0.8% by the employment of the near-critical solvent. In order to compare the catalytic properties of the hybrid catalyst in the near-critical fluid with those in a supercritical fluid, the partial pressure of *n*-hexane was increased to 3.0 MPa, while the partial pressure of syngas was decreased to 1.0 MPa to keep the total pressure at 4.0 MPa. Surprisingly, DME and $CO_2$ were little detected, and hydrocarbons were dominantly produced although the CO conversion decreased due to the decrease in the partial pressure of syngas. The employment of *n*-hexane as the near-critical solvent improves the heat transfer during the reaction, leading to the increase in the LPG yield through the conversion of methanol [21]. It is suggested that the introduction of *n*-hexane as the near-critical solvent improved the conversion of DME to hydrocarbons due to the effect on desorption and good heat transfer in the near-critical phase. Supercritical fluids have unique properties such as superior solubility and transfer characteristics due to gas-like viscosity and diffusivity as well as liquid-like density, which make them attractive for chemical reactions. It is indicated that the near-critical reaction system suppressed the formation of liquid layer of hydrocarbons on the surfaces of zeolite due to desorption effect so that the polymerization reaction of DME was improved. Also, introduction of *n*-hexane as heat-carrier solvent will help the removal of reaction heat from catalysts in the near-critical phase. The model of desorption effect during the reduction is shown in Fig. 2.4.

The yield of $CO_2$ decreased with increasing the partial pressure of *n*-hexane. $CO_2$ is generated through the water-gas shift (WGS) reaction of CO with $H_2O$ over Cu-ZnO. Supercritical fluids in the FT processes extracts $H_2O$ generated during the reaction from the catalyst, while the extraction capability of the fluids to $H_2O$ is proportional to the

partial pressure of the fluids due to low affinity of $H_2O$ to organic solvents [33, 38]. It is thus suggested that the near-critical fluid helped the emission of $H_2O$ from the surfaces of the catalyst, leading to the suppression of the WGS reaction over Cu-ZnO. Considering the use of high-pressure equipment (supercritical system), it generally costs much to set up apparatuses which can be safely operated under sever conditions. Thus, processes with the near-critical *n*-hexane fluid are expected to be economical due to easier handling of apparatuses for the selective production of gasoline-range hydrocarbons from syngas via methanol using hybrid catalysts.

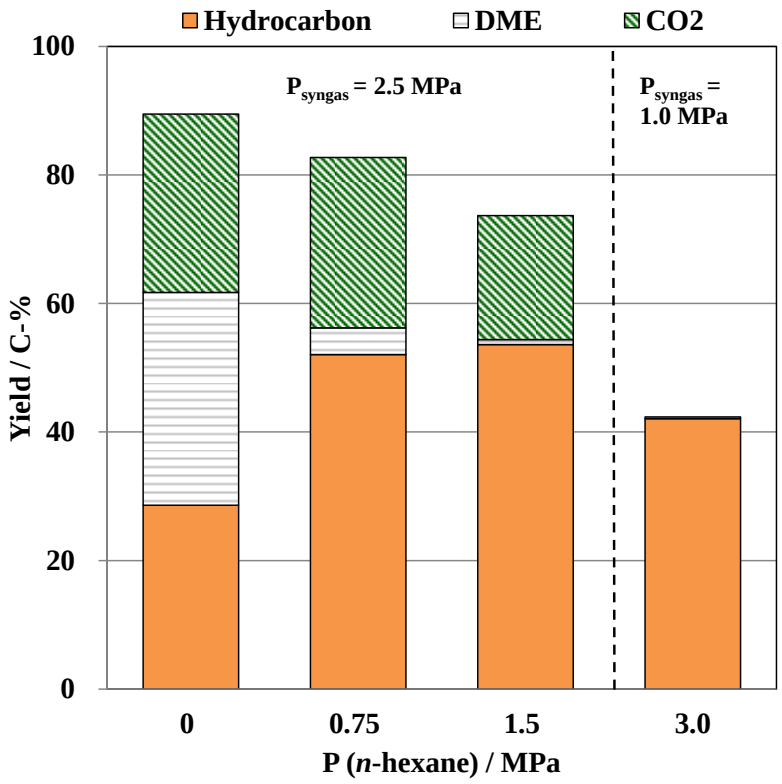


Fig. 2.2. Product yield resulting from conversion of syngas to hydrocarbons over hybrid catalyst composed of Cu-ZnO and 0.5 wt% Pd/ZSM-5 as a function of partial pressure of *n*-hexane. Reaction conditions: cat., 1.0 g hybrid catalyst (0.5 g Cu-ZnO and 0.5 g Pd/ZSM-5); temp., 553 K; $P_{total}$ = 4.0 MPa (balanced by He); $P_{syngas}$ = 2.5 MPa or 1.0 MPa; W/F = 9.7 $g_{\text{-cat}}$ h/$mol_{\text{-syngas}}$; $H_2/CO$ = 1.9.

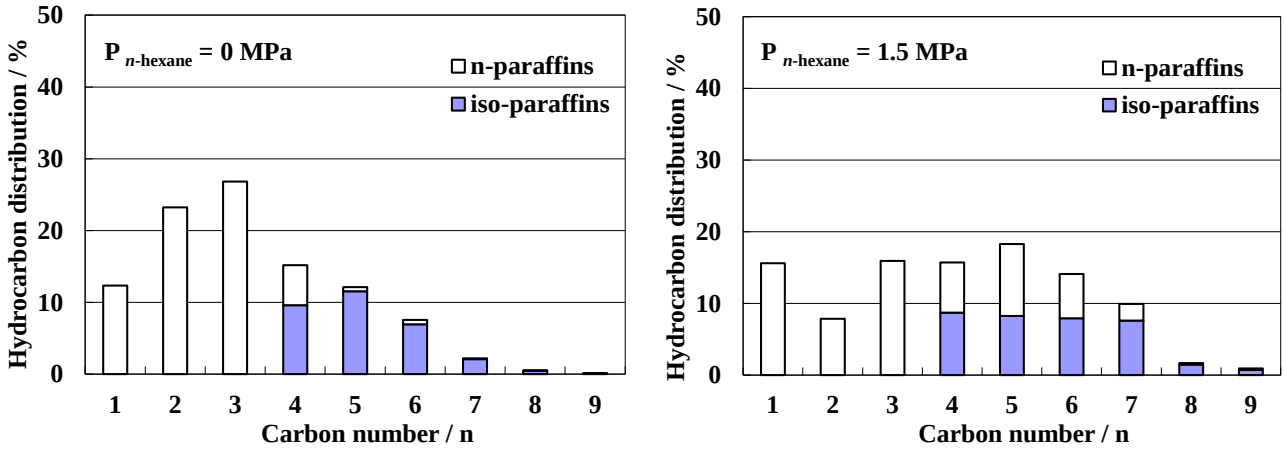


Fig. 2.3. Hydrocarbon distributions resulting from conversion of syngas to hydrocarbons over hybrid catalyst composed of Cu-ZnO and 0.5 wt% Pd/ZSM-5. Reaction conditions: cat., 1.0 g hybrid catalyst (0.5 g Cu-ZnO and 0.5 g Pd/ZSM-5); temp., 553 K; $P_{total}$ = 4.0 MPa (balanced by He); $P_{syngas}$ = 2.5 MPa; W/F = 9.7 $g_{-cat}$ h/$mol_{-syngas}$; $H_2$/CO = 1.9.

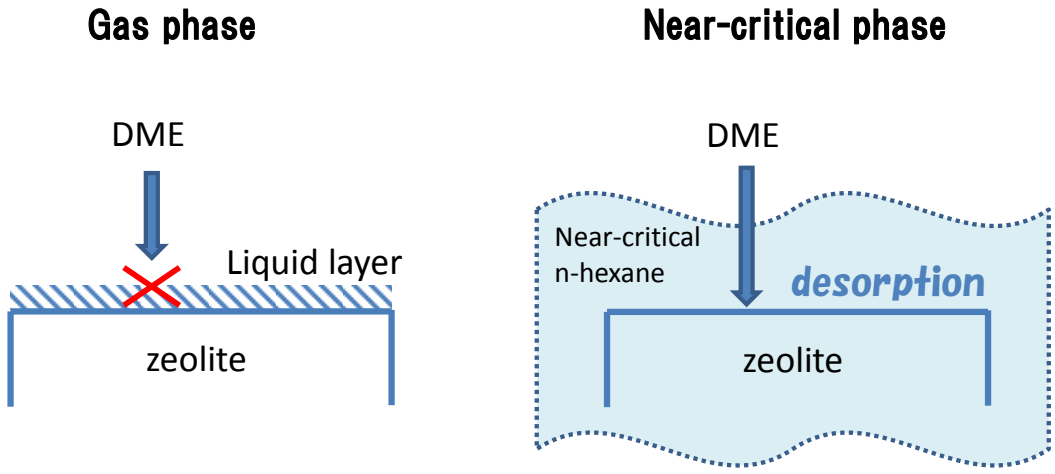


Fig. 2.4. The model of desorption effect during the reduction in near-critical phase

### 2.3.2 Influence of solvent species used in near-critical phase

The influence of solvent species used in near-critical phase during the conversion of syngas to hydrocarbons via methanol was investigated. Three kinds of solvents: *n*-pentane, *n*-hexane and *n*-heptane were chosen as the solvent. The catalyst used was a hybrid catalyst composed of Cu-ZnO and 0.5 wt% Pd/*ns* $Al_2O_3$/ZSM-5. The total pressure in the reaction system was 4.0 MPa while the partial pressure of solvent was 1.5 MPa constant. Fig. 2.5 shows product yields resulting from the syngas conversion over the hybrid catalyst. *N*-pentane, *n*-hexane and *n*-heptane have a critical temperature of 469.4 K, 507.5 K and 540.2 K, and critical pressure of 3.37 MPa, 3.01 MPa and 2.74 MPa, respectively. Reaction temperature and pressure are close to critical condition of these three kinds of solvent. The production of undesirable product $CO_2$ and the intermediate product DME reduced under the near-critical fluid reaction system. Pentane or heptane instead of hexane in reaction system gave similar results in CO conversion and $CO_2$ selectivity. Hexane and heptane have slight higher yield of hydrocarbons than pentane, because closer to the critical point at this reaction condition. All these three kinds of solvent might be suitable for the near-critical fluid reaction system. Actually in commercial use of this process, the solvent will be the components of liquid products without separation. A small quantity of solvent in recycling will increase the selectivity of gasoline-range hydrocarbons in reaction. The amount of product generated from decomposition of solvent would be eliminated in experimental data by the method of internal standard in analysis.

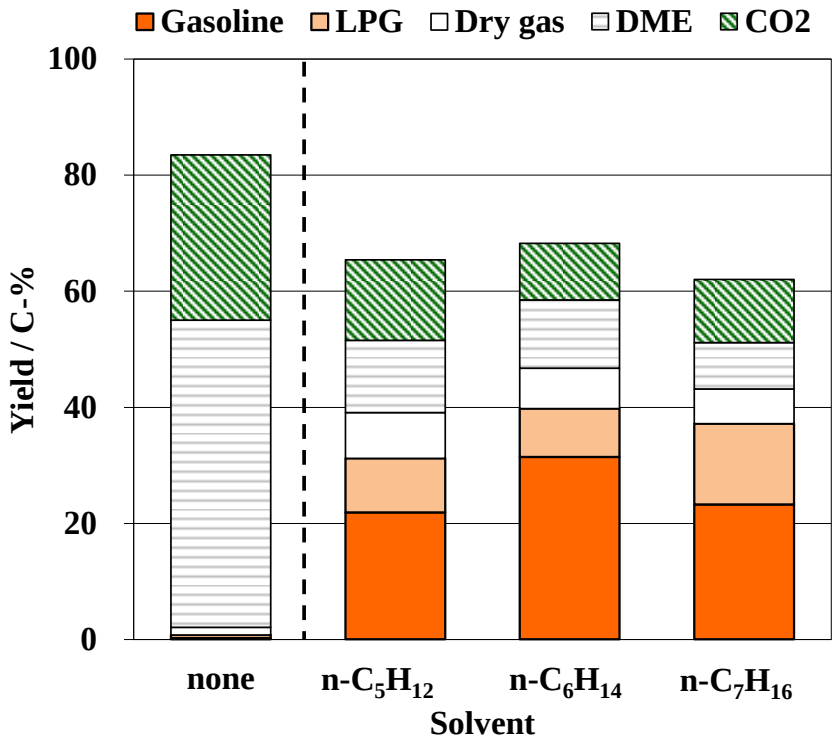


Fig. 2.5. Product yield resulting from conversion of syngas to hydrocarbons over hybrid catalyst composed of Cu-ZnO and 0.5 wt% Pd/*ns* $Al_2O_3$/ZSM-5 as a function of solvent species. Reaction conditions: cat., 1.0 g hybrid catalyst (0.5 g Cu-ZnO and 0.5 g Pd/*ns* $Al_2O_3$/ZSM-5); temp., 553 K; $P_{total}$ = 4.0 MPa; $P_{syngas}$ = 2.5 MPa; W/F = 9.7 $g_{\text{-cat}}$ h/$mol_{\text{-syngas}}$; $H_2$/CO = 1.9.

### 2.3.3 Effect of reaction pressure

Introduction the near-critical solvent in the system could effectively suppress $CO_2$ selectivity and promote the generation of hydrocarbons. However, due to the solvent existing in the reaction process, the partial pressure of syngas will decrease and affect reaction performance. The effect of total reaction pressure on conversion of syngas to hydrocarbons via methanol in near-critical phase was investigated. The catalyst used was a hybrid catalyst composed of Cu-ZnO and 0.5 wt% Pd/*ns* $Al_2O_3$/ZSM-5. The total pressure in the reaction system was varied from 2.0 MPa to 4.0 MPa with the ratio of syngas partial pressure to *n*-hexane partial pressure of 1.67 kept constant. Fig. 2.6 shows product yields resulting from the syngas conversion over the hybrid catalyst. *N*-hexane has a critical temperature of 507.5 K and critical pressure of 3.01 MPa. High total pressure showed a high CO conversion and high products yield. CO conversion increased from ca. 46% to ca. 68% as the total pressure increased from 2.0 to 4.0 MPa. The yield of $CO_2$ was 9.8% at the total pressure of 4.0 MPa with *n*-hexane partial pressure of 1.5 MPa. High pressure requires complex facilities and high power consumption. Therefore, lower reaction pressure favored the utilization of this technology.

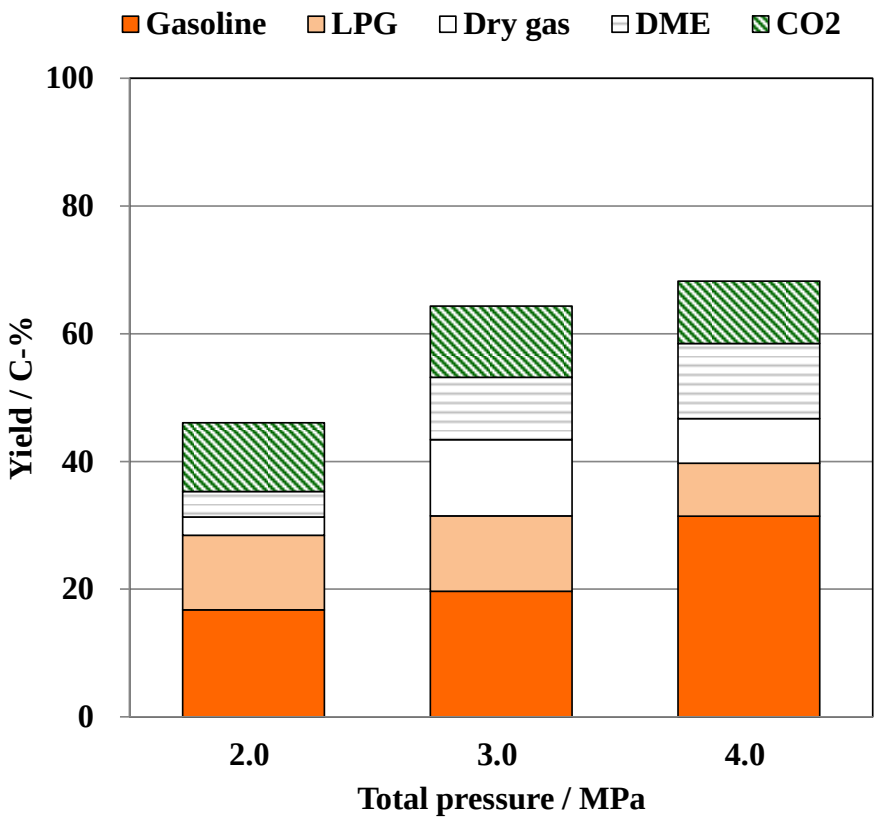


Fig. 2.6. The pressure effect on the performance of conversion syngas to hydrocarbons over hybrid catalyst composed of Cu-ZnO and 0.5 wt% Pd/*ns* $Al_2O_3$/ZSM-5. Reaction conditions: cat., 1.0 g hybrid catalyst (0.5 g Cu-ZnO and 0.5 g Pd/*ns* $Al_2O_3$/ZSM-5); temp., 553 K; $P_{total}$ = 2.0 - 4.0 MPa; $P_{syngas}$ / $P_{n\text{-}hexane}$ = 1.67; W/F = 9.7 $g_{\text{-}cat}$ h/$mol_{\text{-}syngas}$; $H_2$/CO = 1.9.

### 2.3.4 Stability of hybrid catalysts in a near-critical and gas phases

As shown in Fig. 2.7, in the conversion of syngas to hydrocarbons in the near-critical phase of *n*-hexane, the hybrid catalyst consisting of Cu-ZnO and 0.5 wt% Pd/ZSM-5 exhibited the higher CO conversion with the lower selectivity of $CO_2$ in comparison with the reaction in the gas phase under the conditions at 553 K and 4.0 MPa. The CO conversion of ca. 65% was kept until 30 h of the reaction in the near-critical phase. Similar to the reaction in the near-critical phase, in the gas phase, the CO conversion was kept with a constant value of 58% during the reaction although the $CO_2$ selectivity slightly increased at the initial stage of the reaction.

The deactivation of the catalyst can be mitigated through better heat and mass transfer, leading to prolonging the longevity of catalyst. Owing to the advantages mentioned above, the reaction system with a hybrid catalyst consisting of Cu-ZnO and Pd/ZSM-5 in a near-critical phase is promising for commercial application of the synthesis of gasoline fraction hydrocarbons from syngas.

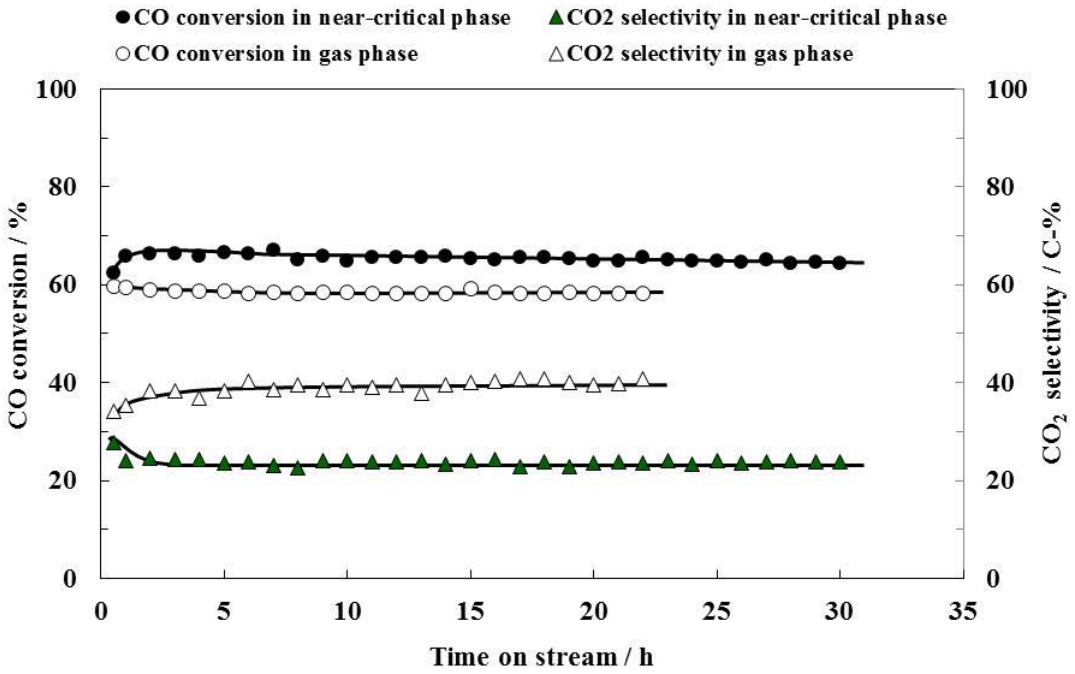


Fig. 2.7. Conversion of syngas to hydrocarbons over the hybrid catalyst consisting of Cu-ZnO and 0.5 wt% Pd/ZSM-5. Reaction conditions: cat., 1.0 g hybrid catalyst (0.5 g Cu-ZnO and 0.5 g Pd/ZSM-5); temp., 553 K; W/F = 9.7 $g_{\text{-cat}}$ h/$mol_{\text{-syngas}}$; $H_2/CO$ = 1.9; $P_{\text{syngas}}/P_{n\text{-hexane}}$ = 2.5 MPa/0 MPa (gas phase); $P_{\text{syngas}}/P_{n\text{-hexane}}$ = 2.5 MPa/1.5 MPa (near-critical phase).

## 2.4. Conclusions

The catalytic performances of hybrid catalysts composed of Cu-ZnO and Pd/ZSM-5 in the syngas conversion to hydrocarbons via methanol in a near-critical *n*-hexane solvent have been studied. The near-critical fluid was effective in the selective production of hydrocarbons in gasoline fraction during the syngas conversion over the hybrid catalyst. In addition, the employment of the near-critical solvent led to depressing the formation of $CO_2$ during the reaction.

References

[1] M. F. Chang, L. Evans, R. Herman, P. Wasielewski, 1976. Gasoline Consumption in Urban Traffic. Transportation Research Record.

[2] C. Wang, D. Zhang, C Fang, Q. Ge, H. Xu, Fuel 134 (2014) 11–16

[3] R. B. Anderson, Fischer–Tropsch Synthesis, Academic Press, New York, 1984.

[4] M. E. Dry, Appl. Catal. A: Gen. 276 (2004) 1–3.

[5] B. H. Davis, Ind. Eng. Chem. Res. 46 (2007) 8938–8945.

[6] H. Schulz, in: B. H. Davis, M.L. Occelli (Eds.), Fischer–Tropsch Synthesis and Hydroformylation on Cobalt Catalysts, CRC Press/Taylor and Francis Group, Boca Raton/London/New York, 2010, pp. 165–183.

[7] L. Shi, Y. Jin, C. Xing, C. Zeng, T. Kawabata, K. Imai, K. Matsuda, Y. Tan, N. Tsubaki, Appl. Catal. A: Gen. 435-436 (2012) 217–224.

[8] B. Todic, T. Bhatelia, G.F. Froment, W. Ma, G. Jacobs, B.H. Davis, D.B. Bukur, Ind. Eng. Chem. Res. 52 (2013) 669–679.

[9] N. E. Tsakoumis, R. Dehghan, R. E. Johnsen, A. Voronov, W. van Beek, J. C. Walmsley, Ø. Borg, E. Rytter, D. Chen, M. Rønning, A. Holmen, Catal. Today 205 (2013) 86–93.

[10] Aghamohammadi, S., Haghighi, M., Chem. Eng. J. 264, (2015) 359–375.

[11] F. Yaripour, Z. Shariatinia, S. Sahebdelfar, A. Irandoukht, Microporous Mesoporous Mater. 203 (2015) 41–53.

[12] Olsbye U, Svelle S, Bjorgen M, Beato P, Janssens TVW, Joensen F, Angew Chem-Int Ed 51(2012) 5810–5831.

[13] M. Stöcker, Microporous Mesoporous Mater. 29 (1999) 3–48.

[14] M. Stöcker, Microporous Mesoporous Mater. 82 (2005) 257–292.

[15] T. Mokrani, M. Scurrell, Catal. Rev. 51 (2009) 1–145.

[16] Y. Li, T. Wang, C. Wu, H. Li, X. Qin, N. Tsubaki, Fuel Processing Technology 91 (2010) 388–393.

[17] Y. Yoneyama, J. He, Y. Morii, S. Azuma, N. Tsubaki, Catalysis Today 104 (2005) 37–40.

[18] P. Mohanty, K.K. Pant, J. Parikh, D.K. Sharma, Fuel Processing Technology 92 (2011) 600–608.

[19] F. G. Botes, W. Böhringer, Applied Catalysis A: General 267 (2004) 217–225.

[20] X. Huang, B. Hou, J.Wang, D. Li, L. Jia, J. Chen, Y. Sun, Applied Catalysis A: General 408 (2011) 38–46.

[21] Q. Zhang, P. Liu, Y. Fujiyama, C. Chen, X.H. Li, Appl. Catal. A: Gen. 401 (2011) 147–152.

[22] M.G. Hiltzler, M. Poliakoff, Chem. Commun. (1997) 1667–1668.

[23] A. Baiker, Chem. Rev. 99 (1999) 453–473.

[24] P.G. Jessop, W. Leitner (Eds.), Chemical Synthesis Using Supercritical Fluids, Wiley, New York, 1999.

[25] C.V. Rode, U.D. Joshi, O. Sato, M. Shirai, Chem. Commun. 9 (2003) 1960–1961.

[26] Y. Matsumura, T. Minowa, B. Potic, S.R.A. Kersten, W. Prins, W.P.M. van Swaaij, B. van de Beld, D.C. Elliott, G.G. Neuenschwander, A. Kruse, M.J. Antal Jr., Biomass Bioenergy 29 (2005) 269–292.

[27] A.A. Peterson, F. Vogel, R.P. Lachance, M. Fröling, M.J. Antal Jr., J.W. Tester, Energy Environ. Sci. 1 (2008) 32–65.

[28] D.C. Elliott, Biofuels Bioprod. Biorefining 2 (2008) 254–265.

[29] A. Yamaguchi, N. Hiyoshi, O. Sato, M. Shirai, Green Chem. 13 (2011) 873–881.

[30] E. Markocic, B. Kramberger, J.G. Van Bennekom, H. Jan Heeres, J. Vos, Z. Knez, Renew. Sustain. Energy Rev. 23 (2013) 40–48.

[31] N. Tsubaki, K. Yoshii, K. Fujimoto, J. Catal. 207 (2002) 371–375.

[32] W. Linghu, X. Li, K. Asami, K. Fujimoto, Fuel Process. Technol. 85 (2004) 1121–1138.

[33] R.M. Malek Abbaslou, J.S. Soltan Mohammadzadeh, A.K. Dalai, Fuel Process. Technol. 90 (2009) 849–856.

[34] A.K. Mogalicherla, N.O. Elbashir, Energy Fuels 25 (2011) 878–889.

[35] E.E. Elmalik, E. Tora, M. El-Halwagi, N.O. Elbashir, Fuel Process. Technol. 92 (2011) 1525–1530.

[36] Q. Zhang, X. Li, K. Asami, S. Asaoka, K. Fujimoto, Fuel Process. Technol. 85 (2004) 1139–1150.

[37] A.K. Mogalicherla, E.E. Elmalik, N.O. Elbashir, Chem. Eng. Process.: Process Intensification 62 (2012) 59–68.

[38] K. Yokota, Y. Hanaoka, K. Fujimoto, Fuel 70 (1991) 989–994.

CHAPTER THREE

# THE DEVELOPMENT OF HYBRID CATALYST CONSISTING OF Cu-ZnO AND METAL-LOADED ZSM-5 FOR SELECTIVE SYNTHESIS OF GASOLINE FROM SYNGAS VIA METHANOL SYNTHESIS


## Abstract

The conversion of syngas (CO + $H_2$) to hydrocarbons in gasoline fraction over a hybrid catalyst composed of Cu-ZnO and Pd/ZSM-5 in a near-critical *n*-hexane solvent was investigated. Methanol was synthesized from syngas over Cu-ZnO; subsequently, was converted to hydrocarbons through the formation of dimethyl ether (DME) over Pd/ZSM-5. A decrease in the particle size of ZSM-5 as well as an increase in a Pd loading led to the selective production of hydrocarbons in the gasoline fraction. The hybrid catalyst containing 0.5 wt% Pd/ZSM-5 with ca. 100 nm in size exhibited 51% gasoline fraction yield with 75% CO conversion. The catalyst stability was also improved by increasing the Pd loading during the reaction. When 0.5 wt% Pd/ZSM-5 and 5 wt% Cu/ZSM-5 among the metal-loaded ZSM-5 catalysts with Pd, Co, Fe or Cu were employed as a portion of the hybrid catalyst, the gasoline-ranged hydrocarbons were selectively produced (the gasoline-ranged hydrocarbons in all hydrocarbons: 59% for the hybrid catalyst with Pd/ZSM-5 and 64% for that with Cu/ZSM-5) with a similar CO conversion during the reaction. An increase in the Cu loading on ZSM-5 resulted in increasing the yield of the gasoline-ranged hydrocarbons, and in decreasing the yield of DME. Furthermore, the hybrid catalyst with Cu/ZSM-5 exhibited no deactivation for 30 h of the reaction. It was revealed that a hybrid catalyst containing Cu/ZSM-5 was efficient in the selective synthesis of gasoline-ranged hydrocarbons from syngas via methanol in the near-critical *n*-hexane fluid.

## 3.1 Introduction

Because of a drastic increase in worldwide energy consumption, the development of hydrocarbon production processes with carbon resources alternative to crude oil has been highly desirable. Syngas ($CO + H_2$), which can be produced from a variety of carbon resources such as natural gas, biomass, and coal, has been focused on as a raw material for the production of fuels and chemicals. Syngas can be converted directly to hydrocarbons through the Fischer-Tropsch synthesis (FTS) [1–7]. Another way of uses of syngas is the production of methanol. Methanol can be utilized for the production of hydrocarbons through the methanol-to-hydrocarbons (MTH) reaction using zeolites or zeolite-type catalysts. In the MTH reaction, hydrocarbon distribution is strongly dependent on the micropore size of zeolites, and the production of heavy hydrocarbons such as diesel fraction hydrocarbons are strictly inhibited [8–12]. Thus, a process of the methanol synthesis from syngas following the MTH reaction would be effective on the selective production of light hydrocarbons with the efficient utilization of the alternative carbon resources.

By employing hybrid catalysts composed of a methanol synthesis catalyst, e.g. $Pd/SiO_2$, Cu-ZnO and Cr-ZnO, and a zeolite catalyst, e.g. ultra-stable Y zeolite (USY) and beta zeolite, the direct synthesis of light hydrocarbons in liquefied petroleum gas (LPG) fraction from syngas has been developed [13–17]. In these LPG synthesis processes, syngas can be primarily converted to methanol over the metal-based catalyst. Subsequent conversion of methanol to hydrocarbons readily takes place over the zeolite which neighbors the metal-based catalyst in the hybrid catalyst. The rapid consumption of methanol gives the methanol synthesis from syngas an advantage over the reverse reaction of methanol to syngas over the metal-based catalysts, leading to higher yield of

hydrocarbons than the calculated value based on the thermodynamic equilibrium [13].

ZSM-5, a MFI-type aluminosilicate material, is well known as a zeolite catalyst having the pore size and acid properties suitable for the production of gasoline-range hydrocarbons in the MTH reaction [8–10]. Considering the selective production of specified fuel hydrocarbons, the employment of a hybrid catalyst containing ZSM-5 would be suitable for the hydrocarbon production from syngas. Furthermore, since olefins are primarily produced in the MTH reaction, metal catalysts with high hydrogenation ability are required for obtaining paraffins as a final product. It was reported that Pd supported on zeolite efficiently converts olefins to paraffins during the conversion of syngas to hydrocarbons [15]. Thus, Pd/ZSM-5 is expected to efficiently produce paraffins in gasoline fraction from methanol that is generated from syngas.

It has been accepted that loading metal species on zeolite not only provides a metal-acid bifunction for a catalyst but induces synergetic effects due to interactions between metal species and acid sites of zeolite. Conte et al. have reported that in the methanol conversion, the selectivity to aromatic compounds was improved by loading metal species on ZSM-5 due to the interaction of acid sites of zeolite with basic sites of metal oxide [18]. The interaction of metal species with acid sites of zeolite involves changes in acid properties of the zeolite as well. The acid strength of ZSM-5 was weakened by the introduction of transition metal species on the surface of ZSM-5, leading to inhibiting undesirable reactions such as the cracking of hydrocarbon products [19]. Furthermore, it has been proposed that hydrogen dissociated on metal species moves onto the surface of a zeolite support to generate active sites [20, 21]. The synergetic effects are strongly dependent on loaded metal species. Thus, it occurs to us to apply metal-loaded ZSM-5 catalysts to the development of a hybrid catalyst for the

selective synthesis of gasoline-ranged hydrocarbons from syngas.

In this study, we investigated the catalytic activity of hybrid catalysts composed of Cu-ZnO and metal-loaded ZSM-5 in a near-critical *n*-hexane solvent in the conversion of syngas to hydrocarbons via methanol. Since low-cost sources are desirable for the preparation of catalysts, copper, cobalt and iron, which are non-precious metals, were employed for the preparation of metal-loaded ZSM-5 to compare their catalytic properties with those of Pd/ZSM-5. We also investigated the effects of the metal loading on the hydrocarbon formation, in particularly gasoline-ranged hydrocarbons yield, as well as the durability during the reaction.

## 3.2 Experimental

### 3.2.1 Catalyst preparation

A hybrid catalyst was prepared by physically mixing the 355-710 μm pellets of a Cu-ZnO methanol synthesis catalyst of 0.5 g with those of a Pd/ZSM-5 catalyst of 0.5 g. Cu-ZnO was a commercial catalyst (MK-121, TOPSØE). Pd/ZSM-5 was prepared by impregnation method with a 4.557 wt% $Pd(NH_3)_2(NO_3)_2$ aqueous solution and commercial ZSM-5 with the $SiO_2/Al_2O_3$ molar ratio of 23 (CBV2314, Zeolyst) or 80 (CBV8014, Zeolyst). $Fe(NO_3)_2 \cdot 9H_2O$, $Co(NO_3)_2 \cdot 6H_2O$ or $Cu(NO_3)_2 \cdot 3H_2O$ were employed for the preparation of each metal salt aqueous solution. Commercial $NH4^+$-type ZSM-5 was calcined at 823 K for 3 h to become proton-type ZSM-5. Proton-type ZSM-5 was immersed in the $Pd(NH_3)_2(NO_3)_2$, $Fe(NO_3)_2 \cdot 9H_2O$, $Co(NO_3)_2 \cdot 6H_2O$ or $Cu(NO_3)_2 \cdot 3H_2O$ aqueous solution with a supported metal weight at room temperature overnight. The proton-type ZSM-5 was immersed in a metal salt aqueous solution with a supported metal weight at room temperature overnight.The resultant was evaporated at 333 K, dried at 393 K for 3 h, and calcined at 823 K for 3 h. In addition, a MFI zeolite was hydrothermally synthesized by using an aluminosilicate gel with the $SiO_2/Al_2O_3$ ratio of 23 and tetrapropylammonium hydroxide (TPAOH) as a structure-directing agent (SDA) at 443 K for 24 h, according to the previous report [22]. The obtained $Na^+$-type MFI zeolite was transformed to a proton-type MFI zeolite by ionexchange treatment with 2.2 M $NH_4NO_3$ aqueous solution followed by calcination at 823 K for 3 h.

### 3.2.2 Characterization

The structure of the catalysts was examined by X-ray diffraction (XRD, Rigaku XRD-DSC-XII). The diffractometer was operated at 40 kV and 20 mA using Cu-Kα radiation source. XRD patterns were recorded at 6 degree/min over the angular range of 5-50°. The $SiO_2/Al_2O_3$ ratios of the samples were determined by X-ray fluorescence analysis (XRF, Rigaku ZSX101E). The BET surface area and micropore volume were estimated from nitrogen adsorption isotherms at 77 K with a Micromeritics ASAP 2010 instrument. Prior to the analyses, the sample was treated at 573 K for 3 h under nitrogen flow in order to remove adsorbed compounds. External surface area ($S_{EXT}$) was estimated by the t-plot method. Field-emission scanning electron microscopic (FE-SEM) images of the catalysts were obtained on an S-5200 microscope (Hitachi) operating at 10-15 kV.

Temperature programmed ammonia desorption ($NH_3$-TPD) profiles were recorded on BELCAT-B (BEL Japan). The sample was pretreated under a He flow at 723 K for 1 h, and then cooled down to 373 K. Ammonia was allowed to make contact with the sample at 373 K for 1 h. Subsequently, the sample was evacuated to remove weakly adsorbed ammonia at 373 K for 30 min. Finally, the sample was heated from 373 K to 883 K at a raising rate of 10 K/min in a He flow. The desorbed ammonia was monitored on a TCD.

Temperature programmed hydrogen desorption ($H_2$-TPD) profiles were recorded on BELCAT-B (BEL Japan). The sample was pretreated under a He flow at 473 K for 5 h, and then reduced under 10 vol% $H_2$ balanced by He at 573 K for 10 h. After cooling down to 323 K, a mixed gas composed of 10 vol% $H_2$ and He balance flowed into the sample for 1 h. Finally, the sample was heated from 323 K to 923 K at raising rate of 10 K/min in a He flow. A mass spectrometer was used to monitor the desorbed hydrogen

(m/e = 2).

3.2.3. Catalytic reaction test

A pressurized flow type of reaction apparatus with a fixed-bed reactor was used for this study. The experimental set-up scheme is shown in Fig. 3.1. The apparatus was equipped with an electronic temperature controller for a furnace, a vaporizer of a solvent, a stainless tubular reactor with an inner diameter of 6 mm, thermal mass flow controllers for gas flows and a back-pressure regulator. A solvent was pumped into the reactor by a high-pressure pump. 1 g of a hybrid catalyst was loaded in the reactor, and inert glass sand was placed above and below the catalyst. The length of the catalyst bed was about 6.0 - 6.5 cm. The catalyst was reduced in a flow of a mixture of 5% hydrogen and 95% nitrogen with 100 mL $min^{-1}$ at 573 K for 3 h. After the reduction of the catalyst, the catalyst was cooled down to 473 K. Syngas (60% $H_2$, 32% CO, 5% $CO_2$, and 3% Ar) and *n*-hexane as a solvent were introduced into the catalyst to make the total pressure inside reach to 4.0 MPa in a He flow, and then the catalyst was heated up to 553 K. The partial pressure of syngas, $P_{syngas}$, of 2.5 MPa was retained, and the partial pressure of *n*-hexane, $P_{n\text{-hexane}}$, was varied from 0 MPa to 1.5 MPa. The catalyst weight to the flow rate ratio ($W/F_{\text{-syngas}}$) was 9.7 $g_{\text{-cat}}$ $h/mol_{\text{-syngas}}$. CO, $CO_2$ and $CH_4$ of the reaction products were analyzed with an on-line gas chromatograph (Shimadzu GC-8A) equipped with a thermal conductivity detector (TCD) and a packed column of activated charcoal. The light hydrocarbon products were analyzed with another on-line gas chromatograph (Shimadzu GC-2014) equipped with a flame ionization detector (FID) and a capillary column of Porapak-Q. The products liquefied by condensation at room

temperature were analyzed with an off-line gas chromatograph (Shimadzu GC-2014) equipped with an FID detector and a capillary column of TC-1. For the analyses of the liquefied products, decahydronaphthalene ($C_{10}H_{18}$) was used as an internal standard.

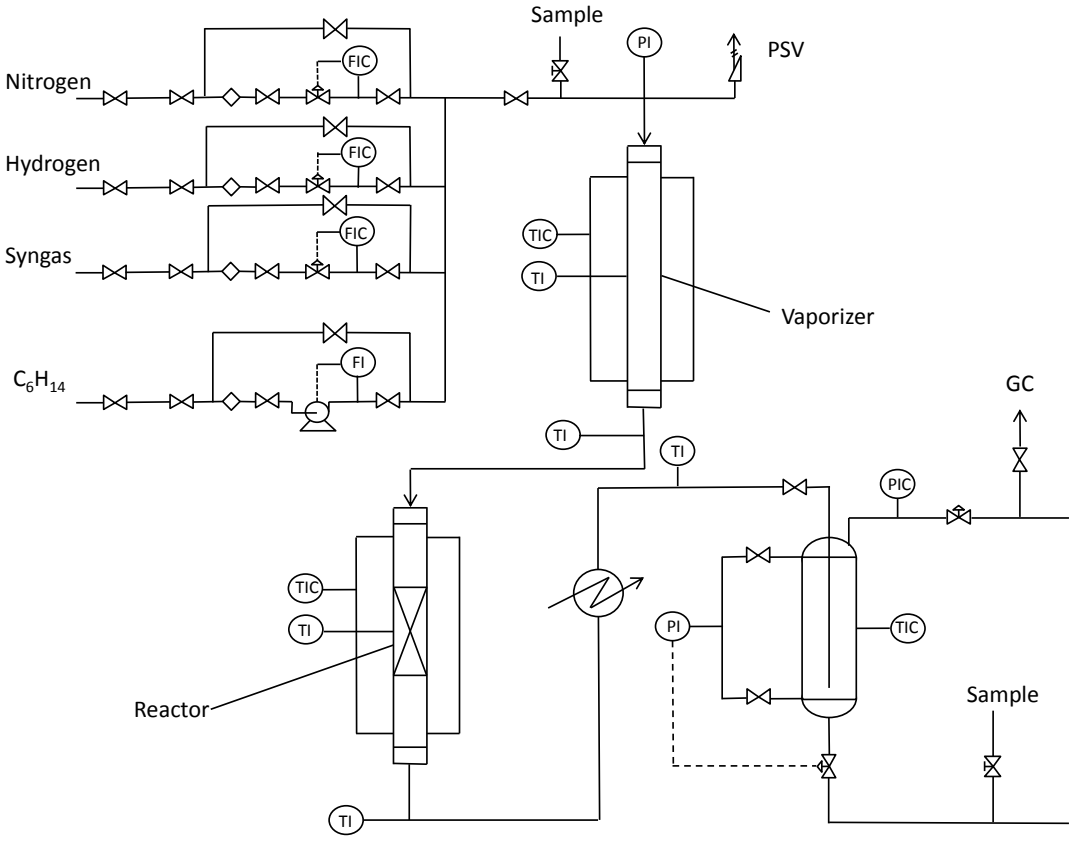


FIC, flow indicator and controller

PIC, pressure indicator and controller

TIC, temperature indicator

PI, pressure indicator

TI, temperature indicator

GC, gas chromatograph

Fig. 3.1. Scheme of experimental set-up.

2.2.4. Calculation method

The conversion of CO was defined as

$$\text{CO conversion (\%)} = \left(1 - \frac{\text{CO out (mol)}}{\text{CO in feed (mol)}}\right) \times 100$$

The yield of C-containing products was defined based on the atomic carbon. The yield of $CO_2$ was defined as

$$CO_2 \text{ yield (C-\%)} = \frac{CO_2 \text{ (mol)}}{\text{CO in feed (mol)}} \times 100$$

The yield of DME was defined as

$$\text{DME yield (C-\%)} = \frac{\text{DME (mol)} \times 2}{\text{CO in feed (mol)}} \times 100$$

The yield of hydrocarbon was defined as

$$C_n \text{ yield (C-\%)} = \frac{C_n \text{ (mol)} \times n}{CO \text{ in feed (mol)}} \times 100$$

## 3.3. Results and discussion

### 3.3.1. Effect of acid amount of ZSM-5 on catalytic activity

Product distribution in the MTH reaction is strongly dependent on physicochemical properties of zeolites including acid amount, pore size and crystal size. In order to investigate the effect of the acid amount of ZSM-5 in the hybrid catalyst on the catalytic properties, the syngas conversion to hydrocarbons was conducted over hybrid catalysts containing ZSM-5 with different $SiO_2/Al_2O_3$ ratios. The results obtained in the reaction are shown in Fig. 3.2. The CO conversion increased with increasing the Al content of ZSM-5. In addition, the increase in the Al content of ZSM-5 increased the yield of the hydrocarbons, while the yield of DME drastically decreased. The trends resulting from the reaction are consistent with those obtained using beta zeolite in the LPG synthesis [23]. Fig. 3.3 shows $NH_3$-TPD profiles of the 0.5 wt% Pd/ZSM-5 catalysts. The peaks which appeared at higher temperature (573 - 873 K) correspond to $NH_3$ desorption from catalytically active acid sites [24, 25]. The acid amount of ZSM-5 was strongly dependent on the Al content of ZSM-5, and the acid amounts estimated from the $NH_3$-TPD profiles were 0.67 mmol $g^{-1}$ and 0.26 mmol $g^{-1}$ for 0.5 wt% Pd/ZSM-5 with the $SiO_2/Al_2O_3$ ratio of 23 and that with the $SiO_2/Al_2O_3$ ratio of 80, respectively. The conversion of methanol or DME to hydrocarbons should depend on the amount of acid sites of zeolite catalysts. The large amount of the acid sites is probably required for the complete conversion of methanol to hydrocarbons via DME at low temperature below 573 K, compared with the MTH reaction carried out at temperatures of 623 - 723 K. Therefore, ZSM-5 with the higher Al content was advantageous to yielding

hydrocarbons from syngas via methanol or DME.

The generation of $CO_2$ was mitigated during the reaction when the Al content of ZSM-5 in the hybrid catalyst decreased (Fig. 3.2). The smaller amount of $H_2O$ could be generated over ZSM-5 with the $SiO_2/Al_2O_3$ ratio of 80 than over ZSM-5 with the $SiO_2/Al_2O_3$ ratio of 23 due to the insufficient conversion of DME to hydrocarbons, resulting in the suppression of the $CO_2$ generation through the WGS reaction.

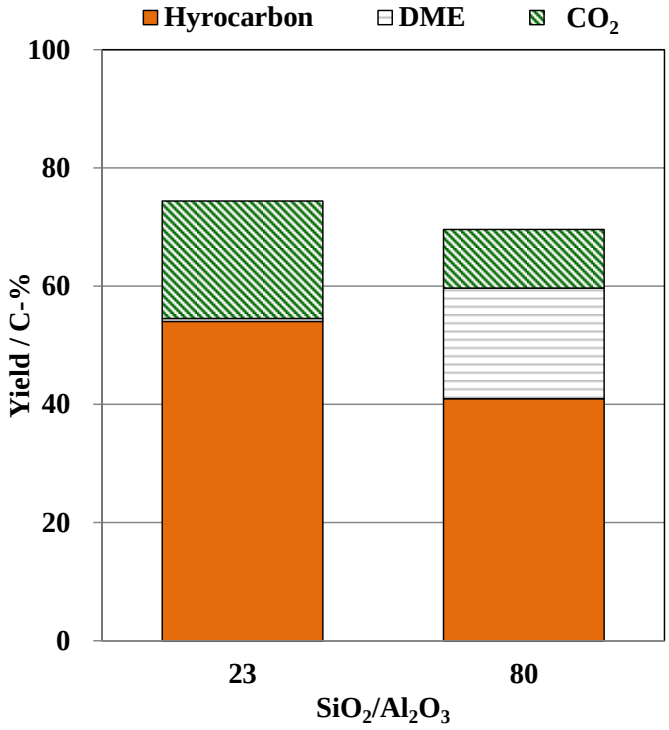


Fig. 3.2. Product yield resulting from conversion of syngas to hydrocarbons over hybrid catalysts composed of Cu-ZnO and 0.5 wt% Pd/ZSM-5 with different $SiO_2/Al_2O_3$ ratios. Reaction conditions: cat., 1.0 g hybrid catalyst (0.5 g Cu-ZnO and 0.5 g Pd/ZSM-5); temp., 553 K; $P_{syngas}$ = 2.5 MPa; $P_{n\text{-hexane}}$ = 1.5 MPa; W/F = 9.7 $g_{\text{-cat}}$ h/$mol_{\text{-syngas}}$; $H_2/CO$ = 1.9.

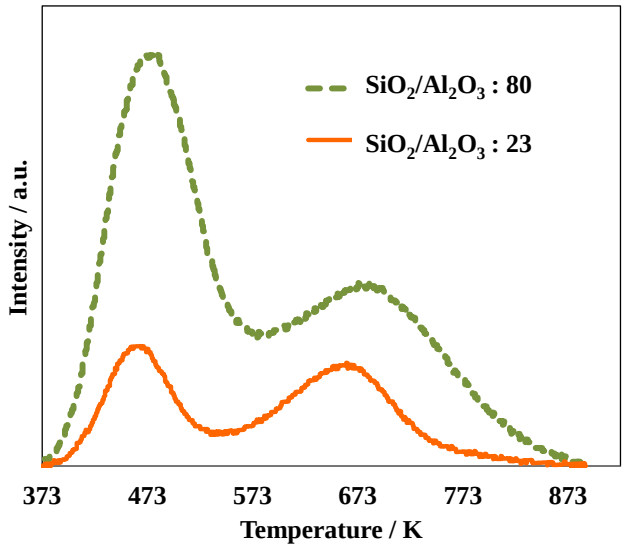


Fig. 3.3. $NH_3$-TPD profiles of 0.5 wt% Pd/ZSM-5 samples with different $SiO_2/Al_2O_3$ ratios.

### 3.3.2. Effect of particle size of ZSM-5 on catalytic activity

The effect of the particle size of Pd/ZSM-5 on the catalytic activity was investigated using ZSM-5 with different particle sizes. Fig. 3.4 shows XRD patterns and SEM images of commercial ZSM-5 (CBV2314, Zeolyst) and hydrothermally synthesized ZSM-5 using tetraorthosilicate as a silica source and TPAOH as an SDA. Both samples exhibited the typical patterns assigned to the MFI structure (Fig. 3.4A). The FE-SEM images revealed that commercial ZSM-5 (ZSM-5-CM) was composed of cuboid blocks with an average size of ca. 600 nm, while hydrothermally synthesized ZSM-5 (ZSM-5-HT) was composed of cubic crystallites about 100 nm in size (Fig. 3.4B). The physicochemical properties of both the ZSM-5 samples are summarized in Table 3.1. The $SiO_2/Al_2O_3$ ratio of 32 for ZSM-5-HT was similar to that of 23 for ZSM-5-CM. The surface area (SBET) of ZSM-5-HT (373 $m^2\ g^{-1}$) was also close to that of ZSM-5-CM (363 $m^2\ g^{-1}$). By contrast, the external surface area (SEXT) of ZSM-5 increased due to a decrease in the particle size.

Table 3.1. Physicochemical properties of commercial and hydrothermal synthesized ZSM-5 catalysts.

| Sample | $SiO_2/Al_2O_3$[a] | Size[b] (nm) | $S_{BET}$[c] ($m^2\ g^{-1}$) | $S_{EXT}$[d] ($m^2\ g^{-1}$) | $V_{micro}$[e] ($cm^3\ g^{-1}$) |
|---|---|---|---|---|---|
| ZSM-5-CM | 23 | 600 | 363 | 54 | 0.13 |
| ZSM-5-HT | 32 | 100 | 373 | 115 | 0.11 |
| ZSM-5-CM | 80 | - | 440 | 183 | 0.13 |

[a] Estimated from XRF measurement.

[b] Average particle size estimated from FE-SEM observations.

[c] $S_{BET}$, surface area estimated by $N_2$ adsorption method.

[d] $S_{EXT}$, external surface area estimated by $N_2$ adsorption method.

[e] $V_{micro}$, micropore volume estimated by $N_2$ adsorption method.

(A)

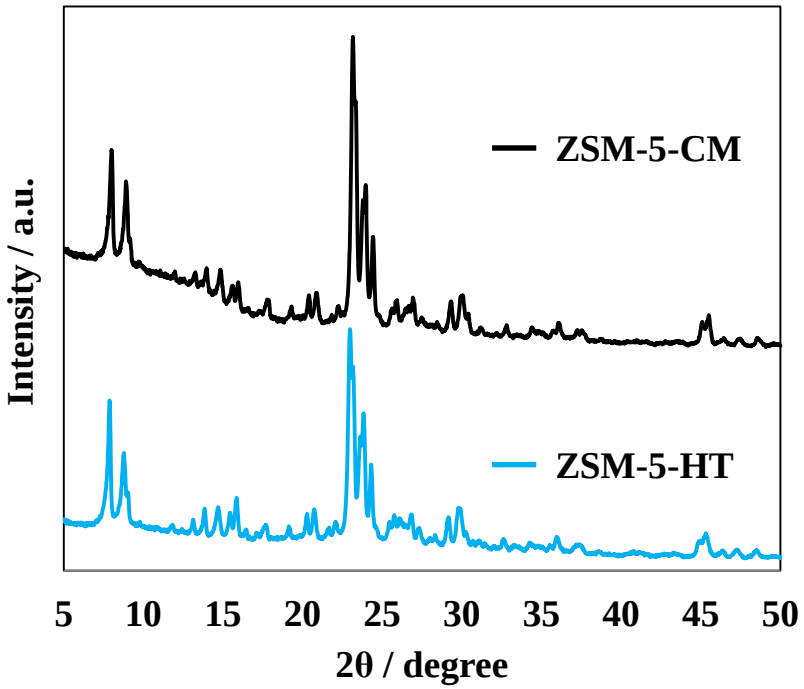


(B)

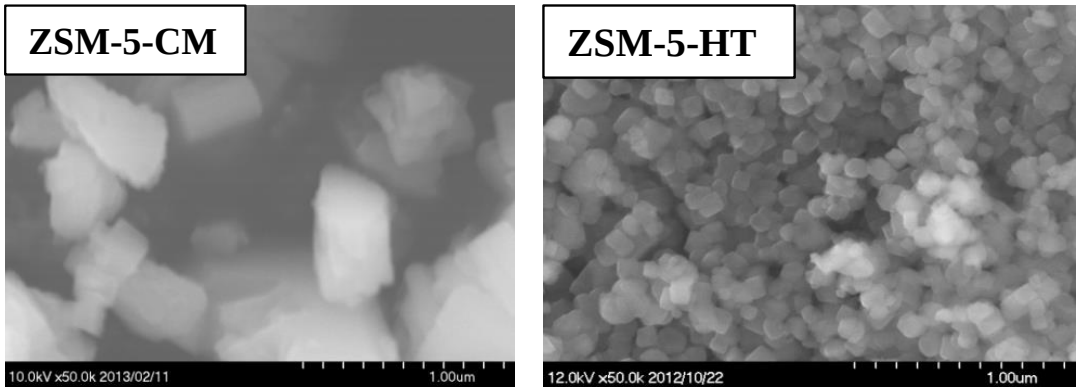


Fig. 3.4. XRD patterns (A) and SEM images (B) of commercial ZSM-5 (CBV2314) (ZSM-5-CM) and hydrothermally synthesized ZSM-5 (ZSM-5-HT).

Fig. 3.5 shows the product yields of ZSM-5-CM and ZSM-5-HT in the syngas conversion to hydrocarbons via methanol. The CO conversion was independent of the particle size of the ZSM-5 sample. In addition, the yields of $CO_2$, DME and the hydrocarbons generated over the hybrid catalyst containing ZSM-5-CM were very similar to those of the hybrid catalyst containing ZSM-5-HT. These results indicate that the particle size of the zeolite influences little the catalytic activity of the zeolite for the methanol conversion to hydrocarbons. By contrast, the product distribution, especially the hydrocarbon distribution, was strongly dependent on the particle size of ZSM-5. Fig. 3.6 shows hydrocarbon distributions over the hybrid catalysts with ZSM-5-CM or ZSM-5-HT at 6.5 h of the reaction time. The selectivity of hydrocarbon fractions ($C_5$ - $C_9$) associated with gasoline increased from 44% to 65% with decreasing the particle size of ZSM-5, while those of methane, ethane and propane decreased with decreasing the particle size. In the MTH reaction, the crystal size of zeolites does not significantly influence the selectivity of various hydrocarbon products. However, a decrease in the crystal size retards the deposition of carbonaceous species in the pores and cavities of zeolites due to the high mass transfer of reactants as well as products, leading to the improvement of the catalyst life [22]. On the other hand, it was reported that the carbonaceous species formed in the cavities of the zeolite induced an effect of transition-state shape selectivity due to the reduction of the pore and cavity spaces, promoting the formation of smaller olefins [26, 27]. ZSM-5-HT composed of smaller particles than those of ZSM-5-CM exhibited the selective production of the hydrocarbons in the gasoline fraction. In ZSM-5-HT, hydrocarbons generated in the pores of the zeolite could more readily transfer out of the pores during the reaction due to the shorter pore channels in comparison with ZSM-5-CM. It is assumed that the

further oligomeration of the products in the pores could be suppressed in ZSM-5-HT, resulting in keeping large cavity spaces. Thus, the efficient transfer of larger hydrocarbons than the LPG and dry gas fractions to out of the pores could take place in ZSM-5-HT. On the other hand, in the cavities of ZSM-5-CM, the transfer of the large hydrocarbons was suppressed by the carbonaceous species deposited, promoting the formation of the small hydrocarbons through the cracking of the large hydrocarbons.

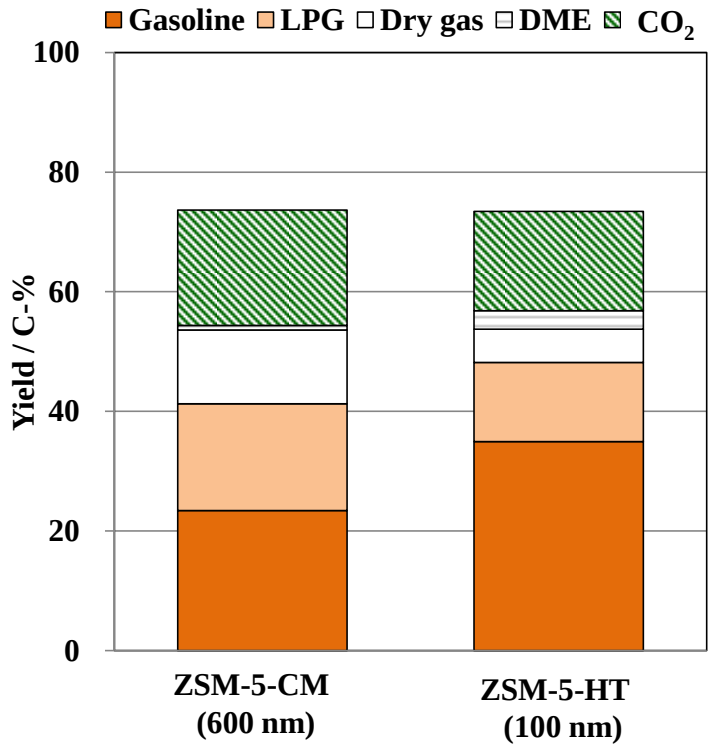


Fig. 3.5. Product yield resulting from conversion of syngas to hydrocarbons over hybrid catalysts composed of Cu-ZnO and 0.5 wt% Pd/ZSM-5 with different particle sizes. Reaction conditions: cat., 1.0 g hybrid catalyst (0.5 g Cu-ZnO and 0.5 g Pd/ZSM-5); temp., 553 K; $P_{syngas}$ = 2.5 MPa; $P_{n\text{-hexane}}$ = 1.5 MPa; W/F = 9.7 $g_{\text{-cat}}$ h/$mol_{\text{-syngas}}$; $H_2$/CO = 1.9.

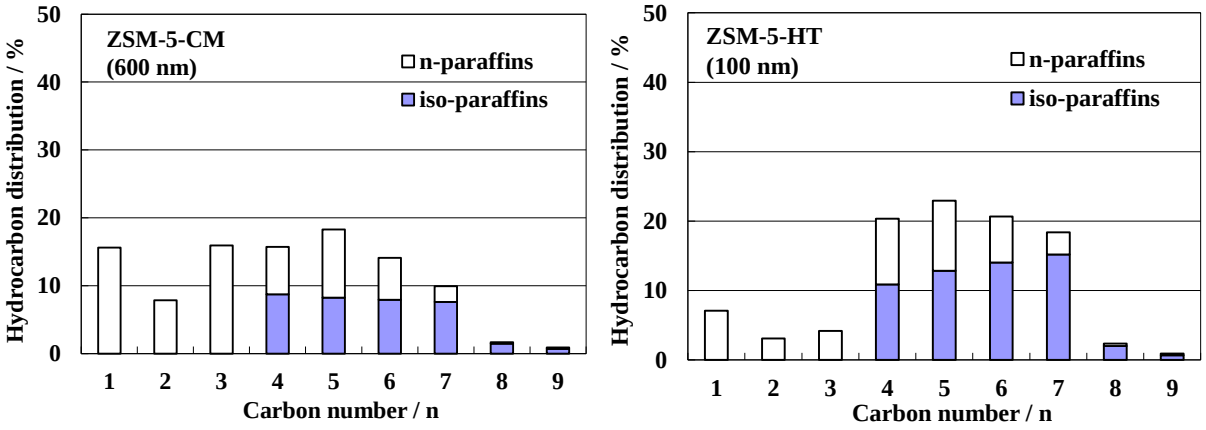


Fig. 3.6. Hydrocarbon distributions resulting from conversion of syngas to hydrocarbons over hybrid catalyst composed of Cu-ZnO and 0.5 wt% Pd/ZSM-5 with different particle sizes. Reaction conditions: cat., 1.0 g hybrid catalyst (0.5 g Cu-ZnO and 0.5 g Pd/ZSM-5); temp., 553 K; $P_{syngas}$ = 2.5 MPa; $P_{n\text{-hexane}}$ = 1.5 MPa; W/F = 9.7 $g_{\text{-cat}}$ h/$mol_{\text{-syngas}}$; $H_2$/CO = 1.9.

### 3.3.3. Effect of mixing way of Cu-ZnO with Pd/ZSM-5 on catalytic properties

In order to investigate the effects of the catalyst preparation method on the catalytic properties, the hybrid catalysts were prepared by two different methods: powder mixing and granule mixing. In the powder mixing, after Cu-ZnO of 0.5 g and Pd/ZSM-5 of 0.5 g were physically mixed with a mortar, the mixed powder was pelletized, crushed, and then sieved to particles with 355 - 710 μm. In order to distinguish the physical mixing method of each pelletized particle of Cu-ZnO and Pd/ZSM-5 described in the experimental section from the powder mixing, the usual preparation method is denoted as granule mixing in Fig. 3.7. The hybrid catalyst prepared by the granule mixing exhibited a slightly higher CO conversion, higher $CO_2$ yield and lower DME yield than that prepared by the powder mixing in the conversion of syngas to hydrocarbons in the near-critical *n*-hexane fluid (Fig. 3.7). In addition, the catalyst prepared by the granule mixing gave the higher yield (ca. 33%) of gasoline fraction hydrocarbons ($C_5$ - $C_9$) than the catalyst prepared by the powder mixing. On the catalyst prepared by the powder mixing, hydrogen dissociated on Cu-ZnO could readily transfer to the neighboring Pd/ZSM-5, resulting in the formation of $CH_4$ through the hydrogenation of CO and $CO_2$ on the Pd particles. Yoshie et al. reported that a hybrid catalyst prepared by the granule mixing showed a high selectivity and activity in the hydrocarbon synthesis from $CO_2$ [28].

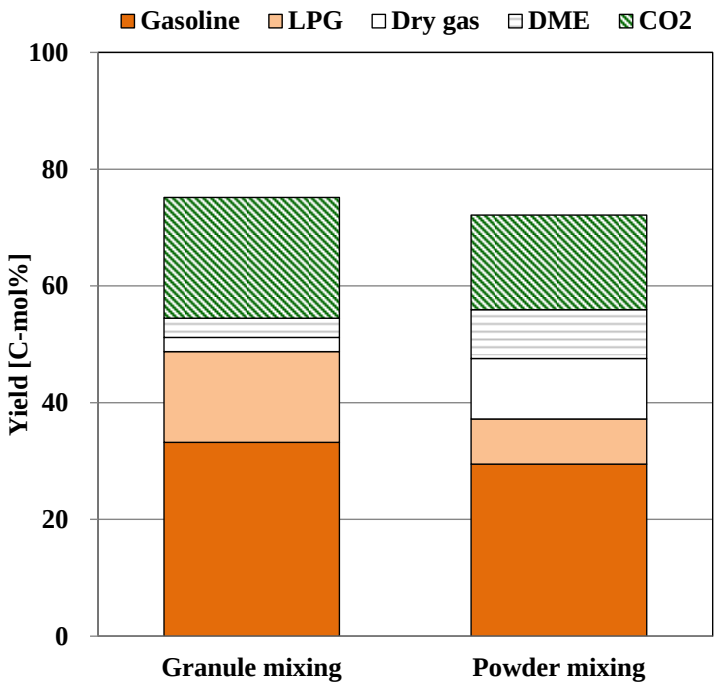


Fig. 3.7. Influence of mixing way of Cu-ZnO with Pd/ZSM-5 on conversion of syngas to hydrocarbons in near-critical phase over hybrid catalysts composed of Cu-ZnO and 0.5 wt% Pd/ZSM-5. Reaction conditions: cat., 1.0 g hybrid catalyst (0.5 g Cu-ZnO and 0.5 g Pd/ZSM-5,); temp., 553 K; $P_{syngas}$ = 2.5 MPa; $P_{n\text{-hexane}}$ = 1.5 MPa; W/F = 9.7 $g_{\text{-cat}}$ h/$mol_{\text{-syngas}}$; $H_2$/CO = 1.9.

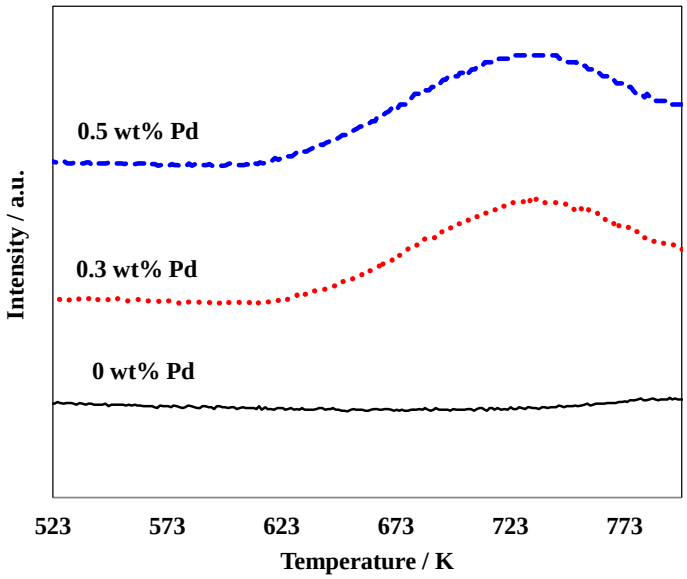


Fig. 3.8. $H_2$-TPD profiles of Pd/ZSM-5-HT samples with different Pd loadings.

### 3.3.4. Effect of palladium loading on ZSM-5 on catalytic properties

Pd on the zeolite plays roles in the efficient hydrogenation of olefins to paraffins in the syngas conversion to hydrocarbons [15]. Since olefins are primarily produced in the methanol conversion to hydrocarbons, Pd is required for the synthesis of saturated hydrocarbons through the hydrogenation. Fig. 3.8 shows $H_2$-TPD profiles of the 0.3 and 0.5 wt% Pd/ZSM-5 samples and the ZSM-5 sample. The adsorption of $H_2$ on ZSM-5 was almost negligible as a result of the observation of no peak derived from desorbed $H_2$ molecules. By contrast, on the Pd/ZSM-5 samples, a broadened peak was observed in the range from 673 K to 773 K, indicating that $H_2$ molecules were adsorbed on only the Pd sites. The amount of the adsorbed $H_2$ was estimated from the profiles to be 0.017 mmol $g^{-1}$ for 0.3 wt% Pd/ZSM-5 and 0.018 mmol $g^{-1}$ for 0.5 wt% Pd/ZSM-5, respectively. Thus, ZSM-5 with the increased Pd loading is capable of preventing the oligomerization of coke precursors through the hydrogenation of the coke precursors to paraffins.

In order to clarify the effects of Pd on the catalytic activity in the syngas conversion, the reaction was carried out employing various Pd loadings on ZSM-5 prepared by the hydrothermal treatment in the hybrid catalyst. The results are shown in Figs. 3.9 and 3.10. The hybrid catalyst containing ZSM-5 exhibited 82% CO conversion at 0.5 h after the reaction started. The CO conversion gradually decreased after the reaction started until the conversion reached to ca. 65% at 4 h of the reaction time. By employing the hybrid catalyst composed of Cu-ZnO and Pd supported on ZSM-5, the deactivation became slow, although the initial CO conversion was almost the same (ca. 80%) regardless of the Pd loadings (Fig. 3.9). The effect of the Pd loadings on the CO

conversion was consistent with that obtained in the LPG synthesis over hybrid catalysts composed of Cu-ZnO and Pd/beta [16]. In addition, the hybrid catalysts containing Pd/ZSM-5 exhibited the higher CO conversion at 6.5 h than that with ZSM-5, while the CO conversion at 6.5 h of 0.3 wt% Pd/ZSM-5. was similar to that of 0.5 wt% Pd/ZSM-5. In the MTH reaction, rapid deactivation occurs due to the deposition of carbonaceous species resulting from the oligomerization of primarily formed unsaturated products on the surface or inside pores of the zeolite [29]. The hydrogenation of the unsaturated products to saturated hydrocarbons over Pd/ZSM-5 would retard the oligomerization to suppress the deactivation.

Fig. 3.10 shows the product yields of the hybrid catalysts containing ZSM-5, 0.3 wt% Pd/ZSM-5 and 0.5 wt% Pd/ZSM-5. The yield of the hydrocarbons (gasoline, LPG and dry gas) was increased by employing Pd/ZSM-5 as a component of the hybrid catalyst. Moreover, the yield of the hydrocarbons in the gasoline fraction increased from 25% to 33% with the increase in the Pd loadings from 0 wt% to 0.5 wt%, while the yield of the dry gas fractions decreased with increasing the Pd loadings. The increase in the Pd loadings would improve the mass transfer of the products during the reaction because the hydrogenation over Pd leads to suppressing the blocking of the pores and cavities of the zeolite by the carbonaceous species. Therefore, the transfer of the gasoline fractions out of the zeolite intracrystallites was promoted with increasing the Pd loadings; simultaneously, the hydrocracking of the products to small fractions was suppressed. The decrease in the yield of the dry gas fractions with increasing the Pd loading also indicates that the direct hydrogenation of CO to methane was not accelerated even when Pd was employed as a hydrogenation catalyst. In addition, the $CO_2$ yield was almost the same regardless of the Pd loadings, although the larger amount of $H_2O$ was generated

over Pd/ZSM-5 compared with ZSM-5 alone as a result of the methanol conversion to hydrocarbons. These results indicate that Pd hardly contributed to the WGS reaction during the syngas conversion to hydrocarbons.

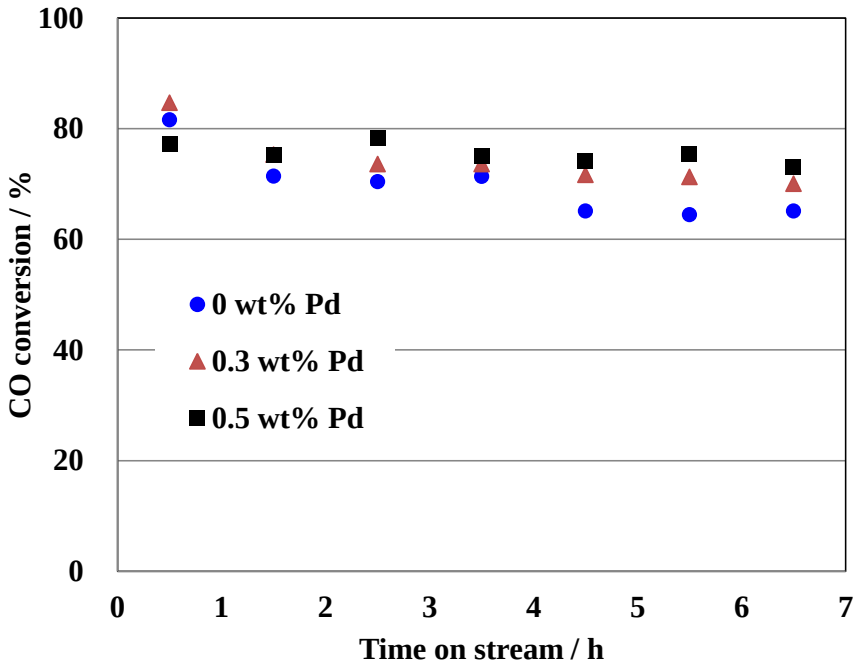


Fig. 3.9. CO conversion over hybrid catalysts composed of Cu-ZnO and Pd/ZSM-5-HT with different Pd loadings. Reaction conditions: cat., 1.0 g hybrid catalyst (0.5 g Cu-ZnO and 0.5 g Pd/ZSM-5); temp., 553 K; $P_{syngas}$ = 2.5 MPa; $P_{n\text{-hexane}}$ = 1.5 MPa; W/F = 9.7 $g_{\text{-cat}}$ h/$mol_{\text{-syngas}}$; $H_2$/CO = 1.9.

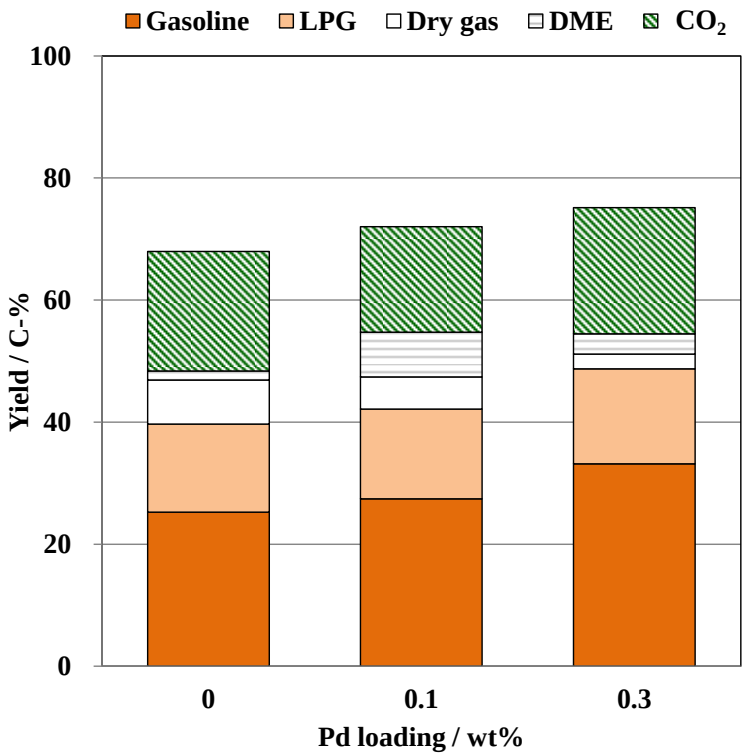


Fig. 3.10. Product yield resulting from conversion of syngas to hydrocarbons over hybrid catalysts composed of Cu-ZnO and Pd/ZSM-5-HT with different Pd loadings. Reaction conditions: cat., 1.0 g hybrid catalyst (0.5 g Cu-ZnO and 0.5 g Pd/ZSM-5); temp., 553 K; $P_{syngas}$ = 2.5 MPa; $P_{n\text{-hexane}}$ = 1.5 MPa; W/F = 9.7 $g_{\text{-cat}}$ h/$mol_{\text{-syngas}}$; $H_2$/CO = 1.9.

### 3.3.5 Hydrocarbon synthesis from syngas over hybrid catalyst consisting of Cu-ZnO and metal-loaded ZSM-5

The catalytic properties of a hybrid catalyst consisting of Cu-ZnO and metal-loaded ZSM-5 were investigated in the conversion of syngas to hydrocarbons in a near-critical *n*-hexane solvent. The metal-loaded ZSM-5 catalysts were prepared by loading 0.5 wt% Pd, 5 wt% Fe, 5 wt% Co or 5 wt% Cu on ZSM-5 with the $SiO_2/Al_2O_3$ ratio of 23. Fig. 3.11 shows product yields after 6.5 h of the reaction at 543 K. Except for the hybrid catalyst with Co/ZSM-5, each catalyst exhibited almost the same yield of the sum of hydrocarbons and DME. Hydrocarbons and DME are produced through the formation of methanol, indicating that the conversion of methanol to DME followed by hydrocarbons is independent of metal species. Pd/ZSM-5 produced selectively hydrocarbons in the gasoline fractions ($C_5$ - $C_9$ saturated hydrocarbons) among the hydrocarbons with a high CO conversion of 67%. When Fe/ZSM-5 was employed as a portion of the hybrid catalyst, the CO conversion as well as the hydrocarbons yield was smaller than those of the other metal-loaded ZSM-5 catalysts, while DME was selectively produced. Thus, the conversion of DME to hydrocarbons did not take place smoothly over the Fe/ZSM-5 catalyst, resulting in decreasing the hydrocarbons yield. In addition, the yield of $CO_2$ generated through the water-gas-shift (WGS) reaction was decreased due to a decrease in $H_2O$ generated through the conversion of DME to hydrocarbons. By contrast, the hybrid catalyst with Co/ZSM-5 gave the highest CO conversion as well as the hydrocarbons yield among the four hybrid catalysts. Among the hydrocarbons, methane in hydrocarbons in dry gas fraction was dominantly produced with the yield of 38%. In the conversion of methanol to hydrocarbons, hydrocarbons with a carbon number of more than 1 are dominantly produced as a result

of the cracking ofintermediates [30, 31]. These results indicated that the Co species on ZSM-5 caused selectively the methanation of CO, $CO_2$ and methanol under the present conditions. The hybrid catalyst with 5 wt% Cu/ZSM-5 showed the CO conversion of 64% and the 28% yield of hydrocarbons in the gasoline fraction, which were very similar to those over that with 0.5 wt% Pd/ZSM-5. The TOFs in terms of the carbon amount (C-mol) of hydrocarbon products per mole of the metal species were estimated to 478 $h^{-1}$ and 8521 $h^{-1}$ for 5 wt% Cu/ZSM-5 and 0.5 wt% Pd/ZSM-5, respectively. Although the TOFs were much different between the two catalysts, the hydrocarbon distributions were almost the same. Thus, the hydrocarbon formation from methanol or DME would be dependent on the acidity of ZSM-5, and 5 wt% Cu on ZSM-5 would have almost the same catalytic properties for the WGS reaction and the methanation as those of 0.5 wt% Pd on ZSM-5.

Fig. 3.12 shows hydrocarbon distributions over the hybrid catalysts with 0.5 wt% Pd/ZSM-5 or 5 wt% Cu/ZSM-5. Both catalysts exhibited almost the same hydrocarbon distributions, and $C_7$ hydrocarbons were selectively produced. Only saturated hydrocarbons with a carbon number of less than 10 were obtained as products during the reaction. Among the gasoline-ranged hydrocarbons, the formation of *iso*-paraffins was more favorable than *n*-paraffins probably due to the isomerization of produced hydrocarbons over acid sites of ZSM-5. Furthermore, mono-branched paraffins such as 2-methylhexane and 3-methylpentane were mainly obtained as *iso*-paraffins. The carbon ratios of (*iso*-paraffins + cycloparaffins)/*n*-paraffins were 4.6 and 7.2 for 0.5 wt% Pd/ZSM-5 and 5 wt% Cu/ZSM-5, respectively. Metal species such as Pt and Pd, with a high hydrogenation ability, coexisting with a solid acid catalyst supplies dissociated hydrogen species to the surface of the solid acid catalyst to generate active acid sites,

which play an important role in the isomerization of alkane [20, 21, 32 - 35]. The amount of the Cu species on ZSM-5 was larger than that of the Pd species on ZSM-5. Thus, it is suggested that in the case of the hybrid catalyst with Cu/ZSM-5 the larger number of acid sites were generated from hydrogen dissociated on the metal species to cause the isomerization of hydrocarbon products without the cracking of hydrocarbons.

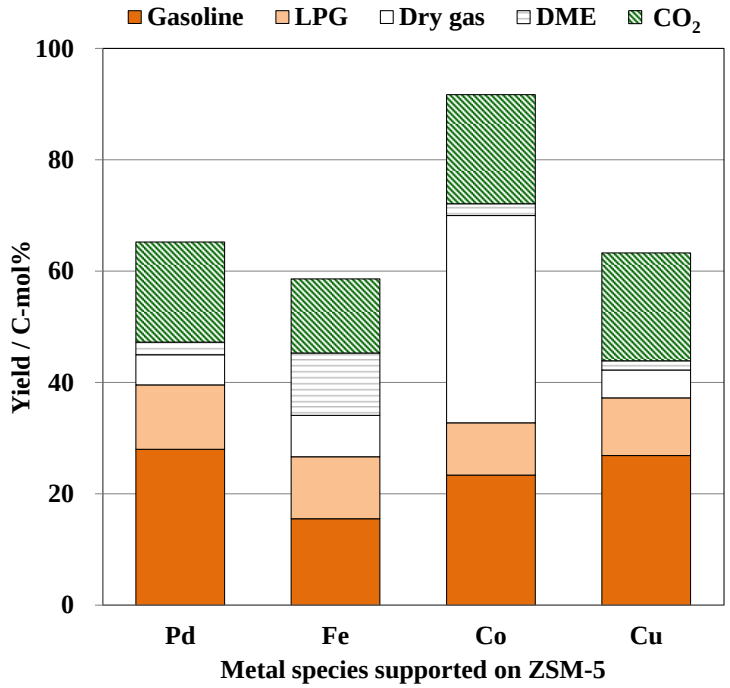


Fig. 3.11. Product yield resulting from conversion of syngas to hydrocarbons over hybrid catalysts consisting of Cu-ZnO and metal-loaded ZSM-5. Reaction conditions: catalyst, 1.0 g (0.5 g Cu-ZnO and 0.5 g metal-loaded ZSM-5); temperature, 543 K; $P_{syngas}$ = 2.5 MPa; $P_{n\text{-hexane}}$ = 1.5 MPa; W/Fsyngas = 9.7 $g_{\text{-catalyst}}$ h $mol^{-1}$; $H_2/CO$ = 1.9.

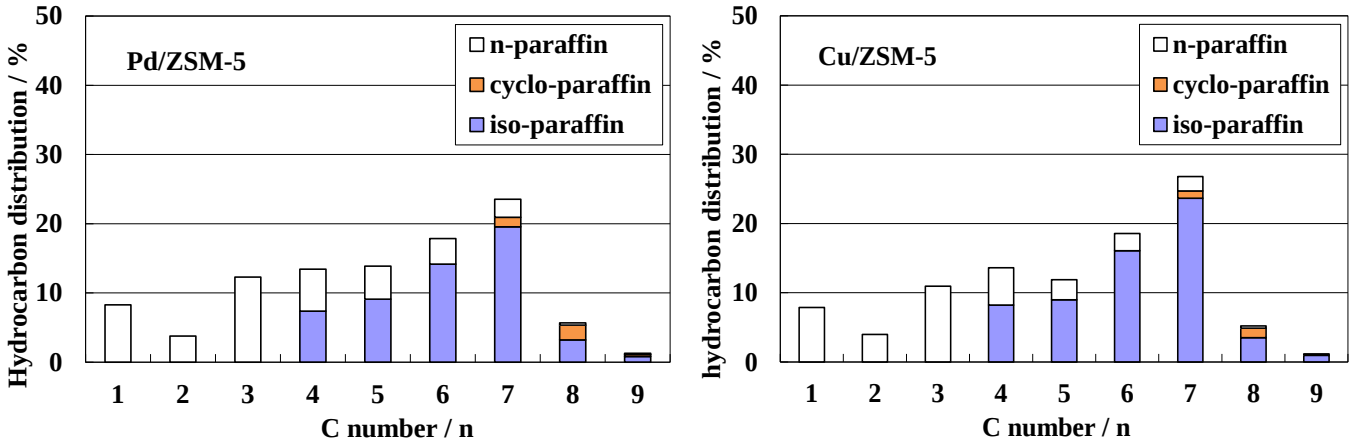


Fig. 3.12. Hydrocarbon distribution resulting from conversion of syngas to hydrocarbons over hybrid catalysts with 0.5 wt% Pd/ZSM-5 or 5 wt% Cu/ZSM-5. Reaction conditions: catalyst, 1.0 g (0.5 g Cu-ZnO and 0.5 g metal-loaded ZSM-5); temperature, 543 K; $P_{syngas}$ = 2.5 MPa; $P_{n\text{-hexane}}$ = 1.5 MPa; $W/F_{syngas}$ = 9.7 $g_{\text{-catalyst}}$ h $mol^{-1}$; $H_2/CO$ = 1.9.

### 3.3.6 Effect of copper loaded on ZSM-5 on catalytic properties

The hydrogenation ability of the Cu species on ZSM-5 would play an important role in supplying acidic species to the surface of ZSM-5 as well as in hydrogenating olefins, which were primarily produced from DME, to paraffins. In addition, the hydrogenation ability is important to decompose carbonaceous species deposited in/on ZSM-5 because a rapid deactivation occurs due to the deposition of coke resulting from the further oligomerization of the carbonaceous species to cover the acid sites and/or to block the pores of the zeolite [36]. In order to investigate the effects of the Cu species on ZSM-5 on the durability of the catalyst, the conversion of syngas to hydrocarbons was conducted over the hybrid catalysts with the different Cu loadings on ZSM-5. Fig. 3.13 shows time course plots of the CO conversions over the hybrid catalysts containing Cu/ZSM-5 with the different Cu loadings. The initial CO conversion was reached to ca. 67%, independent of the Cu loadings, indicating that the Cu species on ZSM-5 did not influence the conversion of syngas to methanol followed by DME. In the case of employing ZSM-5 without the Cu species, the CO conversion rapidly decreased after the reaction started until the conversion reached to 57% after 6.5 h. By loading even small amount of the Cu species on ZSM-5, the deactivation became slow. When 3 wt% Cu species was loaded on ZSM-5, the rapid deactivation was obviously suppressed compared with 0 wt% and 1 wt% Cu/ZSM-5, resulting in the CO conversion of 65% after 6.5 h of the reaction time. The inhibition of the deactivation by loading the Cu species on ZSM-5 is consistent with the previous report employing hybrid catalysts with Pd/ZSM-5 [23, 37]. By contrast, a further increase in the Cu loading caused the deactivation at the initial periods of the reaction again; in addition, decreased the CO

conversion. However, the CO conversions of the hybrid catalysts with 5 wt% or 8 wt% Cu/ZSM-5 became constant after 2.5 h of the reaction time, while the slight deactivation was observed over the hybrid catalyst with 3 wt% Cu/ZSM-5 during the reaction.

Hydrogen uptakes determined from the hydrogen chemisorption measurement were 2.4 μmol $g^{-1}$, 3.6 μmol $g^{-1}$, and 3.6 μmol $g^{-1}$ for 1 wt%, 5 wt%, and 8 wt% Cu/ZSM-5, respectively. The hydrogen uptake was increased by increasing the Cu loading. Thus, it is assumed that the Cu species on ZSM-5 inhibited the formation of heavy coke through the hydrogenation of carbonaceous species, leading to the suppression of the deactivation.

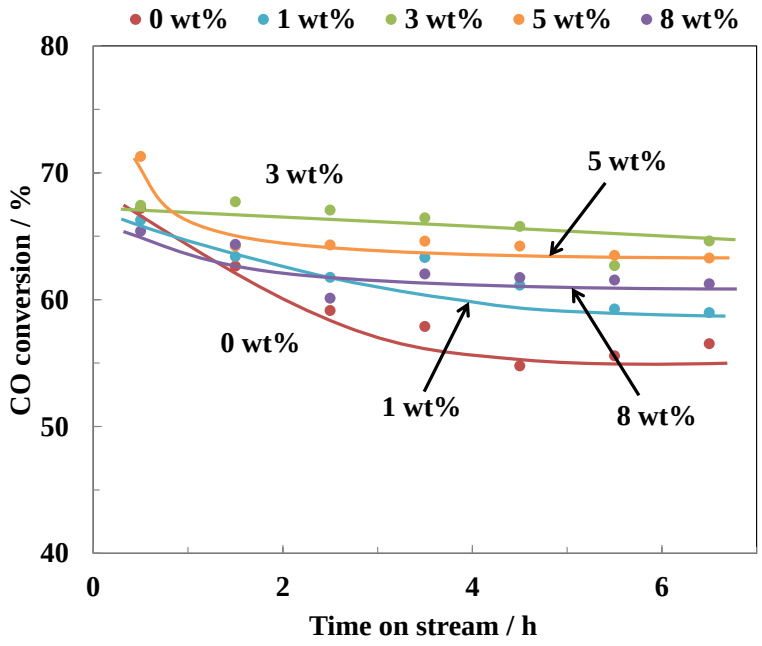


Fig. 3.13. CO conversion over hybrid catalysts composed of Cu-ZnO and Cu/ZSM-5 with different Cu loading amounts. Reaction conditions: catalyst, 1.0 g (0.5 g Cu-ZnO and 0.5 g Cu/ZSM-5); temperature, 543 K; $P_{syngas}$ = 2.5 MPa; $P_{n\text{-hexane}}$ = 1.5 MPa; W/Fsyngas = 9.7 $g_{\text{-catalyst}}$ h $mol^{-1}$; $H_2$/CO = 1.9.

Fig. 3.14 shows product yields at the initial period and after 6.5 h of the reaction at 543 K. In order to investigate the product distribution without the influence of the deactivation, the product yields at the initial period of the reaction were compared on the basis of a similar CO conversion. At the initial period, although the hydrocarbon yield of the hybrid catalyst with 1 wt% Cu/ZSM-5 was smaller than that of the hybrid catalyst with H-ZSM-5, the gasoline-ranged hydrocarbon yields of both the catalysts were almost the same values. Increasing the Cu loading resulted in an obvious increase in the gasoline-ranged hydrocarbons yield with the yields of hydrocarbons in LPG and dry gas fractions unchanged. Since $CO_2$ is generated from CO through the WGS reaction, a high hydrocarbon yield leads to the generation of a large amount of $H_2O$ to encourage the $CO_2$ production through the WGS reaction. However, the $CO_2$ yield was decreased by increasing the Cu loading. It is indicated that the Cu species on ZSM-5 had less influence on the WGS reaction under the present conditions.

At 6.5 h after the reaction started, the product distribution was dependent on the Cu loading as well. An increase in the Cu loading resulted in increasing the gasoline-ranged hydrocarbons yield and in decreasing the DME yield. When increasing the Cu loading amount up to 5 wt%, the hydrocarbons yield slightly decreased with the slight increase in the gasoline-ranged hydrocarbons yield. It is implied that the Cu species on ZSM-5 would cover the acid sites causing the cracking of hydrocarbons, leading to the improvement in the yield of the gasoline-ranged hydrocarbons.

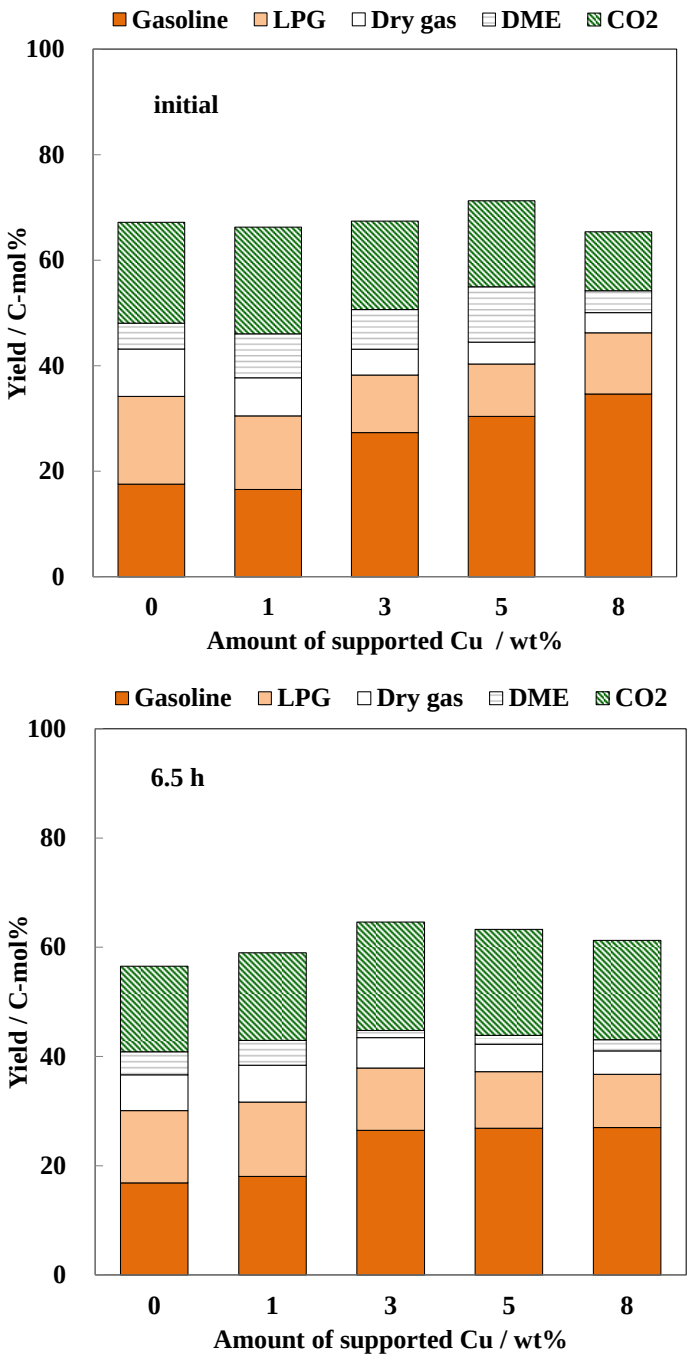


Fig. 3.14. Product yield resulting from conversion of syngas to hydrocarbons over hybrid catalysts with Cu/ZSM-5 with different Cu loadings. Reaction conditions: catalyst, 1.0 g (0.5 g Cu-ZnO and 0.5 g Cu/ZSM-5); temperature, 543 K; $P_{syngas}$ = 2.5 MPa; $P_{n\text{-hexane}}$ = 1.5 MPa; $W/F_{syngas}$ = 9.7 $g_{\text{-catalyst}}$ h $mol^{-1}$; $H_2/CO$ = 1.9.

Acid sites of a catalyst should play an important role in the conversion of methanol to DME followed by hydrocarbons. Fig. 3.15 shows $NH_3$-TPD profiles of Cu/ZSM-5 with the different Cu loadings. The acid amounts estimated from the peak at higher temperature were 0.99 mmol $g^{-1}$, 0.63 mmol $g^{-1}$, 0.52 mmol $g^{-1}$, 0.48 mmol $g^{-1}$, and 0.59 mmol $g^{-1}$ for H-ZSM-5, 1 wt%, 3 wt%, 5 wt%, and 8 wt% Cu/ZSM-5, respectively. The peak at higher temperature was decreased by increasing the Cu loading. When the Cu loading was increased up to 3 wt%, a shoulder peak appeared at around 300 K. The peak at higher temperature (573 - 873 K) corresponds to $NH_3$ desorption from catalytically active acid sites [38, 39]. It is suggested that the Cu species interacted with the acid sites of ZSM-5 to make their acid strength weaker. The high Cu loading (3 - 8 wt%) catalysts exhibited a new peak at around 550 K, and the peak was increased by increasing the Cu loading. Since the large peak was observed on Cu/ZSM-5 with the high Cu loading of 8 wt%, the peak can be derived from $NH_3$ adsorbed on the Cu species, which is consistent with the previous reports [40 - 42]. As shown in Fig. 3.14, the gasoline-ranged hydrocarbons yield was drastically improved when the Cu loading was increased up to 3 wt%, while the slight increase in the gasoline-ranged hydrocarbons yield was observed by the further increase in the Cu loading, which was in line with the changes in the peak at the higher temperature in the $NH_3$-TPD profiles. Therefore, it is suggested that the weak acid sites generated by loading the Cu species on ZSM-5 played an important role in the selective synthesis of the gasoline-ranged hydrocarbons without the polymerization and cracking of products because of mild acid strength.

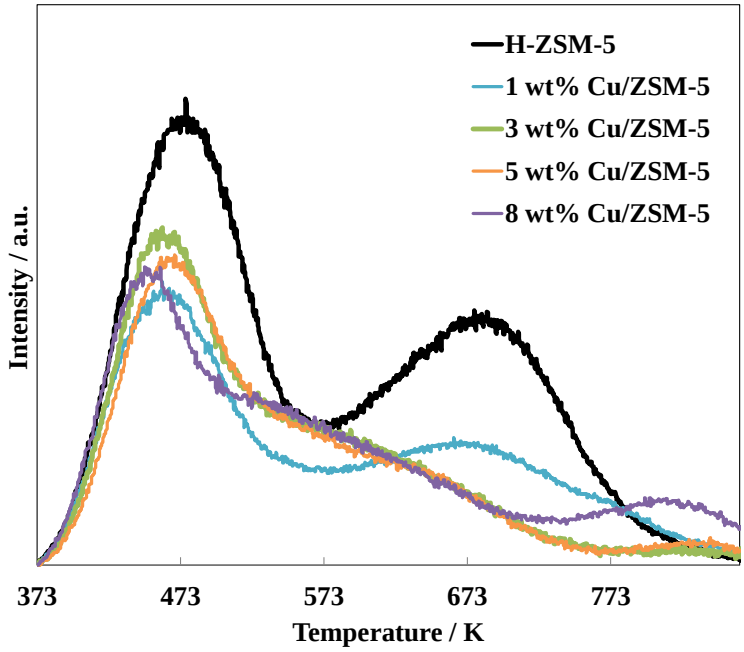


Fig. 3.15. Temperature programmed ammonia desorption ($NH_3$-TPD) profiles of Cu/ZSM-5 with different Cu loading amounts.

### 3.3.7 Durability of hybrid catalyst with Cu/ZSM-5

In order to investigate the durability of the hybrid catalyst with Cu/ZSM-5 in the syngas conversion, the changes in the CO conversion and product selectivities along with time-on-stream were examined in a long-run reaction at 553 K. It is reported that by loading Pd on ZSM-5, a high CO conversion was retained without the rapid deactivation and changes in product distributions in the conversion of syngas to the gasoline-ranged hydrocarbons [37]. As shown in Fig. 3.16, the initial CO conversion of the hybrid catalyst with 0.5 wt% Pd/ZSM-5 reached to 80%, while the hybrid catalyst with 5 wt% Cu/ZSM-5 exhibited 77% initial CO conversion. In the case of the hybrid catalyst with Pd/ZSM-5, the CO conversion gradually decreased until around 7 h after the reaction started, and then, the conversion of ca. 70% was kept until 30 h of the reaction time. By contrast, the CO conversion of the hybrid catalyst with Cu/ZSM-5 was kept constant with the value of ca. 74% during the reaction. Although $CO_2$ selectivity of the hybrid catalyst with Cu/ZSM-5 was slightly smaller than that of the hybrid catalyst with Pd/ZSM-5, the hybrid catalyst with Cu/ZSM-5 exhibited the higher DME selectivity than the hybrid catalyst with Pd/ZSM-5 during the reaction. These findings indicate that Cu/ZSM-5 constantly transformed methanol generated from syngas into DME followed by hydrocarbons without the rapid deposition of carbonaceous species on the catalyst during the reaction. Furthermore, the Cu species on ZSM-5 did not encourage the CO consumption through the WGS reaction compared with Pd/ZSM-5. Owing to the advantages mentioned above, Cu species is promising for the development of bifunctional catalysts in the selective synthesis of hydrocarbons from syngas, instead of precious metals such as Pd and Pt.

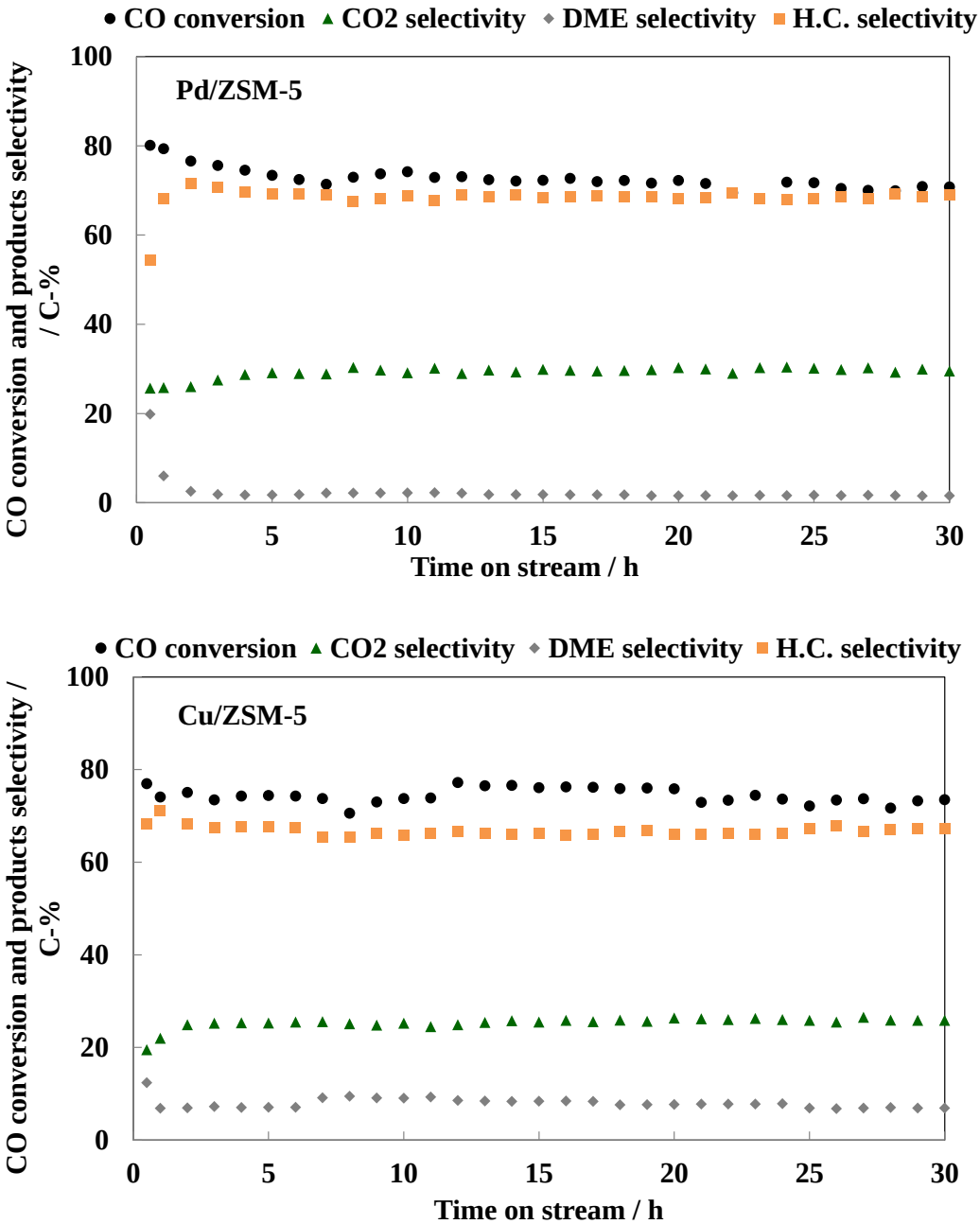


Fig. 3.16. Conversion of syngas to hydrocarbons over hybrid catalysts with 0.5 wt% Pd/ZSM-5 and 5 wt% Cu/ZSM-5. Reaction conditions: catalyst, 1.0 g (0.5g Cu-ZnO and 0.5 g metal-loaded ZSM-5); temperature, 553 K; $P_{syngas}$ = 2.5 MPa; $P_{n\text{-hexane}}$ = 1.5 MPa; $W/F_{syngas}$ = 9.7 $g_{\text{-catalyst}}$ h $mol^{-1}$; $H_2/CO$ = 1.9.

## 3.4. Conclusions

The catalytic performance of hybrid catalysts consisting of Cu-ZnO coupled with metal-loaded ZSM-5 have been studied in the syngas conversion to hydrocarbons via methanol in a near-critical *n*-hexane solvent.

The characteristics of Pd/ZSM-5 influenced the synthesis of the hydrocarbons in the syngas conversion. An increase in the acid amount of ZSM-5 was effective on the generation of hydrocarbons in the syngas conversion to hydrocarbons at lower temperature than those applied in the MTH reaction. Hydrocarbon distribution was strongly dependent on the particle size of ZSM-5 and Pd loading. A decrease in the particle size of ZSM-5 and an increase in the Pd loading improved the yield of hydrocarbons in gasoline fraction with high catalytic stability. It is likely that the improvement of the mass transfer due to the decrease of the particle size and the hydrogenation of unsaturated hydrocarbons over Pd suppress the deposition of carbonaceous species. Subsequently, the pore and cavity spaces in the zeolite can be retained, leading to the smooth mass transfer of large hydrocarbons out of the intracrystallites. Therefore, Pd/ZSM-5 composed of nano-sized particles is effective on the selective production of gasoline fractions from syngas via methanol with the near-critical fluid.

The hybrid catalyst consisting of 5 wt% Cu/ZSM-5 coupled with Cu-ZnO exhibited very similar catalytic performances to those over the hybrid catalyst containing 0.5 wt% Pd/ZSM-5, and produced selectively gasoline-ranged hydrocarbons from syngas. The Cu loaded on ZSM-5 influenced the deactivation rate as well as the product distribution. An increase in the Cu loading increased the gasoline-ranged hydrocarbons yield without

the cracking of the products, and shortened time before the catalytic activity became stable with keeping a high CO conversion. The high Cu loading on ZSM-5 decreased the amount of the acid sites and weakened the acid strength of ZSM-5, which were estimated from $NH_3$-TPD profiles. These findings suggest that Cu species would interact with the acid sites of ZSM-5 to make the acid strength mild, leading to suppressing the excess polymerization and the cracking of products with keeping high ability of the methanol conversion to hydrocarbons. In addition, the Cu species on ZSM-5 exhibited less ability for the water-gas-shift reaction, resulting in the good catalytic stability without excess consumption of CO. Therefore, Cu/ZSM-5 as a portion of a hybrid catalyst is effective in the selective synthesis of the gasoline-ranged hydrocarbons from syngas.

References

[1] R.B. Anderson, Fischer–Tropsch Synthesis, Academic Press, New York, 1984.

[2] M.E. Dry, Appl. Catal. A: Gen. 276 (2004) 1–3.

[3] B.H. Davis, Ind. Eng. Chem. Res. 46 (2007) 8938–8945.

[4] H. Schulz, in: B.H. Davis, M.L. Occelli (Eds.), Fischer–Tropsch Synthesis and Hydroformylation on Cobalt Catalysts, CRC Press/Taylor and Francis Group, Boca Raton/London/New York, 2010, pp. 165–183.

[5] L. Shi, Y. Jin, C. Xing, C. Zeng, T. Kawabata, K. Imai, K. Matsuda, Y. Tan, N. Tsubaki, Appl. Catal. A: Gen. 435-436 (2012) 217–224.

[6] B. Todic, T. Bhatelia, G.F. Froment, W. Ma, G. Jacobs, B.H. Davis, D.B. Bukur, Ind. Eng. Chem. Res. 52 (2013) 669–679.

[7] N.E. Tsakoumis, R. Dehghan, R.E. Johnsen, A. Voronov, W. van Beek, J.C. Walmsley, Ø. Borg, E. Rytter, D. Chen, M. Rønning, A. Holmen, Catal. Today 205 (2013) 86–93.

[8] M. Stöcker, Microporous Mesoporous Mater. 29 (1999) 3–48.

[9] M. Stöcker, Microporous Mesoporous Mater. 82 (2005) 257–292.

[10] T. Mokrani, M. Scurrell, Catal. Rev. 51 (2009) 1–145.

[11] B. Vora, J.Q. Chen, A. Bozzano, B. Glover, P. Barger, Catal. Today 141 (2009) 77–83.

[12] J.F. Haw, W. Song, D.M. Marcus, J.B. Nicholas, Acc. Chem. Res. 36 (2003) 317–326.

[13] Q. Zhang, X. Li, K. Asami, S. Asaoka, K. Fujimoto, Fuel Process. Technol. 85 (2004) 1139–1150.

[14] K. Asami, Q. Zhang, X. Li, S. Asaoka, K. Fujimoto, Catal. Today 106 (2005) 247–

251.

[15] Q. Ge, X. Li, H. Kaneko, K. Fujimoto, J. Mol. Catal. A 278 (2007) 215–219.

[16] Q. Ge, Y. Lian, X. Yuan, X. Li, K. Fujimoto, Catal. Commun. 9 (2008) 256–261.

[17] X. Ma, Q. Ge, J. Ma, H. Xu, Fuel Process. Technol. 109 (2013) 1–6.

[18] Conte, M., Lopez-Sanchez, J. A., He, Q., Morgan, D. J., Ryabenkova, Y., Bartley, J. K., Carley, A. F., Taylor, S. H., Kiely, C. J.; Khalid, K., Catal. Sci. Technol. 2 (2012) 105–112.

[19] Chang, Y. F., Somorjai, G. A., Heinemann, H., J. Catal., 154 (1995) 24–32.

[20] Fujimoto, K., Maeda, K., Aimoto, K., Appl. Catal. A, 91 (1992) 81–86.

[21] Zhang, A., Nakamura, I., Aimoto, K., Fujimoto, K., Ind. Eng. Chem. Res., 34 (1995) 1074–1080.

[22] H. Mochizuki, T. Yokoi, H. Imai, R. Watanabe, S. Namba, J.N. Kondo, T. Tatsumi, Microporous Mesoporous Mater. 145 (2011) 165–171.

[23] Q. Zhang, P. Liu, Y. Fujiyama, C. Chen, X.H. Li, Appl. Catal. A: Gen. 401 (2011) 147–152.

[24] M. Niwa, N. Katada, Catal. Surv. Jpn. 1 (1997) 215–226.

[25] K. Suzuki, Y. Aoyagi, N. Katada, M. Choi, R. Ryoo, M. Niwa, Catal. Today 132 (2008) 38–45.

[26] D. Chen, K. Moljord, T. Fuglerud, A. Holmen, Microporous Mesoporous Mater. 29 (1999) 191–203.

[27] D. Chen, K. Moljord, A. Holmen, Microporous Mesoporous Mater. 164 (2012) 239–250.

[28] S. Yoshie, F. Masahiro, K. Roger, A. Hisanori, Q. Xu, Stud. Surf. Sci. Catal. 114 (1998) 327–332.

[29] H. Schulz, Catal. Today 154 (2010) 183–194.

[30] Stöcker, M., Micropor. Mesopor. Mater., 29 (1999) 3–48.

[31] Mokrani, T., Scurrell, M. Catal. Rev. Sci. Eng., 51 (2009) 1–145.

[32] Ebitani, K., Tsuji, J., Hattori, H., J. Catal., 130 (1990) 257–267.

[33] Ebitani, K., Tsuji, J., Hattori, H., Kita, H., J. Catal., 135 (1992) 609–617.

[34] Roland, U., Braunschweig, T., Roessner, F., J. Mol. Catal. A, 127 (1997) 61–84.

[35] Weitkamp, J., Chem Cat Chem, 4 (2002) 292–306.

[36] Schulz, Catal. Today, 154 (2010) 183–194.

[37] Ma, T., Imai, H., Suehiro, Y., Chen, C., Kimura, T., Asaoka, S.; Li, X., Catal. Today 228 (2014) 167–174.

[38] Niwa, M., Katada, N., Catal. Surv. Asia, 1 (1997) 215–226.

[39] Suzuki, K., Aoyagi, Y., Katada, N., Choi, M., Ryoo, R., Niwa, M., Catal. Today 132 (2008) 38–45.

[40] Mihai, O., Widyastuti, C. R., Andonova, S., Kamasamudram, K., Li, J., Joshi, S. Y., Currier, N. W., Yezerets, A., Olsson, L., J. Catal. 311 (2014) 170–181.

[41] Kubo, K., Iida, H., Namba, S., Igarashi, A., Catal. Commun. 29 (2012) 162–165.

[42] Halász, J., Varga, J., Schöbel, G., Kiricsi, I., Hernádi, K., Hannus, I., Varga, K., Fejes, P., Stud. Surf. Sci. Catal. 96 (1995) 675–685.

CHAPTER FOUR

# DIRECT SYNTHESIS OF GASOLINE FROM $H_2$–DEFICIENT SYNGAS IN FISCHER-TROPSCH SYNTHESIS OVER HYBRID CATALYST


## Abstract

The effects of metal species in an Fe-based catalyst on structural properties were investigated through the synthesis of Fe-based catalysts containing various metal species such, as Mn, Zr, and Ce. The addition of themetal species to the Fe-based catalyst resulted in high dispersions of the Fe species and high surface areas due to the formation of mesoporous voids about 2 - 4 nm surrounded by the catalyst particles. The metal-added Fe-based catalysts were employed together with Co-loaded beta zeolite for the synthesis of hydrocarbons from syngas with a lower $H_2$/CO ratio of 1 than the stoichiometric $H_2$/CO ratio of 2 for the Fischer-Tropsch synthesis (FTS). Among the catalysts, the Mn-added Fe-based catalyst exhibited a high activity for the water-gas shift (WGS) reaction with a comparative durability, leading to the enhancement of the CO hydrogenation in the FTS in comparison with Co-loaded beta zeolite alone. Furthermore, the loading of Pd on the Mn-added Fe-based catalyst enhanced the catalytic durability due to the hydrogenation of carbonaceous species by the hydrogen activated over Pd.

## 4.1. Introduction

The use of biomass materials as renewable resources has been focused on for the production of sustainable liquefied fuels as well as the fixation of emitted $CO_2$ [1, 2], the so called "biomass-to-liquid (BTL) process." In the BTL process, the gasification of biomass materials produces mainly syngas composed of carbon monoxide and hydrogen; subsequently, syngas can be directly converted to hydrocarbons as liquefied fuels such as diesel fuel through the Fischer-Tropsch synthesis (FTS) over Fe- and Co-based catalysts. Syngas obtained from biomass materials usually contains lower ratios of hydrogen to carbon monoxide than syngas derived from natural gas; the $H_2$/CO molecular ratio is below 2 [3, 4]. However, the $H_2$/CO ratio of 2 is required for the stoichiometric hydrogenation of carbon monoxide to hydrocarbons in the FTS; furthermore, the reaction rate in the FTS is positively dependent on the partial pressure of hydrogen [5 - 7]. Therefore, from the viewpoint of the efficient production of hydrocarbons from the $H_2$-deficient syngas, methods for increasing the $H_2$/CO ratio during the FTS are highly desirable.

The water-gas shift (WGS) reaction is an important process for the production of hydrogen through the reaction of carbon monoxide with water. In the FTS, even if the steam is not introduced into a reaction system, water is produced through the CO hydrogenation. Thus, the use of a WGS catalyst together with an FTS catalyst can continuously supply hydrogen required for the FTS through the WGS reaction with generated water and a portion of CO in syngas. For the conversion of $H_2$-deficient syngas to hydrocarbons, Fe based catalysts have been attractive since Fe-based catalysts have high activities for both the WGS reaction and the FTS to attain an efficient utilization of carbon monoxide [8 - 13]. Furthermore, the catalytic activity of Fe-based

catalysts can be promoted by the introduction of metal species such as Cu, Mn, Ce, and Zr to the catalysts because of the enhancement of the reducibility of Fe species ($Fe_2O_3$ → $Fe_3O_4$) [14 - 17] as well as high dispersions of nanosized Fe crystallites [18–20]. However, in the FTS over the Fe-based catalyst, both the WGS reaction and the FTS can simultaneously proceed; meanwhile, carbonaceous species, which are formed in the carbon growth, are deposited on the catalyst to cause the deactivation by the covering of active sites of the catalyst [13, 21, 22].

The combination of catalysts with different functions is expected to be effective in the construction of processes where different reactions occur simultaneously and/or sequentially. It has been reported that the selective synthesis of specific hydrocarbons from syngas was attained using an FTS catalyst together with a zeolite as an acid catalyst [23 - 25]. The FTS catalyst produced hydrocarbons from syngas, and the zeolite converted the produced hydrocarbons to specific hydrocarbons through the isomerization/cracking. In the synthesis of hydrocarbons through the formation of methanol, a methanol synthesis catalyst such as Cu-ZnO was employed together with a zeolite to show high catalytic activity [26 - 28]. In addition, the methanol synthesis catalyst was not covered with carbonaceous species which were deposited on the zeolite, leading to the improvement of the catalyst life. When a WGS catalyst is employed together with an FTS catalyst in the synthesis of hydrocarbons from $H_2$-deficient syngas, it is expected that the FTS reaction would proceed more efficiently by increasing the hydrogen concentration through the WGS reaction in comparison with the FTS catalyst alone. Furthermore, the catalyst activity of the WGS catalyst would be retained because carbonaceous species which are deposited on the FTS catalyst cannot move to the WGS catalyst.

In the present study, we investigated the catalytic properties of hybrid catalysts composed of a catalyst for the WGS reaction and a catalyst for the FTS in the conversion of $H_2$-deficient syngas to hydrocarbons. In particular, the catalytic activity of the WGS catalyst was focused on for the enhancement of the CO hydrogenation by the supply of hydrogen. Since Co-based catalysts have a higher activity for the CO hydrogenation than Fe-based catalysts [29], the Co based catalyst and the Fe-based catalyst were employed as an FTS catalyst and a WGS catalyst, respectively. We also investigated the effect of the addition of metal species to the Fe-based WGS catalyst on the physicochemical and catalytic properties.

## 4.2. Experimental

### 4.2.1. WGS catalyst preparation.

Metal-added Fe-based WGS catalysts, M-FeCu (M = Zr, Mn, and Ce), were prepared by the coprecipitation method using $Fe(NO_3)_3 \cdot 9H_2O$ (Kanto Chem. Co.), $Cu(NO_3)_2 \cdot 3H_2O$ (Kanto Chem. Co.), $ZrO(NO_3)_2 \cdot 2H_2O$ (Kanto Chem. Co.), $Mn(NO_3)_2 \cdot 6H_2O$ (Kanto Chem. Co.), and $Ce(NO_3)_3 \cdot 6H_2O$ (Kanto Chem. Co.) as Fe, Cu, Zr, Mn, and Ce sources, respectively. 2 M $Na_2CO_3$ aqueous solution was dropped into a mixed aqueous solution of $Fe(NO_3)_3 \cdot 9H_2O$, $Cu(NO_3)_2 \cdot 3H_2O$, and $M(NO_3)_x \cdot nH_2O$ to adjust a pH value of the solution at around 8 at 353K. Continuously, the resultant gel was stirred at 353K for 1 h. The obtained product was recovered by filtration, washed with hot deionized water to remove sodium cations, and dried at 393K for 12 h. A $KNO_3$ aqueous solution was added to the product by impregnation method. The mixture was evaporated at 333K, dried at 393K for 3h, and calcined at 673K for 3h. The nominal weight ratio of the Fe-based catalyst was 100 Fe: 1 Cu: 2 K, and the added amount of M was 0 wt.%, 10 wt.%, and 20 wt.% on the basis of the weight of the Fe-based catalyst.

A Pd-modified WGS catalyst was prepared by impregnation method with 4.6 wt.% $Pd(NH_3)_2(NO_3)_2$ aqueous solution. The 10 wt.% Mn-containing FeCu catalyst was immersed in the aqueous solution with Pd for preparing 1 wt.% Pd loaded Mn-FeCu at room temperature overnight. The resultant was evaporated at 333 K, dried at 393 K for 3 h, and calcined at 823 K for 3 h.

4.2.2. FTS catalyst preparation.

A Co supported on beta zeolite catalyst (Co/$\beta$) with a nominal Co loading of 20 wt.% was applied as an FTS catalyst. Co/$\beta$ was prepared by impregnation method using $Co(NO_3)_2 \cdot 6H_2O$ (Kanto Chem. Co.) aqueous solution and commercial beta zeolite (CP814E,Zeolyst). Prior to the impregnation, commercial $NH_4^+$-type beta zeolite was calcined at 823 K for 3 h to become proton type beta zeolite. Proton-type beta zeolite was immersed in the $Co(NO_3)_2 \cdot 6H_2O$ aqueous solution at room temperature overnight. The resulting mixture was evaporated at 333 K, dried at 393 K for 3 h, and calcined at 573 K for 3 h.

4.2.3. Characterization.

XRD patterns were collected on a Smart Lab (Rigaku) instrument using a Cu-K$\alpha$ X-ray source (40 kV, 20 mA). Nitrogen adsorption-desorption measurements were conducted at 77 K on a BELSORP-mini II (MicrotracBEL Corp.) instrument. Prior to the measurement, the WGS catalyst was evacuated at 473 K for 2 h. The BET (Brunauer-Emmett-Teller) specific surface area was calculated from the adsorption data. The pore size distribution was estimated from the desorption data by BJH (Barrett-Joyner-Halenda) method. Field-emission scanning microscopic (FE-SEM) images of the samples were obtained on an S-5200 microscope (Hitachi) operating at 1.0 - 5.0 kV. The sample was mounted on a carbon-coated microgrid (Okenshoji Co.) without any metal coating. Transmission electron microscope (TEM) images of the powder samples were obtained on a TEM instrument (JEOL) operating at 100 - 300 kV. Elemental analyses of the WGS catalyst were performed on a JXA- 8100 electron probe micro analyzer (EPMA, JEOL) operating at 15 kV and a backscatter electronic beam

diameter of 10 $\mu$m. Hydrogen temperature-programmed reduction ($H_2$ - TPR) profiles of the samples were recorded on a BELCAT (MicrotracBEL Corp.) apparatus. Typically, the sample was pretreated at 673 K in He (50 mL $min^{-1}$) for 1h and then was cooled to 323 K. Then, the sample was heated up to 973 K at a ramping rate of 5 K $min^{-1}$ with 10% $H_2$/He flow (30 mL $min^{-1}$) passed through the reactor. A mass spectrometer was used to monitor the water flow (m/e = 18) generated through the reduction of the sample by hydrogen.

4.2.4. Syngas conversion to hydrocarbons.

A pressurized flow type of reaction apparatus with a fixed-bed reactor was used to carry out the conversion of syngas to hydrocarbons. The experimental set-up scheme is shown in Fig. 4.1. The apparatus was equipped with an electronic temperature controller for a furnace, a vaporizer of a solvent, a stainless tubular reactor with an inner diameter of 6 mm, thermal mass flow controllers for gas flows and a back-pressure regulator. A hybrid catalyst was obtained by physically mixing 0.5 g of 355 - 710 $\mu$m pellets of the WGS catalyst with 1.5 g of 355 - 710 $\mu$m pellets of the FTS catalyst. 2.0 g of the hybrid catalyst was centered in a stainless tubular reactor with an inner diameter of 6 mm. The length of the catalyst bed was about 13 - 14 cm. Prior to the reaction, the hybrid catalyst was reduced in a hydrogen flow of 50 mL $min^{-1}$ at 673 K for 3 h and then cooled down to room temperature. Syngas (48.5 vol.% $H_2$, 48.5 vol.% CO, and 3 vol.% Ar) was introduced into the catalyst bed to make the pressure inside reach 1.0 MPa, and then the catalyst was heated up to 513 K. The catalyst weight to the flow rate ratio ($W/F_{\text{-syngas}}$) was 16.3 $g_{\text{-cat.}}$ h $mol^{-1}$. CO, $CO_2$, and $CH_4$ in the outlet gas which passed through the catalyst bed were analyzed with an on-line gas chromatograph (Shimadzu GC-8A)

equipped with a thermal conductivity detector (TCD) and a packed column of activated charcoal. The light hydrocarbons in the reaction products were analyzed with another on-line gas chromatograph (Shimadzu GC-2014) equipped with a flame ionization detector (FID) and a capillary column of InertCap 1. The products liquefied by condensation at room temperature were analyzed with an off-line gas chromatograph (Shimadzu GC-2014) equipped with an FID detector and a capillary column of TC-1. For the analyses of the liquefied products, decahydronaphthalene (*n*-$C_{10}H_{18}$) was used as an internal standard.

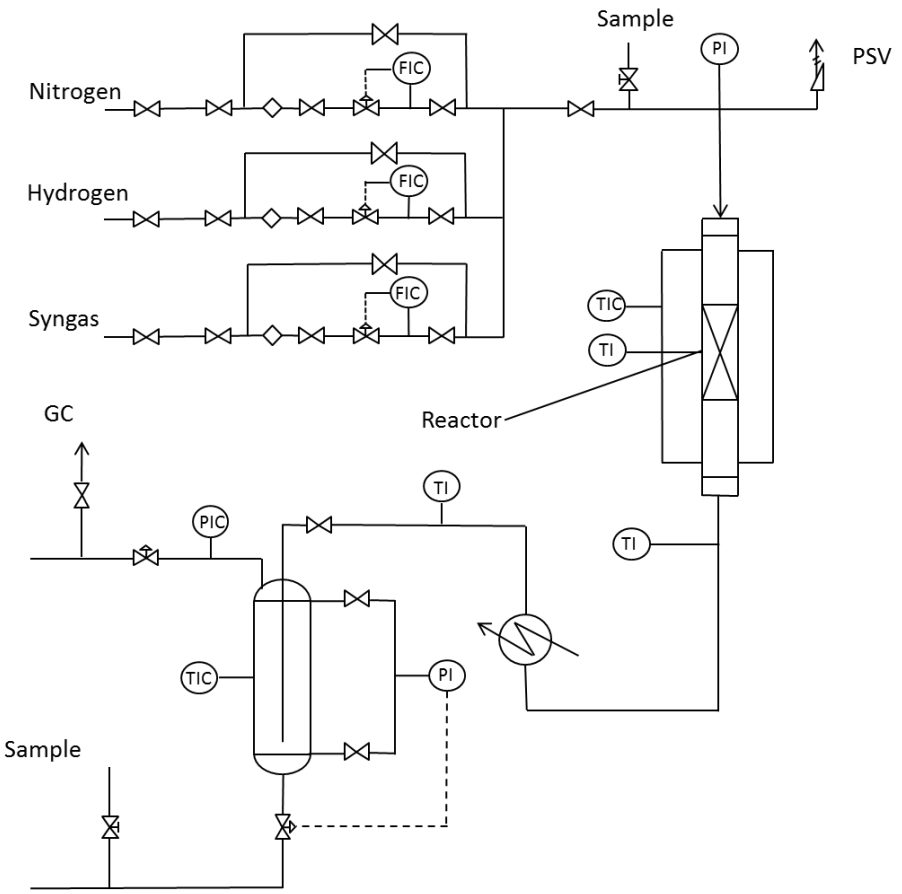


FIC, flow indicator and controller

PIC, pressure indicator and controller

TIC, temperature indicator controller

PI, pressure indicator

TI, temperature indicator

GC, gas chromatograph

Fig. 4.1. Scheme of experimental set-up.

## 4.3. Results and discussion

### 4.3.1. Preparation of metal-added Fe-based WGS Catalyst.

XRD patterns of calcined conventional Fe-based WGS catalyst (FeCu) and metal-added Fe-based catalysts are shown in Figure 4.2. Calcined FeCu exhibited an XRD typical of hematite. When Zr, Mn, or Ce species was introduced to the FeCu sample during the coprecipitation, only broadened peaks were observed at around 35° and 63.5° without any discernable peaks attributed to metal and metal oxide phases. Even when the amount of the added Zr species was increased up to 20 wt.%, no change was observed in the XRD pattern; only broadened peaks appeared at around 35° and 63.5°. In the synthesis of Fe-based FTS catalysts, the introduction of metal species such as Cr, Mo, and Mn to the catalyst leads to the formation of small oxide crystallites less than 4 - 5nm in size [18, 19]. These results suggest that the addition of the metal species to the Fe-based catalyst would promote the dispersion of the Fe species and the other metal species to form nanosized composites, independent of the added metal species.

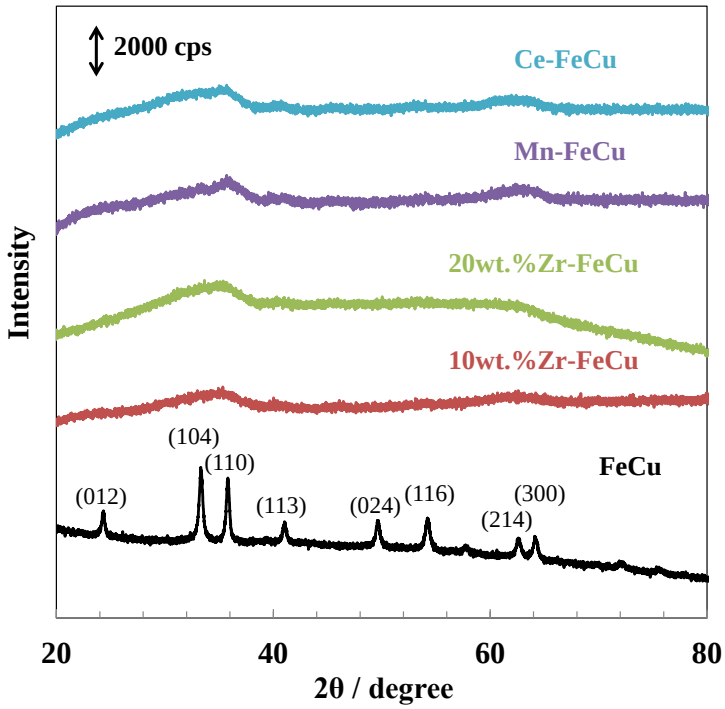


Fig. 4.2. XRD patterns of FeCu and metal-added Fe-based samples.

Figure 4.3 shows the $N_2$ adsorption-desorption isotherms and pore size distributions estimated by BJH method for the FeCu and metal-added Fe-based samples. All the samples showed a type IV isotherm, which is classified by IUPAC, with hysteresis. The FeCu sample exhibited the hysteresis at high relative pressures ($P/P_0$ = 0.8 - 0.95), which was derived from voids among the FeCu particles. By contrast, the hysteresis of the $N_2$ isotherms for the metal-added Fe-based samples appeared at $P/P_0$ = 0.45 - 0.75, regardless of the added metal species. In the pore size distribution, the metal-added Fe-based samples exhibited a peak in a range of diameters of mesopores (more than 2 nm), while no sharp peak was observed for the FeCu sample. Since Fe-based catalysts prepared by conventional coprecipitation method are not mesoporous materials, the

peaks in the pore size distribution can be assigned to mesopore-like voids surrounded by nanosized particles of the Fe-based catalyst. The BET surface areas, pore volumes, and pore sizes of the calcined catalysts are summarized in Table 4.1.The BET surface area was drastically increased by the addition of the metal species to the Fe-based catalyst because of the formation of the mesoporous voids. Moreover, the BET surface area was independent of the added amount of the metal species; the BET surface areas were found to be 175 and 181 $m^2$ $g^{-1}$ for 10 wt.% Zr-FeCu and 20 wt.% Zr-FeCu, respectively. Figure 4.4 shows FE-SEM images of calcined FeCu and the metal-added Fe-based samples. FeCu was composed of small particles ca. 60 nm in size. On the other hand, the SEM images of the metal-added Fe-based samples showed significantly large masses resulting from the agglomeration of small particles, regardless of the added metal species. The morphology of the metal-added Fe-based samples was also evaluated by TEM observations (Figure 4.5). It was found that particles ca. 4 - 5nm in size were agglomerated to form large masses, independent of the added metal species. These findings were consistent with the XRD findings. In addition, a number of voids were observed in the large agglomerates (Figures 4.4(c) and 4.4(f)), whose voids were in agreement with the mesoporous voids estimated by the $N_2$ adsorption measurement.

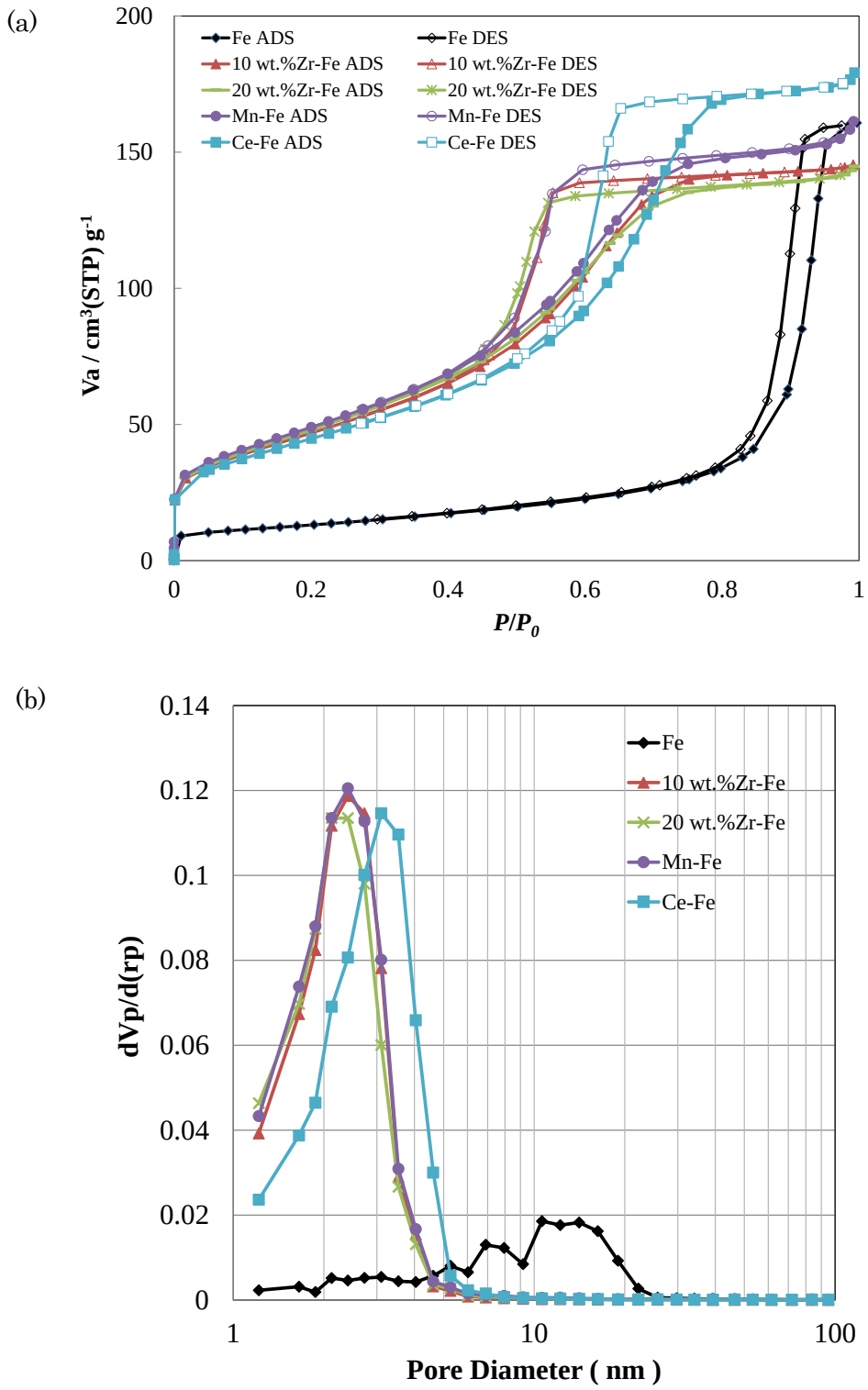


Fig. 4.3. $N_2$ adsorption and desorption isotherms (a) and pore size distributions (b) of FeCu and metal-added Fe-based samples.

Table 4.1. Physicochemical properties of Fe-based samples.

| Catalyst | Surface area[a] ($m^2$ $g^{-1}$) | Pore volume[a] ($cm^3$ $g^{-1}$) | Pore size[a] (nm) |
|---|---|---|---|
| FeCu | 46 | 0.25 | 11 |
| Zr-FeCu (10 wt.% Zr) | 175 | 0.22 | 2.1 |
| Zr-FeCu (20 wt.% Zr) | 181 | 0.22 | 2.1 |
| Mn-FeCu | 183 | 0.25 | 2.1 |
| Ce-FeCu | 163 | 0.27 | 2.7 |

[a]Estimated by $N_2$ adsorption-desorption method.

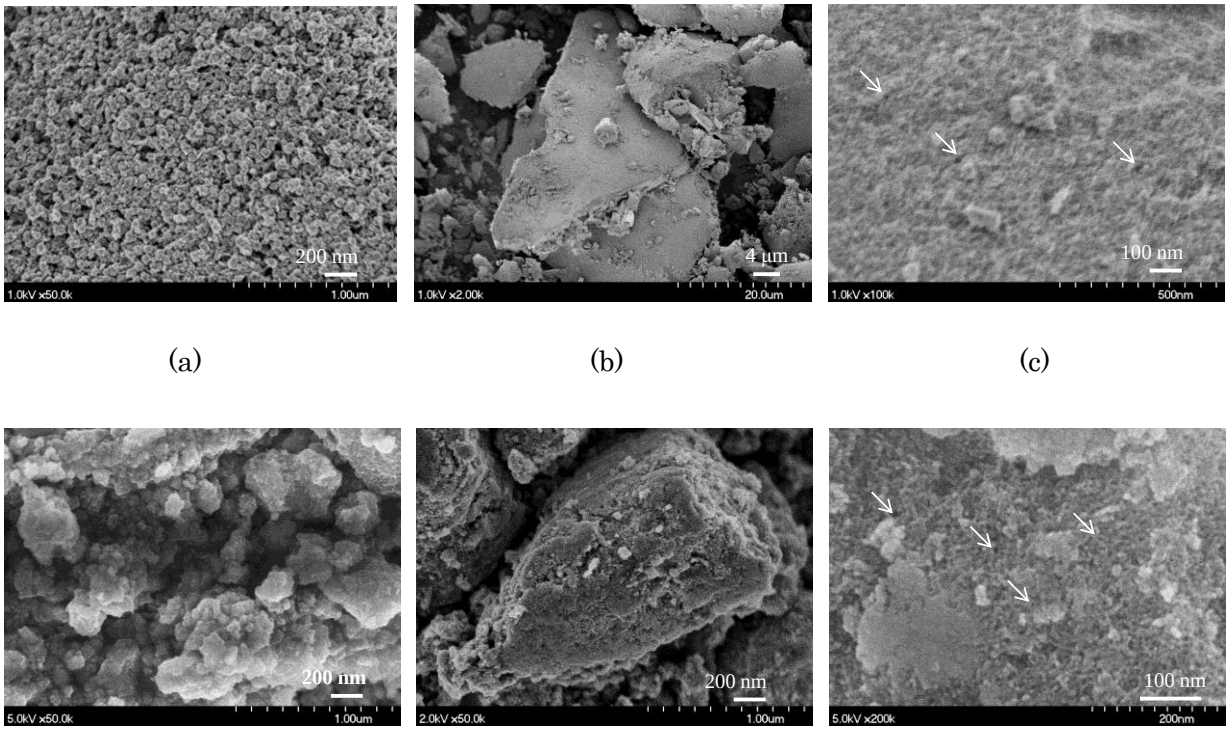


Fig. 4.4. FE-SEM images of (a) FeCu, (b, c) 10wt.% Zr-FeCu, (d) Mn-FeCu, and (e, f) Ce-FeCu. Voids are indicated by white arrows.

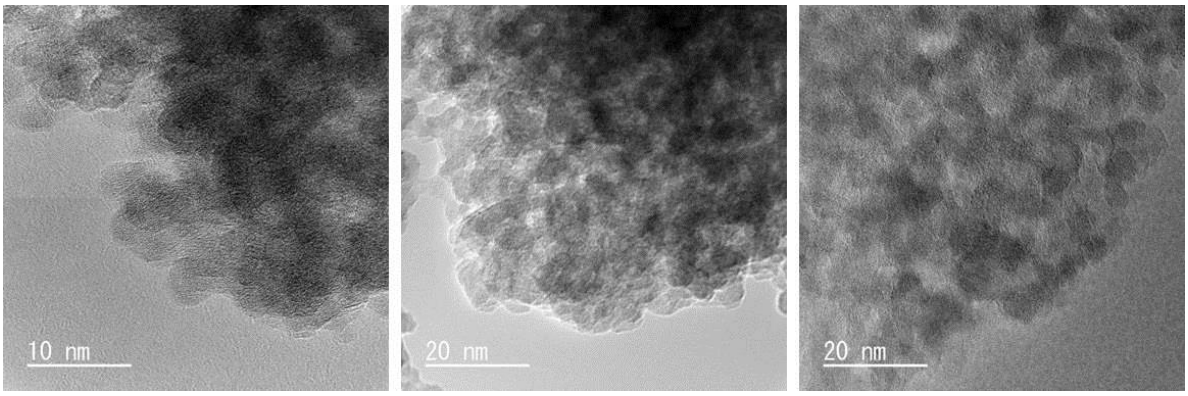


(a) (b) (c)

Fig. 4.5. TEM images of (a) 10 wt.% Zr-FeCu, (b) Mn-FeCu, and (c) Ce-FeCu.

The elemental analyses of the metal-added Fe-based samples were conducted with EPMA (Figure 4.6). Homogeneous dispersion of Fe species was observed on all the samples. Zr species and Ce species were homogeneously dispersed on the 10 wt.% Zr-FeCu and Ce-FeCu samples, respectively. These findings were consistent with the XRD findings. By contrast, the gatherings of Mn species were observed on the Mn-FeCu sample although Mn species were spread out on the sample. No peak derived from Fe-Mn composites or Mn oxides was observed in the XRD pattern of Mn-FeCu, suggesting that crystalline agglomerations composed of Mn species were not formed even if Mn species were gathered in the sample.

The reducibility of the metal-added Fe-based catalysts was estimated from the $H_2$-TPR profiles (Figure 4.7). The FeCu catalyst exhibited two peaks attributed to $H_2O$ generated through the reduction by $H_2$ at around 600 and 900 K, which corresponds to $H_2$-TPR profile observed in the twostep reduction of hematite, that is, $Fe_2O_3 \rightarrow Fe_3O_4 \rightarrow Fe$ [15, 30, 31], indicating that the first peak at lower temperature is ascribed to the reduction of $Fe_2O_3$ to $Fe_3O_4$, and the second peak at higher temperature is ascribed to

further reduction of $Fe_3O_4$. The reduction of Fe species can be promoted by the addition of Cu species, leading to a shift of a peak attributed to the reduction of $Fe_2O_3$ to $Fe_3O_4$ to lower temperature in $H_2$-TPR profiles [14 - 16], whereas K species suppresses the reduction of Fe and Cu species due to the interaction between the K species and the metal species [32, 33]. Thus, it is suggested that the reducibility of the Fe species may not be promoted in the FeCu catalyst due to the presence of the K species although the Cu species coexisted in the catalyst. All the metal-added Fe-based samples exhibited two peaks derived from the reduction of the Fe species at around 600 and 900 K, which was similar to the finding in $H_2$-TPR of the FeCu sample. However, the first peak of all the metal added Fe-based catalysts was shifted to higher temperatures in comparison with that of the FeCu sample. In addition, the temperature where the first peak appeared was slightly increased with an increase in the amount of added Zr. In an Fe-based FTS catalyst containing $SiO_2$, the reducibility of Fe oxides is not influenced by the coexistence of Zr, regardless of the amount of Zr [18, 19]. By contrast, Qing et al. have reported that in the $H_2$-TPR profiles a first peak of a calcined composite of Fe and Zr without $SiO_2$ appeared at higher temperature than that of hematite due to the cover of Fe sites with enriched Zr [34]. The addition of Mn or Ce species to Fe-based catalysts causes the interaction between the Fe species and the metal species, leading to the delay of the reduction of the Fe species [20, 35 - 37]. According to the findings reported above, it is suggested that in the metal added Fe-based catalysts the reduction of the Fe species was suppressed to shift the first peak to higher temperature in the $H_2$-TPR profile due to the interaction of the Fe species and the metal species resulting from the addition of the large amount of the metal species although the Fe species were highly dispersed.

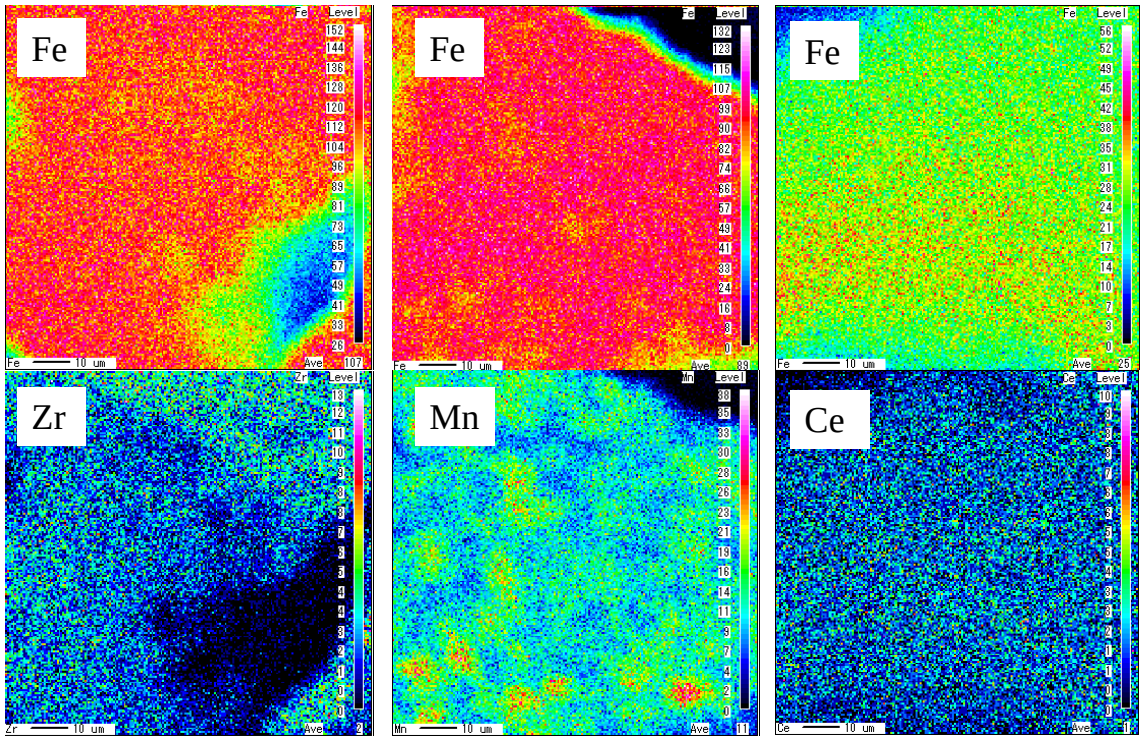


(a) (b) (c)

Fig. 4.6. EPMA mapping images of (a) 10wt.% Zr-FeCu, (b) Mn-FeCu, and (c) Ce-FeCu.

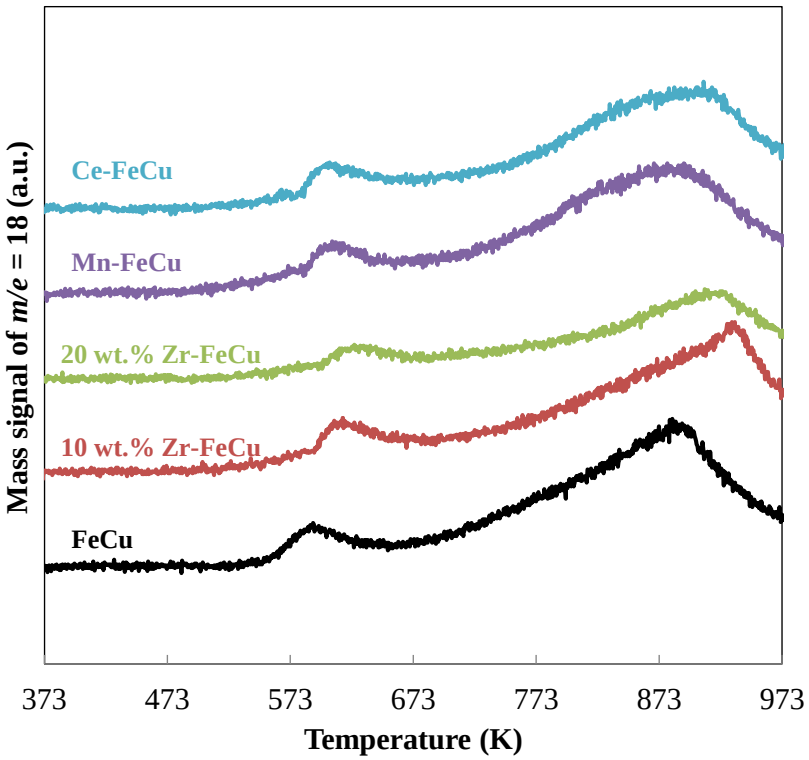


Fig. 4.7. $H_2$-TPR profiles of FeCu and metal-added Fe-based samples.

4.3.2. Syngas-to-hydrocarbons reaction.

Since syngas produced from biomass contains generally lower hydrogen concentrations than syngas produced from $CH_4$ [4], it must be necessary to simultaneously generate hydrogen during the conversion of syngas to hydrocarbons in order to improve the producibility of hydrocarbons. The use of a hybrid catalyst composed of an FTS catalyst and a WGS catalyst will efficiently produce hydrocarbons from $H_2$-deficient syngas as follows: (1) the CO hydrogenation to hydrocarbons over an FTS catalyst results in the generation of $H_2O$; (2) generated $H_2O$ reacts with CO over a WGS catalyst to generate hydrogen; and (3) generated hydrogen is used in the FTS:

(1), (3) $CO + H_2 \rightarrow -(CH_2)- + H_2O$

(2) $CO + H_2O \rightarrow CO_2 + H_2$

4.3.2.1. Effect of metal species in WGS catalyst on catalytic properties.

We investigated the catalytic properties of a hybrid catalyst containing the metal-added Fe-based catalyst as a WGS catalyst in the conversion of $H_2$-deficient syngas to hydrocarbons. Considering the use of syngas produced from biomass, syngas with the $H_2$/CO molar ratio of 1 was employed as a reactant gas in the present study. The metal added Fe-based catalyst was centered together with 20 wt.% Co supported on beta zeolite (Co/$\beta$) as an FTS catalyst in the reactor. Figure 4.8 shows the results of the conversion of $H_2$-deficient syngas to hydrocarbons over Co/$\beta$ and the hybrid catalysts as a function of time on stream. Figure 4.8(a) clearly shows the improvement of the CO conversion by employing the Fe-based WGS catalyst together with the FTS catalyst through the reaction times. When Co/$\beta$ was used alone, the formation of $CO_2$ was not observed during the reaction (Figure 4.8(b)), indicating that CO was converted through

only the FTS over Co/$\beta$ due to a low ability of Co species for the WGS reaction [38]. By contrast, the formation of $CO_2$ was observed when the hybrid catalysts containing the Fe-based WGS catalyst were used, regardless of the added metal species. Since no steam was introduced to the catalyst bed in the present study, $CO_2$ should be produced through the WGS reaction with $H_2O$ generated in the CO hydrogenation over Co/$\beta$, and hydrogen was simultaneously generated. Thus, it is indicated that the improvement of the CO conversion of the hybrid catalyst was derived from the WGS reaction. Moreover, it is also assumed that the hydrogenation concentration in the reaction system would be increased through the WGS reaction.

As shown in Figure 4.8(b), the formation of $CO_2$ was also dependent on the Fe-based WGS catalysts; the space time yields (STY) of $CO_2$ at 0.5 h were in the order of FeCu > Mn-FeCu > Ce-FeCu > 10 wt.% Zr-FeCu > 20 wt.% Zr-FeCu. The formation rate of $CO_2$ of all the catalysts was gradually declined through the reaction. After 6.5 h of the reaction time, the hybrid catalyst with Mn-FeCu exhibited the highest $CO_2$ formation rate, and the other hybrid catalysts with the metal added Fe-based catalyst showed similar $CO_2$ formation rates. These results indicate that Mn species in the Fe-based catalyst enhanced the catalytic activity for the WGS reaction and the catalyst durability in the CO hydrogenation, leading to an increase in the CO conversion, while Zr andCe species hardly had positive effects for the WGS activity. In contrast, the CO conversion of Zr-FeCu was similar to that of Mn-FeCu, suggesting that Zr species improved the activity of the Febased catalyst for the FTS. However, increasing the amount of Zr from 10 wt.% to 20 wt.% decreased the CO conversion due to the decrease in the amount of the Fe species in the catalyst. The doping of metal species to Fe-based catalysts showed positive effects on catalytic performances for the CO hydrogenation and the WGS

reaction [18 - 20, 34, 39, 40]. In the present study, the improvement of the catalytic activity would be derived from the high dispersion of the Fe species and the formation of active sites by the interaction of the Fe species with the Mn or Zr species. In the case of Ce-FeCu, the improvement of both activities for the CO hydrogenation and the WGS reaction was not observed due to low steam concentrations [41].

Table 4.2 summarizes the catalytic properties of the hybrid catalysts in the conversion of $H_2$-deficient syngas to hydrocarbons. The formation rate of hydrocarbons of the hybrid catalyst was increased by adding the metal species to FeCu in comparison with the hybrid catalyst containing FeCu. In the hydrocarbon distributions, the formation of $C_5$ - $C_{11}$ hydrocarbons, which corresponds to gasoline fractions, was improved by using the hybrid catalysts, in particularly the hybrid catalysts containing Mn-FeCu or Ce-FeCu that exhibited high values of the $C_5$ - $C_{11}$ hydrocarbon distribution. By contrast, the formation of hydrocarbons with carbon number more than 12 was suppressed when the Fe-based catalyst was employed together with Co/$\beta$. Lohitharn et al. have reported that transition-metal-added Fe-based catalysts showed a similar hydrocarbon selectivity to that of an Fe based catalyst without the addition of metal species [18, 19]. Thus, it is suggested that beta zeolite in the hybrid catalyst influenced the hydrocarbon distribution due to a high ability of the isomerization/cracking of hydrocarbons. Considering the generation of hydrogen through the WGS reaction over the Fe-based catalyst as shown in Figure 4.8(b), it is assumed that the increase in the hydrogen concentration would lead to the improvement of the spillover effect for the cracking of large hydrocarbons over acid sites or to the suppression of the carbon chain growth due to the hydrogenation of carbonaceous intermediates.

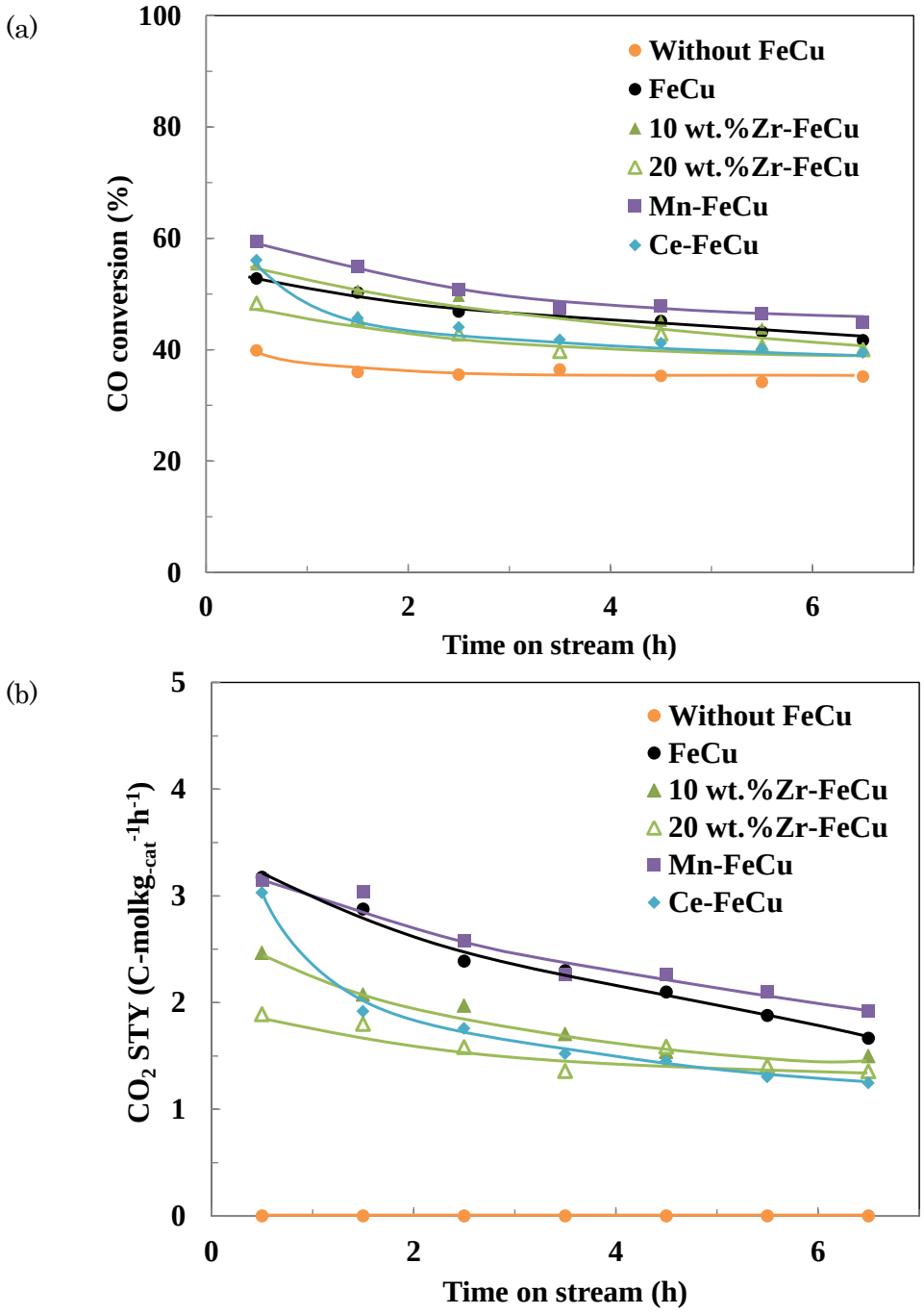


Fig. 4.8. CO conversion (a) and the formation rate of $CO_2$ (b) in the conversion of syngas to hydrocarbons over hybrid catalysts containing FeCu and metal-added Fe-based catalysts. Reaction conditions: cat.: 1.5 g Co/$\beta$, 1.95 g hybrid catalyst (1.5 g Co/$\beta$ and 0.45 g FeCu) and 2.0 g hybrid catalyst (1.5 g Co/$\beta$ and 0.5 g metal-added Fe-based catalyst); pressure: 1.0MPa; W/F = 16.3 $g_{\text{-cat.}}h\ mol^{-1}$; $H_2/CO = 1$.

Table 4.2. The results of the conversion of syngas to hydrocarbons over hybrid catalysts for reaction time of 6.5 h at 513K [a].

| | Without FeCu | FeCu[b] | Zr-FeCu (10 wt.% Zr) | Zr-FeCu (20 wt.% Zr) | Mn-FeCu | Ce-FeCu | Pd/Mn-FeCu |
|---|---|---|---|---|---|---|---|
| CO conv. (%) | 35.2 | 41.7 | 45.1 | 40 | 45 | 39.5 | 44.8 |
| $CO_2$ STY (mol $kg^{-1}$ $h^{-1}$) | 0 | 1.75 | 1.5 | 1.36 | 1.92 | 1.25 | 2.65 |
| H.C. STY (mol $kg^{-1}$ $h^{-1}$) | 2.48 | 2.16 | 2.38 | 2.30 | 2.61 | 2.54 | 2.35 |
| H.C. distribution (C-%) | | | | | | | |
| $C_1$ | 31.8 | 36.7 | 33.8 | 34.3 | 33.2 | 31.4 | 36.6 |
| $C_2$ - $C_4$ | 13.5 | 12.7 | 11.3 | 12.7 | 10.4 | 11.5 | 11.8 |
| $C_5$ - $C_{11}$ | 38.5 | 43.9 | 41.1 | 36.7 | 45.9 | 48.2 | 41.9 |
| $C_{12+}$ | 16.1 | 6.7 | 13.7 | 16.3 | 10.5 | 8.9 | 9.7 |

[a]Reaction conditions: cat.: 2.0 g hybrid catalyst (1.5 g Co/$\beta$ and 0.5 g Fe-based catalyst); pressure: 1.0MPa; W/F = 16.3 $g_{-cat.}$ $hmol^{-1}$; $H_2/CO$ = 1.

[b]1.95 g hybrid catalyst (1.5 g Co/$\beta$ and 0.45 g Fe-based catalyst).

4.3.2.2. Stabilization of WGS catalyst by loading of Pd.

The catalytic activity for the WGS reaction has been improved by loading Pd on WGS catalysts due to the promotion of the redox properties of iron oxides [42]. In addition, an increase in the hydrogen concentration through the WGS reaction will lead to suppressing the deactivation [43]. In order to improve the activity and durability of the Fe-based WGS catalyst, 1 wt.%Pd species was loaded on 10 wt.% Mn-FeCu by impregnation with 4.6 wt.% $Pd(NH_3)_2(NO_3)_2$ aqueous solution. The catalytic properties of the hybrid catalyst composed of the Pd/Mn-FeCu with Co/$\beta$ were evaluated in the conversion of $H_2$-deficient syngas to hydrocarbons. The results are shown in Table 4.2 and Figure 4.9. Pd/Mn-FeCu exhibited a similar CO conversion to that of Mn-FeCu during the reaction. Meanwhile, the formation of $CO_2$ ($H_2$ generation) in the WGS reaction was improved by loading Pd on Mn-FeCu. Furthermore, the gradual deactivation was observed on Mn-FeCu in the WGS reaction, while the $CO_2$ formation rate over Pd/Mn-FeCu was kept at ca. 2.6 mol kmol $kg^{-1}$ $h^{-1}$ even after 6.5 h of the reaction. In our previous findings, the deactivation derived from the deposition of carbonaceous species was suppressed by loading metal species with a high hydrogenation ability on ZSM-5, which was a part of a hybrid catalyst, in the syngas conversion to hydrocarbons via the methanol formation [44, 45]. Thus, Pd species on Mn-FeCu was supposed to readily activate hydrogen generated through the WGS reaction to decompose carbonaceous species, which were formed through the FTS, on active sites of the catalyst, leading to the mitigation of the deactivation of the WGS catalyst.

In the hydrocarbon distribution, the loading of Pd species enhanced the formation of light hydrocarbons; in particular the selectivity to methane was increased to 36.6% in

comparison with that of Mn-FeCu (Table 4.2). The high hydrogenation ability of Pd may lead to accelerate the hydrogenation of carbonaceous intermediates on active sites to form hydrocarbons with short chains prior to sufficient chain growth.

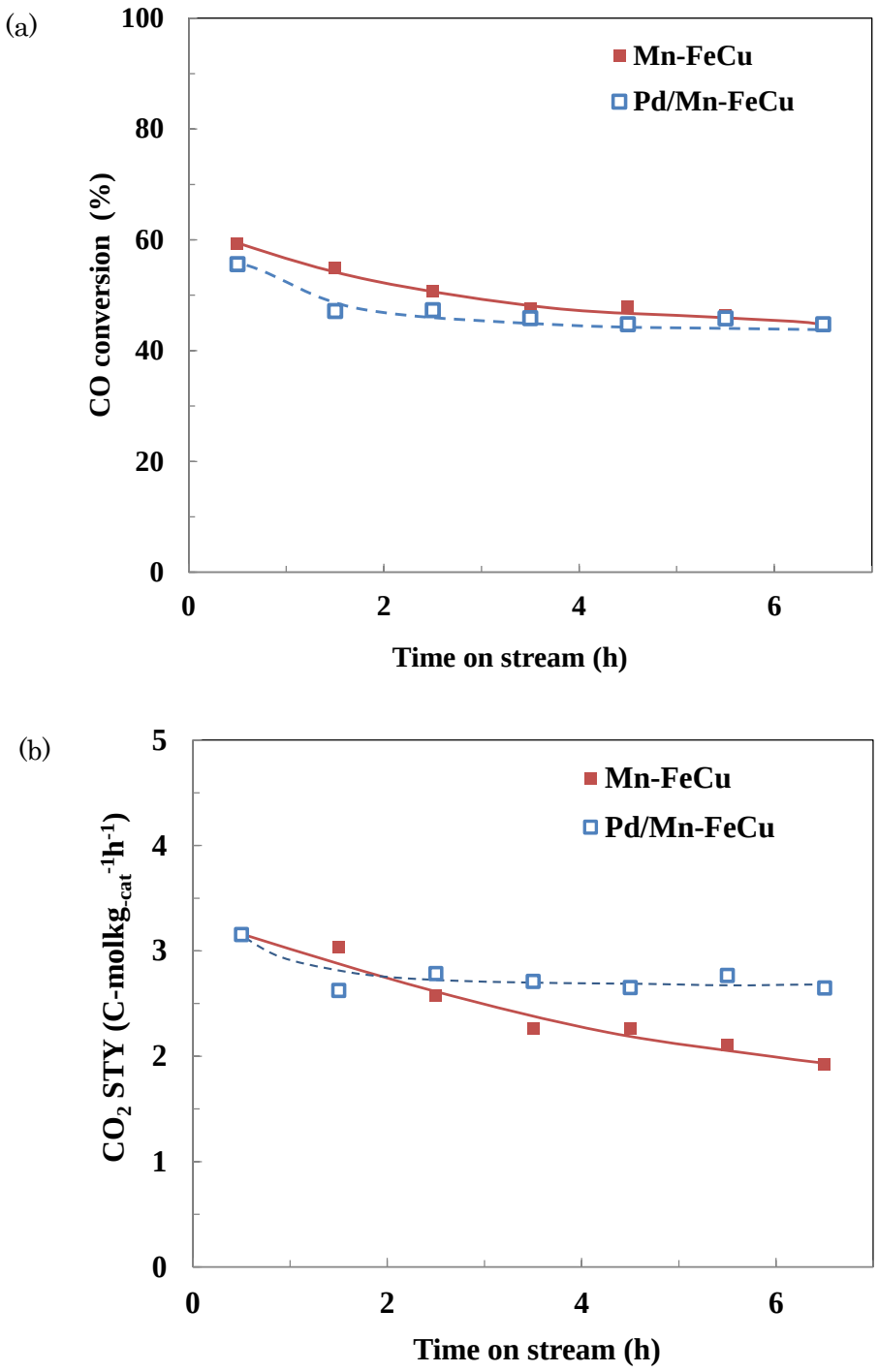


Fig. 4.9. CO conversion (a) and the formation rate of $CO_2$ (b) in the conversion of syngas to hydrocarbons over hybrid catalysts containing Mn-FeCu and Pd/Mn-FeCu. Reaction conditions: cat.: 2.0 g hybrid catalyst (1.5 g Co/$\beta$ and 0.5 g Fe-based catalyst); pressure, 1.0MPa; W/F = 16.3 $g_{\text{-cat.}}$ hmol−1; $H_2$/CO = 1.

## 4.4. Conclusions

Metal-composite Fe-based catalysts with nanosized crystallites were synthesized by the addition of metal species such as Mn, Zr, and Ce into an Fe-based catalyst. The metal-added Fe-based catalysts exhibited much higher specific surface area than the conventional Fe-based catalyst due to the formation of mesoporous voids surrounded by the nanosized crystallites. The metal-added Fe-based catalyst as a WGS catalyst was mixed with Co/$\beta$ as an FTS catalyst to prepare a hybrid catalyst. The catalytic properties of the hybrid catalyst were investigated in the hydrocarbon production from syngas with the low $H_2$/CO ratio of 1, where hydrogen was deficient for the conversion of all CO to hydrocarbons. The use of the hybrid catalyst resulted in the formation of $CO_2$, which corresponds to the simultaneous generation of hydrogen through the WGS reaction, regardless of the type of the added metal species, although no $CO_2$ was formed over Co/$\beta$ alone. Among the catalysts, the hybrid catalyst containing the Mn-added Fe-based catalyst exhibited the highest activity for the CO hydrogenation and the WGS reaction with the CO conversion of 45.0%, the STY of hydrocarbons of 2.61 mol kmol $kg^{-1}$ $h^{-1}$, and the STY of $CO_2$ of 1.92 mol $kg^{-1}$ $h^{-1}$ after 6.5 h of the reaction; furthermore, a high durability of the catalyst was observed during the reaction. Moreover, the loading of Pd species on the Mn-added Fe-based catalyst improved the durability due to the high hydrogenation ability of Pd species.

References

[1] P. K. Swain, L. M. Das, and S. N. Naik, Renewable and Sustainable Energy Reviews, vol. 15, no. 9, pp. 4917–4933, 2011.

[2] L. Yang, X. Ge, C. Wan, F. Yu, and Y. Li, Renewable and Sustainable Energy Reviews, vol. 40, pp. 1133–1152, 2014.

[3] M. E. Dry, Catalysis Today, vol. 71, no. 3-4, pp. 227–241, 2002.

[4] L. Wei, J. A. Thomasson, R. M. Bricka, R. Sui, J. R. Wooten, and E. P. Columbus, Transactions of the ASABE, vol. 52, no. 1, pp. 21–37, 2009.

[5] M. E. Dry, Applied Catalysis A: General, vol. 138, no. 2, pp. 319–344, 1996.

[6] F. G. Botes and B. B. Breman, Industrial and Engineering Chemistry Research, vol. 45, no. 22, pp. 7415–7426, 2006.

[7] I. C. Yates and C. N. Satterfield, Energy & Fuels, vol. 5, no. 1, pp. 168–173, 1991.

[8] K. W. Jun, H. S. Roh, K. S. Kim, J. S. Ryu, and K. W. Lee, Applied Catalysis A: General, vol. 259, no. 2, pp. 221–226, 2004.

[9] N. Escalona, S. Fuentealba, and G. Pecchi, Applied Catalysis A: General, vol. 381, no. 1-2, pp. 253–260, 2010.

[10] M. Iglesias, R. Edzang, and G. Schaub, Catalysis Today, vol. 215, pp. 194–200, 2013.

[11] B. H. Davis, Catalysis Today, vol. 84, no. 1-2, pp. 83–98, 2003.

[12] S. Lögdberg, D. Tristantini, Ø. Borg et al., Applied Catalysis B: Environmental, vol. 89, no. 1-2, pp. 167–182, 2009.

[13] E. de Smit and B. M. Weckhuysen, Chemical Society Reviews, vol. 37, no.12, pp. 2758–2781, 2008.

[14] H. H. Storch, N. Golumbic, and R. B. Anderson, The Fischer-Tropsch and Related

Synthesis, Wiley, New York, NY, USA, 1951.

[15] Y. Jin and A. K. Datye, Journal of Catalysis, vol. 196, no. 1, pp. 8–17, 2000.

[16] H.-J. Wan, B.-S. Wu, C.-H. Zhang et al., Catalysis Communications, vol. 8, no. 10, pp. 1538–1545, 2007.

[17] R. J. O'Brien, L. G. Xu, R. L. Spicer, S. Q. Bao, D. R. Milburn, and B. H. Davis, Catalysis Today, vol. 36, no. 3, pp. 325–334,1997.

[18] N. Lohitharn, J. G. Goodwin Jr., and E. Lotero, Journal of Catalysis, vol. 255, no. 1, pp. 104–113, 2008.

[19] N. Lohitharn and J. G. Goodwin Jr., Journal of Catalysis, vol. 257, no. 1, pp. 142–151, 2008.

[20] L. Bai, H. W. Xiang, Y. W. Li, Y. Z. Han, and B. Zhong, Fuel, vol. 81, no. 11-12, pp. 1577–1581, 2002

[21] J. W. Niemantsverdriet, A. M. van der Kraan, W. L. van Dijk, and H. S. van der Baan, Journal of Physical Chemistry, vol. 84, no. 25, pp. 3363–3370, 1980.

[22] S. A. Eliason and C. H. Bartholomew, Applied Catalysis A: General, vol. 186, no. 1-2, pp. 229–243, 1999.

[23] N. Tsubaki, Y. Yoneyama, K. Michiki, and K. Fujimoto, Catalysis Communications, vol. 4, no. 3, pp. 108–111, 2003.

[24] M. Yao, N. Yao, Y. Shao et al., Chemical Engineering Journal, vol. 239, pp. 408–415, 2014.

[25] A. Martínez, S. Valencia, R. Murciano, H. S. Cerqueira, A. F. Costa, and E. F. S. Aguiar, Applied Catalysis A: General, vol. 346, no. 1-2, pp. 117–125, 2008.

[26] Q. Zhang, X. Li, K. Asami, S. Asaoka, and K. Fujimoto, Fuel Processing Technology, vol. 85, pp. 1139–1150, 2004.

[27] Q. Ge, X. Li, H. Kaneko, and K. Fujimoto, Journal of Molecular Catalysis A: Chemical, vol. 278, no. 1-2, pp. 215–219, 2007.

[28] X. Ma, Q. Ge, J. Ma, and H. Xu, Fuel Processing Technology, vol. 109, pp. 1–6, 2013.

[29] H. Torres, G. Torres, and P. Krijn, ACS Catalysis, vol. 3, no. 9, pp. 2130–2149, 2013.

[30] K. Jothimurugesan, J. G. Goodwin Jr., S. K. Gangwal, and J. J. Spivey, Catalysis Today, vol. 58, no. 4, pp. 335–344, 2000.

[31] D. B. Bukur and C. Sivaraj, Applied Catalysis A: General, vol. 231, no. 1-2, pp. 201–214, 2002.

[32] H. Zhang, H. Ma, H. Zhang, W. Ying, and D. Fang, "Effects of Zr and K promoters on precipitated iron-based catalysts for Fischer-Tropsch synthesis," Catalysis Letters, vol. 142, no. 1, pp. 131–137, 2012.

[33] M. Ding, J. Tu, M. Qiu, T. Wang, L. Ma, and Y. Li, Applied Energy, vol. 138, pp. 584–589, 2015.

[34] M. Qing, Y. Yang, B. Wu et al., Journal of Catalysis, vol. 279, no. 1, pp. 111–122, 2011.

[35] M. Ding, M. Qiu, J. Liuet al., Fuel, vol. 109, pp. 21–27, 2013.

[36] M. D. Lee, J. F. Lee, C. S. Chang, and T. Y. Dong, Applied Catalysis, vol. 72, no. 2, pp. 267–281, 1991.

[37] Z. Tao, Y. Yang, H. Wan et al., Catalysis Letters, vol. 114, no. 3-4, pp. 161–168, 2007.

[38] A. Griboval-Constant, A. Butel, V. V. Ordomsky, P. A. Chernavskii, and A. Y. Khodakov, Applied Catalysis A: General, vol. 481, pp. 116–126, 2014.

[39] H. Wang, Y. Yang, J. Xu, H. Wang, M. Ding, and Y. Li, Journal of Molecular Catalysis A: Chemical, vol. 326, no. 1-2, pp. 29–40, 2010.

[40] F. Meshkani and M. Rezaei, Renewable Energy, vol. 74, pp. 588–598, 2015.

[41] G. K. Reddy, P. Boolchand, and P.G. Smirniotis, Journal of Catalysis, vol. 282, no. 2, pp. 258–269, 2011.

[42] Y. Sekine, T. Chihara, R.Watanabe,Y. Sakamoto, M. Matsukata, and E. Kikuchi, Catalysis Letters, vol. 140, no. 3-4, pp. 184–188, 2010.

[43] G. P. van der Laan and A. A. C. M. Beenackers, Catalysis Reviews: Science and Engineering, vol. 41, no. 3-4, pp. 255–318, 1999.

[44] T. Ma, H. Imai, Y. Suehiro, C. Chen, T. Kimura, S. Asaoka, X. Li, Catalysis Today, vol. 228, pp. 167–174, 2014.

[45] T. Ma, H. Imai, M. Yamawaki, K. Terasaka, and X. Li, Catalysts, vol. 4, no. 2, pp. 116–128, 2014.

# CHAPTER FIVE

# GENERAL CONCLUSIONS

## 5.1 General conclusions

This research focused on selective synthesis of gasoline-range hydrocarbons from syngas on hybrid catalyst through methanol synthesis and FTS process. The purpose of this study was to develop the hybrid catalyst's activity, selectivity, and stability for direct synthesis gasoline from syngas by MTG route and FTS route, respectively.

For methanol synthesis route, the catalytic performances of hybrid catalysts composed of Cu-ZnO and metal/ZSM-5 in the syngas conversion to hydrocarbons via methanol in a near-critical *n*-hexane solvent have been studied. Points are as follows:

1. The near-critical fluid was effective in the selective production of hydrocarbons in gasoline fraction during the syngas conversion over the hybrid catalyst.
2. The employment of the near-critical solvent led to depressing the formation of $CO_2$ during the reaction.
3. The characteristics of Pd/ZSM-5 influenced the synthesis of the hydrocarbons in the syngas conversion. An increase in the acid amount of ZSM-5 was effective on the generation of hydrocarbons in the syngas conversion to hydrocarbons at lower temperature than those applied in the MTH reaction. Hydrocarbon distribution was strongly dependent on the particle size of ZSM-5 and Pd loading. A decrease in the particle size of ZSM-5 and an increase in the Pd loading improved the yield of hydrocarbons in gasoline fraction with high catalytic stability. It is likely that the improvement of the mass transfer due to the decrease of the particle size and the hydrogenation of unsaturated hydrocarbons over Pd suppress the deposition of

carbonaceous species. Subsequently, the pore and cavity spaces in the zeolite can be retained, leading to the smooth mass transfer of large hydrocarbons out of the intracrystallites. Therefore, Pd/ZSM-5 composed of nano-sized particles is effective on the selective production of gasoline fractions from syngas via methanol with the near-critical fluid.

4. The hybrid catalyst consisting of 5 wt% Cu/ZSM-5 coupled with Cu-ZnO exhibited very similar catalytic performances to those over the hybrid catalyst containing 0.5 wt% Pd/ZSM-5, and produced selectively gasoline-ranged hydrocarbons from syngas.
5. The Cu loaded on ZSM-5 influenced the deactivation rate as well as the product distribution. An increase in the Cu loading increased the gasoline-ranged hydrocarbons yield without the cracking of the products, and shortened time before the catalytic activity became stable with keeping a high CO conversion. The high Cu loading on ZSM-5 decreased the amount of the acid sites and weakened the acid strength of ZSM-5, which were estimated from $NH_3$-TPD profiles. These findings suggest that Cu species would interact with the acid sites of ZSM-5 to make the acid strength mild, leading to suppressing the excess polymerization and the cracking of products with keeping high ability of the methanol conversion to hydrocarbons. In addition, the Cu species on ZSM-5 exhibited less ability for the water-gas-shift reaction, resulting in the good catalytic stability without excess consumption of CO. Therefore, Cu/ZSM-5 as a portion of a hybrid catalyst is effective in the selective synthesis of the gasoline-ranged hydrocarbons from syngas.

For FTS reaction with $H_2$-deficient syngas as feed gas, the metal-added Fe-based catalyst as a WGS catalyst was mixed with Co/β as an FTS catalyst to prepare a hybrid catalyst. The effect of different metal addition on the structure and WGS activity of Fe-based catalysts were investigated. Points are as follows:

1. The effects of metal species in an Fe-based catalyst on structural properties were investigated through the synthesis of Fe-based catalysts containing various metal species, such as Mn, Zr, and Ce. The metal-added Fe-based catalysts exhibited much higher specific surface area than the conventional Fe-based catalyst due to the formation of mesoporous voids surrounded by the nanosized crystallites. The use of the hybrid catalyst resulted in the formation of $CO_2$, which corresponds to the simultaneous generation of hydrogen through the WGS reaction, regardless of the type of the added metal species, although no $CO_2$ was formed over Co/$\beta$ alone.
2. Among the catalysts, the hybrid catalyst containing the Mn-added Fe-based catalyst exhibited the highest activity for the CO hydrogenation and the WGS reaction with the CO conversion of 45.0%, the STY of hydrocarbons of 2.61mol kmol $kg^{-1}$ $h^{-1}$, and the STY of $CO_2$ of 1.92mol $kg^{-1}$ $h^{-1}$ after 6.5 h of the reaction; furthermore, a high durability of the catalyst was observed during the reaction.
3. Moreover, the loading of Pd species on the Mn-added Fe-based catalyst improved the durability due to the high hydrogenation ability of Pd species.

## 5.2 Perspective

Firstly, this study comes up with a new idea of using near-critical solvents in synthesizing gasoline in a single pot from syngas through methanol. Owing to the advantages mentioned above, the hybrid catalysts of Cu-ZnO and Cu/ZSM-5 in a near-critical phase are promising for commercial application of direct synthesis of gasoline-range hydrocarbons from syngas.

Besides, most of the FT technologies developed in last two decades are based on the low-temperature FT (473-513 K, LTFT) process. These processes have involved syngas with a high $H_2$/CO ratio, which is generated by vaporeforming, autothermal reforming, or partial oxidation using natural gas as a feedstock. In this study, the design of a hybrid catalyst composed with cobalt, iron and $\beta$ catalysts provided a new solution for direct synthesis of gasoline-range hydrocarbons, using $H_2$-deficient biosyngas as feed gas in the LTFT process. And more work on the catalyst optimization need to be carried out for environmental and sustainable development in future.

ACKNOWLEDGMENT

I would like to express my sincerer appreciation to my advisor Professor Xiaohong Li for her warm encouragement and kind guidance which supported me during these past five years. She is my great mentor who has raised me up to a new level of my research and also my life. I would also like to thank Doctor Hiroyuki Imai, Professor Sachio Asaoka and Professor Qianwen Zhang for their help, scientific advice and suggestions.

Besides my advisor, I would like to thank the rest of my thesis committee: Professor Kenji Asami, Professor Kazuharu Yoshizuka and Professor Kazumi Horiguchi, for their encouragement insightful comments and questions.

My warm thanks are due to Doctor Toshiyuki Kimura and Doctor Chun Chen who gave many directions and help. They guided me to use the experimental facilities and analytical instruments. Moreover, I want to thank all members of Li Lab. and Imai Lab.: especially Kentaro Takasaki, Yuuki Furukado, Manami Yamawaki, Tomohiro Shige, Taisuke Sugio, Tomohiro Akiba and Shinya Nakagawa.

A special thanks to my family. Words cannot express how grateful I am to my parents for all of the sacrifices that made on my behalf. Their love and care for me was what sustained me thus far. At the end I would like express appreciation to my husband for supporting me spiritually.

LIST OF PUBLICATIONS

1. **Ting Ma**, Hiroyuki Imai, Yoshifumi Suehiro, Chun Chen, Toshiyuki Kimura, Sachio Asaoka, Xiaohong Li, " Selective synthesis of gasoline from syngas in near-critical phase" , Catalysis Today, Volume 228, Pages 167-174 (2014)
2. **Ting Ma**, Hiroyuki Imai, Manami Yamawaki, Kazusa Terasaka, Xiaohong Li, "Selective synthesis of gasoline-ranged hydrocarbons from syngas over hybrid catalyst consisting of metal-loaded ZSM-5 coupled with copper-zinc oxide", Catalysts, Volume 4, Pages 116-128 (2014)
3. **Ting Ma**, Hiroyuki Imai, Tomohiro Shige, Taisuke Sugio, Xiaohong Li, "Synthesis of hydrocarbons from $H_2$-deficient syngas in Fischer–Tropsch synthesis over Co-based catalyst coupled with Fe-based catalyst as water-gas shift reaction", Journal of Nanomaterials, Volume 2015 (2015)
4. Qianwen Zhang, **Ting Ma**, Ming Zhao, Teppei Tomonobu, Xiaohong Li, "Direct Synthesis of LPG from Syngas in Slurry Phase", Catalysis Science & Technology, 2016, in press

LIST OF CONFERENCE

International conference

1. **Ting Ma**, Jin Wang, Toshiyuki Kimura, Xiaohong Li and Sachio Asaoka, "Synthesis of LPG gas via methanol on nano-sized $Al_2O_3$/H-FeGaAlMFI catalyst", The 11th China-Japan Symposium on Coal and C1 Chemistry, Yinchuan, China (Aug. 3-7, 2011)
2. **Ting Ma**, Yoshihumi Suehiro, Chun Chen, Toshiyuki Kimura, Hiroyuki Imai, Sachio Asaoka, Xiaohong Li, "Selective Synthesis of Gasoline from syngas in near-critical phase", The 10th Natural Gas Conversion Symposium, Doha, Qatar (Mar. 2-7, 2013)
3. **Ting Ma**, Hiroyuki Imai, Chun Chen, Yoshihumi Suehiro, Sachio Asaoka, Xiaohong Li, "Gasoline Production from Syngas over Hybrid Catalysts in Near-Critical Phase", The 7th International Symposium on Acid-Base Catalysis (ABC-7), Tokyo, Japan (May 12-15, 2013)
4. **Ting Ma**, Manami Yamawaki, Yoshifumi Suehiro, Hiroyuki Imai, Xiaohong Li, "Effects of added oxide on catalytic properties of mixed catalysts in gasoline synthesis from syngas", The 12th Japan-China Symposium on Coal and C1 Chemistry, Fukuoka, Japan (Oct. 28-31, 2013)
5. **Ting Ma**, Hiroyuki Imai, Tomohiro Shige, Taisuke Sugio, Xiaohong Li, "Synthesis of hydrocarbons from $H_2$-deficient syngas in Fischer–Tropsch synthesis over Co-based catalyst coupled with Fe-based catalyst as water-gas shift reaction", The 13th Japan-China Symposium on Coal and C1 Chemistry, Dunhuang, China (Aug. 31 – Sep.3, 2015)

National conference

6. **馬　婷**, 木村　俊之, 黎　暁紅, 浅岡　佐知夫, “ノルマルヘキサンの骨格異性化における Pd/*ns* $Al_2O_3$/BEA 触媒の協奏効果”, 第 41 回石油・石油化学討論会 山口大会, 山口 (Nov. 10-11, 2011)
7. **馬　婷**, 木村　俊之, 陳　春, 今井　裕之, 浅岡　佐知夫, 黎　暁紅, “Gas-to-Liquid 反応における亜臨界条件での二酸化炭素生成への影響”, 第 110 回触媒討論会, 福岡 (Sep. 24-26, 2012)
8. 木村　俊之, **馬　婷**, 今井　裕之, 浅岡　佐知夫, 黎　暁紅, “合成ガスからの低級炭化水素合成におけるナノポーラスハイブリッド触媒の協奏効果”, 第 110 回触媒討論会, 福岡 (Sep. 24-26, 2012)
9. **馬　婷**, 木村　俊之, 陳　春, 今井　裕之, 浅岡　佐知夫, 黎　暁紅, “合成ガスからのガソリン留分合成における炭化水素添加効果”, 第 42 回石油・石油化学討論会 秋田大会, 秋田 (Oct. 11-12, 2012)
10. **馬　婷**, 山脇　真奈美, 今井　裕之, 黎　暁紅, “金属とゼオライトの混合触媒による合成ガスからのガソリン留分炭化水素の合成”, 第 43 回石油・石油化学討論会 北九州大会, 北九州 (Nov. 14-15, 2013)
11. **馬　婷**, 山脇　真奈美, 今井　裕之, 黎　暁紅, “銅系触媒による合成ガスからのガソリン留分炭化水素の合成”, 第 113 回触媒討論会, 豊橋 (Mar. 26-27, 2014)
12. **馬　婷**, 重　智廣, 杉尾　太輔, 今井　裕之, 黎　暁紅, “ハイブリット触媒を用いたバイオマス由来の合成ガスからのガソリン留分合成”, 第 44 回石油・石油化学討論会　旭川大会, 旭川 (Oct. 16-17, 2014)
13. 山脇　真奈美, **馬　婷**, 寺坂　一沙, 今井　裕之, 黎　暁紅, “Cu 系触媒を用いた合成ガスからガソリン留分炭化水素の製造”, 第 44 回石油・石油化学討

論会　旭川大会, 旭川 (Oct. 16-17, 2014)

14. **馬　婷**, 重　智廣, 杉尾　太輔, 今井　裕之, 黎　暁紅, “三元触媒を用いたバイオマス由来の合成ガスからのガソリン留分合成”, 第 115 回触媒討論会, 東京 (Mar. 23-24, 2015)